

# **High-Quality Detection in Heavy-Traffic Avionic Communication System Using Interference Cancellation Techniques**

**Anh-Minh Ngoc Nguyen**

Dissertation submitted to the Faculty of the  
Virginia Polytechnic Institute and State University  
in partial fulfillment of the requirements for the degree of

Doctor of Philosophy  
in  
Electrical Engineering

Dr. Amir I. Zaghoul, Chair  
Dr. William H. Tranter  
Dr. Lamine M. Mili  
Dr. Timothy Pratt  
Dr. Yuriko Renardy  
Dr. Leone Monticone

*Keywords:* Aeronautical mobile communication, avionic communication, Sequential (Successive) Interference Cancellation, SIC, Parallel Interference Cancellation, PIC, multi-user detection, heavy-traffic environment, co-channel interference

September 2005  
Arlington, Virginia

# Abstract

## **High-Quality Detection in Heavy-Traffic Avionic Communication System Using Interference Cancellation Techniques**

by

Minh Nguyen

This dissertation focuses on quantifying the effects of multi-user co-channel interference for an avionic communication system operating in a heavy-traffic aeronautical mobile environment and proposes advanced interference cancellation techniques to mitigate the interference.

The dissertation consists of two parts. The first part of the work investigates the use of a visualization method to quantify and characterize the multi-user co-channel interference (multiple access interference) effects impinging on an avionic communication system. The interference is caused by complex interactions of thousands of RF signals transmitted from thousands of aircraft; each attempts to access a common communication channel, which is governed by a specific channel contention access protocol. The visualization method transforms the co-channel interference, which is specified in terms of signal-overlaps (signal collisions), from a visual representation to a matrix representation for further statistical analysis. It is found that the statistical Poisson and its cumulative distribution provide the best estimates of multi-user co-channel interference. It is shown, using Monte Carlo simulation, that the co-channel interference of a victim aircraft operating in the heavy-traffic environment could result in as high as *eight* signal-overlaps. This constitutes to approximately 83.4% of success rate in signal detection for the entire three thousand aircraft environment using conventional FSK

receiver. One key finding shows that high-quality communications, up to 98.5% success rate, is achievable if only *three* overlapping signals can be decoded successfully. The interference results found in the first part set the stage for interference cancellation research in the second part.

The second part of the work proposes the use of advanced interference cancellation techniques, namely sequential interference cancellation (SIC) and parallel interference cancellation (PIC), as potential solutions to mitigating the interference effects. These techniques can be implemented in radio receivers to perform multi-signal decoding functionality to remove the required interferers (*three* overlapping signals) so that high-quality communication, as described in the first part, can be achieved. Various performance graphs are shown for B-FSK and B-PSK for both SIC and PIC techniques. One key finding is that the system performance can be improved substantially to an additional 15% in signal reception success rate by using SIC or PIC. This means that critical information transmitted from 450 aircraft (out of approximately three thousand aircraft in the environment) is preserved and successfully decoded. Multi-signal decoding using these interference cancellation receivers comes at a small penalty of 2 - 4.5 dBs in  $E_b/N_o$  when sufficient signal-to-interference (SIR) ratio (7-12 dB) is provided.

## Acknowledgements

First and foremost, I would like to thank my advisor Dr. Amir. I. Zaghoul, who has consistently provided support, tutelage, encouragement and advice throughout the years of my doctoral study. Dr. Zaghoul's insight, everlasting helpfulness, understanding and genuine concern for his students made working with him such a memorable experience. His breadth and scope of knowledge about communication system was valuable in defining and scoping the research and his inputs and meticulous attention helped improve the presentation of this dissertation. I would like to thank my committee members, Dr. William H. Tranter, Dr. Lamine M. Mili, Dr. Timothy Pratt, Dr. Yuriko Renardy, and Dr. Leone Monticone for their time and counsel, especially those who went the extra miles to facilitate distant communications between Blacksburg, Northern Virginia, West Virginia, and France.

I would like to extend my sincere gratitude to MITRE colleagues who have provided unselfish support, advice, encouragement and assistance throughout the years, dating back before I even started my first day in the PhD program. First, I would like to thank Dr. Reza Eftekari, David Hamrick, Dr. Lisandro del Cid, Dean Lamiano and Dr. Leone Monticone for recommending me into the competitive Advanced Graduate Degree Program (AGDP) program at MITRE. I would like to thank Dean Lamiano and Dr. Lisandro del Cid for their support, encouragement, understanding as well as their invaluable technical inputs and meticulous reviews for all of my technical conference and journal publications. Many thanks to Dr. Lisandro del Cid for providing funding so that I could attend, present, and publish papers at technical conferences and journal publications.

I would like to thank Dr. Michael Tran, Dr. Leone Monticone, and Dr. Warren Wilson for many valuable technical discussions, which led to the development and

implementation of the visualization method to quantify co-channel interference as described in Chapter 3.

I would like to thank Dr. Chris Hegarty for his research ideas, as well as his initial advice that helped me started on the right direction to further study multi-user detection as a solution for multiple access co-channel interference. I would like to thank John Fite for unselfishly sharing his invaluable knowledge on multi-user detection that led to the design, development and implementation of the sequential interference cancellation receiver as described in Chapter 4. I would like to thank Chris Moody and Rob Strain for sharing their expertise about the operation of Universal Access Transceiver system. I would like to thank Dr. Tae Kim for his encouragement, his willingness to share numerous technical discussions as well as his own experience in the AGDP program.

I am very grateful to my wife Chi for all her love, support, encouragement, and understanding throughout my busy times with the program. I would like to express my deepest gratitude to my parents for their unconditional love, support, encouragement, and many, many, many sacrifices they have made just to show me that through hard work, dedication, determination and love, dreams do come true. My family has been my pillars of strength throughout the years. This PhD degree is for you!

## Accomplishments

### IEEE Conference Paper Award

- A paper, entitled “Extension on Characterizing Packet Interference in a High-Density Traffic Environment” by M. Nguyen and A. Zaghoul was awarded “*Best of Track*” in the Communication, Navigation and Surveillance (CNS) Networks track at the IEEE Digital Avionics System Conference in Salt Lake City, Ohio, October 2004.

### Patents

- Two patents (pending)

### Conference and Journal Publications

- M. Nguyen, A. Zaghoul, “On the Characterization of Co-Channel Interference in an Aeronautical Mobile Environment,” paper accepted in April 2005, to be published in the *IEEE Transactions on Vehicular Technology*.
- M. Nguyen, A. Zaghoul, “Sequential Interference Cancellation Receiver for Future Aeronautical Mobile Communications,” to be submitted to the *IEEE Transactions on Aerospace and Electronic Systems*.
- M. Nguyen, A. Zaghoul, “Parallel Interference Cancellation Receiver for Future CNS Systems, to be submitted to the *IEEE Transactions on Aerospace and Electronic Systems*.

- M. Nguyen, A. Zaghoul, “High-Quality Communication in Heavy-Traffic ATC Environment Using Interference Cancellation Receiver”, accepted, to be published in the *Proceedings of twenty-fourth IEEE Digital Avionics System Conference*, Washington, DC, October 30<sup>th</sup> - November 3<sup>rd</sup>, 2005.
  
- M. Nguyen, A. Zaghoul, “Interference Cancellation Receiver,” *NASA’s Integrated Communications, Navigation and Surveillance (I-CNS) Conference*, Fairfax, Virginia, May 2-6, 2005.
  
- M. Nguyen, A. Zaghoul, “Extension on Characterizing Packet Interference in a High-Density Traffic Environment,” in *Proceedings of twenty-third IEEE Conference on Digital Avionics Systems*, Salt Lake City, Utah, October 24-28, 2004.
  
- M. Nguyen, A. Zaghoul, “A Method for Characterizing Packet Interference in a High-Density Traffic Environment,” in *Proceedings of sixtieth IEEE Conference on Vehicular Technology*, Los Angeles, California, September 26-29, 2004.

# CONTENTS

<b>CHAPTER 1 : INTRODUCTION .....</b>	<b>1</b>
1.1 BACKGROUND.....	1
1.2 PURPOSE .....	3
1.3 MOTIVATION.....	4
1.4 PREVIOUS WORK.....	5
1.4.1 Multiple access interference analysis.....	5
1.4.2 Multi-User Detection (MUD).....	5
1.5 PARALLEL WORK IN THE FIELD.....	10
1.6 CONTRIBUTION .....	10
1.7 ORGANIZATION OF DISSERTATION .....	11
<b>CHAPTER 2 : AERONAUTICAL MOBILE COMMUNICATION SYSTEM OPERATING IN A HEAVY-TRAFFIC ENVIRONMENT.....</b>	<b>13</b>
2.1 OVERVIEW .....	13
2.2 AVIONIC COMMUNICATION SYSTEM DESCRIPTION .....	15
2.3 HEAVY-TRAFFIC AERONAUTICAL ENVIRONMENT DESCRIPTION.....	22
2.4 SUMMARY .....	28
<b>CHAPTER 3 : CHARACTERIZATION OF MULTIPLE ACCESS INTERFERENCE IN THE HEAVY-TRAFFIC ENVIRONMENT .....</b>	<b>30</b>
3.1 METHOD FOR EVALUATING MULTIPLE ACCESS INTERFERENCE.....	31
3.2 SIMULATION.....	33
3.2.1 Assumptions.....	34
3.2.2 Data input.....	34
3.2.3 Simulation engine .....	36
3.2.4 CASE I: Worst-case estimates of interference.....	37
3.2.5 CASE II: Realistic estimates of interference.....	40
3.3 RESULTS AND INTERPRETATION .....	51
3.4 CONCLUSION AND RECOMMENDATION .....	53
3.5 ACKNOWLEDGEMENT.....	54
<b>CHAPTER 4 : SEQUENTIAL INTERFERENCE CANCELLATION (SIC) RECEIVER.....</b>	<b>56</b>
4.1 SIC RECEIVER STRUCTURE.....	58
4.2 SIMULATION ASSUMPTIONS .....	60
4.3 SIC BASED ON <i>B-FSK</i> DE/MODULATION .....	61
4.3.1 Analytical performance evaluation.....	61
4.3.2 Case 1. Performance of SIC for decoding <u>two</u> overlapping co-channel FSK signals .....	69
4.3.3 Case 2. Performance of SIC for decoding <u>three</u> overlapping co-channel FSK signals.....	73
4.4 SIC BASED ON <i>B-PSK</i> DE/MODULATION .....	79
4.4.1 Analytical performance evaluation.....	80
4.4.2 Case 1. Performance of SIC for decoding <u>two</u> overlapping co-channel B-PSK signals.....	80
4.4.3 Case 2. Performance of SIC for decoding <u>three</u> overlapping co-channel B-PSK signals....	84
4.5 CONCLUSION AND RECOMMENDATION .....	90
4.6. ACKNOWLEDGEMENT.....	92
<b>CHAPTER 5 : PARALLEL INTERFERENCE CANCELLATION (PIC) RECEIVER .....</b>	<b>93</b>
5.1 PIC RECEIVER STRUCTURE.....	93
5.2 SIMULATION ASSUMPTIONS.....	94
5.3 PIC BASED ON <i>B-FSK</i> DE/MODULATION .....	95
5.3.1 Case 1. Performance of PIC for decoding <u>two</u> overlapping co-channel B-FSK signals .....	95
5.3.2 Case 2. Performance of PIC for decoding <u>three</u> overlapping co-channel B-FSK signals..	101
5.4 CONCLUSION AND RECOMMENDATION .....	107



5.5.	ACKNOWLEDGEMENT.....	108
<b>CHAPTER 6 : SIC, PIC AND THEIR IMPLEMENTATION CONSIDERATIONS .....</b>		<b>109</b>
6.1	A POSSIBLE RECEIVER ARCHITECTURE FOR THE IMPLEMENTATION OF SIC AND PIC.....	109
6.2	PERFORMANCE COMPARISON BETWEEN SIC AND PIC.....	115
<b>CHAPTER 7 : CONCLUSION AND FUTURE DIRECTIONS .....</b>		<b>118</b>
<b>APPENDIX A. SIMULATION INTEGRITY.....</b>		<b>123</b>
<b>APPENDIX B. ANTENNA AND SWITCHING MECHANISM TO IMPROVE SYSTEM PERFORMANCE .....</b>		<b>125</b>
<b>APPENDIX C. SIC RECEIVER FOR DECODING FOUR BFSK AND BPSK SIGNALS.....</b>		<b>130</b>
<b>REFERENCES .....</b>		<b>132</b>
<b>VITA .....</b>		<b>139</b>

# LIST OF FIGURES

FIGURE 1-1. CONVENTIONAL RECEIVER.....	6
FIGURE 1-2. OPTIMUM RECEIVER.....	7
FIGURE 1-3. DECORRELATOR RECEIVER .....	8
FIGURE 1-4. MINIMUM MEAN-SQUARE ERROR RECEIVER .....	8
FIGURE 2-1. AIRCRAFT POSITION, VELOCITY, WEATHER, TRAFFIC, ADVISORY INFORMATION.....	14
FIGURE 2-2. THE AVIONIC RADIO AND DISPLAY PANEL [UPS03].....	14
FIGURE 2-3. VARIOUS TYPES OF INFORMATION DISPLAY.....	15
FIGURE 2-4. THE AVIONIC SYSTEM OPERATIONAL CONCEPT .....	16
FIGURE 2-5. MESSAGE FRAME .....	16
FIGURE 2-6. MEASURED RF SIGNAL OF THE AVIONIC COMMUNICATION SYSTEM .....	17
FIGURE 2-7. RF SIGNAL REQUIREMENTS [RTCA02] .....	18
FIGURE 2-8. POWER RAMP-UP OF THE RF SIGNAL .....	18
FIGURE 2-9. REQUIRED TRANSMIT SPECTRAL MASK .....	20
FIGURE 2-10. RAISED COSINE IMPULSE RESPONSE IN TIME DOMAIN .....	20
FIGURE 2-11. RAISED COSINE IMPULSE RESPONSE IN FREQUENCY DOMAIN .....	21
FIGURE 2-12. TRANSMIT SPECTRUM COMPLIES WITH .....	21
FIGURE 2-13. HEAVY-TRAFFIC ENVIRONMENT (PLAN VIEW) .....	22
FIGURE 2-14. HEAVY-TRAFFIC ENVIRONMENT (3-D) .....	23
FIGURE 2-15. HEAVY-TRAFFIC ENVIRONMENT (SIDE VIEW) .....	24
FIGURE 2-16. VICTIM AIRCRAFT IN HEAVY-TRAFFIC ENVIRONMENT .....	24
FIGURE 2-17. AIRCRAFT FLYING BELOW 20,000 FEET .....	25
FIGURE 2-18. AIRCRAFT DISTRIBUTION IN HEAVY –TRAFFIC ENVIRONMENT .....	27
FIGURE 3-1. MESSAGE-OVERLAPS EXAMPLE.....	31
FIGURE 3-2. MESSAGE-OVERLAPS CONCEPT USING VISUAL REPRESENTATION .....	32
FIGURE 3-3. SQUARE MATRIX CONVERSION .....	32
FIGURE 3-4. SIMULATION SETUP .....	34
FIGURE 3-5. WORST-CASE SCENARIO FOR CASE I .....	38
FIGURE 3-6. MOST-LIKELY SCENARIO FOR CASE I.....	38
FIGURE 3-7. BEST-CASE OVERLAP STATISTICS .....	39
FIGURE 3-8. AGGREGATE MESSAGE-OVERLAP STATISTICS FOR CASE I.....	40
FIGURE 3-9. RECEIVED POWER HISTOGRAM WHEN VICTIM AIRCRAFT IS AT 10,000 FEET .....	42
FIGURE 3-10. RECEIVED POWER HISTOGRAM WHEN VICTIM AIRCRAFT IS AT 20,000 FEET .....	42
FIGURE 3-11. RECEIVED POWER HISTOGRAM WHEN VICTIM AIRCRAFT IS AT 30,000 FEET .....	42
FIGURE 3-12. RECEIVED POWER HISTOGRAM WHEN VICTIM AIRCRAFT IS AT 40,000 FEET .....	42
FIGURE 3-13. MAXIMUM COMMUNICATIONS RANGE .....	43
FIGURE 3-14. AIRCRAFT CONTAINED WITHIN MAXIMUM COMMUNICATIONS RANGE.....	44
FIGURE 3-15. RECEIVER PERFORMANCE.....	45
FIGURE 3-16. MESSAGE SUCCESS RATE .....	46
FIGURE 3-17. BER PERFORMANCE IN THE PRESENCE OF ONE INTERFERER.....	47
FIGURE 3-18. MSR PERFORMANCE IN THE PRESENCE OF ONE INTERFERER .....	47
FIGURE 3-19. BER PERFORMANCE IN THE PRESENCE OF TWO INTERFERERS (LINEAR SCALE) .....	48
FIGURE 3-20. BER PERFORMANCE IN THE PRESENCE OF .....	48
FIGURE 3-21. BER PERFORMANCE IN THE PRESENCE OF MULTIPLE INTERFERERS.....	49
FIGURE 3-22. MSR PERFORMANCE IN THE PRESENCE OF MULTIPLE INTERFERERS .....	49
FIGURE 3-23. AGGREGATE MESSAGE-OVERLAP STATISTICS FOR CASE II .....	50
FIGURE 3-24. MESSAGE-OVERLAPS RESULTS FOR CASE I AND CASE II .....	51
FIGURE 4-1. LIMITATION OF TODAY’S RADIO RECEIVERS. ....	57
FIGURE 4-2. INTERFERENCE CANCELLATION RADIO RECEIVER ARCHITECTURE. ....	59
FIGURE 4-3. DETECTING THE LARGE SIGNAL IN THE PRESENCE OF .....	62

FIGURE 4-4. DETECTING THE SMALL SIGNAL IN THE.....	64
FIGURE 4-5. TWO CO-CHANNEL SIGNAL OVERLAPS. ....	69
FIGURE 4-6. BER VS SIR PERFORMANCE OF THE TWO B-FSK SIGNALS. ....	70
FIGURE 4-7. PERFORMANCE OF THE SMALL B-FSK SIGNAL. ....	71
FIGURE 4-8. PERFORMANCE OF THE LARGE B-FSK SIGNAL.....	72
FIGURE 4-9. PERFORMANCE OF LARGE AND SMALL FSK SIGNALS AT SIR = 7 DB. ....	73
FIGURE 4-10. THREE CO-CHANNEL SIGNAL OVERLAPS. ....	74
FIGURE 4-11. BER VS SIR PERFORMANCE OF THE THREE B-FSK SIGNALS. ....	75
FIGURE 4-12. PERFORMANCE OF THE LARGE B-FSK SIGNAL.....	76
FIGURE 4-13. PERFORMANCE OF THE MEDIUM B-FSK SIGNAL. ....	77
FIGURE 4-14. PERFORMANCE OF THE SMALL B-FSK SIGNAL. ....	78
FIGURE 4-15. PERFORMANCE OF ALL THREE SIGNALS AT SIR = 7 DB.....	79
FIGURE 4-16. BER VS SIR PERFORMANCE OF THE TWO B-PSK SIGNALS. ....	81
FIGURE 4-17. PERFORMANCE OF THE SMALL B-PSK SIGNAL. ....	82
FIGURE 4-18. PERFORMANCE OF THE LARGE B-PSK SIGNAL.....	83
FIGURE 4-19. PERFORMANCE OF LARGE AND SMALL B-PSK SIGNALS.....	84
FIGURE 4-20. BER VS SIR PERFORMANCE OF THE TWO SIGNALS. ....	85
FIGURE 4-21. PERFORMANCE OF THE LARGE B-PSK SIGNAL.....	86
FIGURE 4-22. PERFORMANCE OF THE MEDIUM B-PSK SIGNAL. ....	87
FIGURE 4-23. PERFORMANCE OF THE SMALL B-PSK SIGNAL. ....	88
FIGURE 4-24. PERFORMANCE OF ALL THREE B-PSK SIGNALS AT SIR = 7 DB.....	89
FIGURE 4-25. PERFORMANCE OF ALL THREE B-PSK SIGNALS AT SIR = 10 DB.....	89
FIGURE 5-1. PARALLEL INTERFERENCE CANCELLATION RECEIVER STRUCTURE .....	94
FIGURE 5-2. PIC STRUCTURE TO DECODE TWO CO-CHANNEL FSK SIGNALS.....	96
FIGURE 5-3. SOME OVERLAPPING CONFIGURATIONS OF TWO SIGNALS .....	96
FIGURE 5-4. BER VS SIR PERFORMANCE OF TWO.....	97
FIGURE 5-5. PERFORMANCE OF THE LARGE B-FSK SIGNAL (PIC).....	98
FIGURE 5-6. PERFORMANCE OF THE SMALL B-FSK SIGNAL (PIC).....	99
FIGURE 5-7. PERFORMANCE OF LARGE AND SMALL SIGNALS AT SIR = 7 DB .....	100
FIGURE 5-8. PERFORMANCE OF LARGE AND SMALL SIGNAL AT SIR = 10 DB.....	100
FIGURE 5-9. PIC STRUCTURE TO DECODE THREE OVERLAPPING FSK SIGNALS .....	101
FIGURE 5-10. SEVERAL OVERLAPPING CONFIGURATIONS .....	102
FIGURE 5-11. BER VS SIR PERFORMANCE OF THE THREE B-FSK SIGNALS. ....	103
FIGURE 5-12. PERFORMANCE OF LARGE B-FSK SIGNAL (PIC).....	104
FIGURE 5-13. PERFORMANCE OF THE MEDIUM B-FSK SIGNAL. ....	105
FIGURE 5-14. PERFORMANCE OF THE SMALL B-FSK SIGNAL .....	106
FIGURE 5-15. PERFORMANCE OF ALL THREE SIGNALS AT SIR = 7dB .....	107
FIGURE 5-16. PERFORMANCE OF ALL THREE SIGNALS AT SIR = 10 DB.....	107
FIGURE 5-17. PERFORMANCE OF ALL THREE SIGNALS AT SIR = 12 DB.....	107
FIGURE 5-18. PERFORMANCE OF ALL THREE SIGNALS AT SIR = 15 DB.....	107
FIGURE 6-1. TYPICAL HETERODYNE RECEIVER WITH MULTI-SIGNAL PROCESSOR .....	109
FIGURE 6-2. MULTI-SIGNAL POSSESSOR CONSISTING SIC DETECTOR.....	110
FIGURE 6-3. SYNCHRONIZATION PROCESS FOR THE AVIONIC SYSTEM .....	111
FIGURE 6-4. SYNCHRONIZATION PERFORMANCE IN AWGN.....	112
FIGURE 6-5. SYNCHRONIZATION PERFORMANCE IN .....	112
FIGURE 6-6. SYNCHRONIZATION PERFORMANCE IN THE PRESENCE OF TWO INTERFERERS.....	114
FIGURE 6-7. PIC AND SIC PERFORMANCE FOR 3 OVERLAPPING CO-CHANNEL SIGNALS .....	115
FIGURE 6-8. COMPARISON BETWEEN SIC (LEFT) AND PIC (RIGHT) FOR LARGE SIGNAL .....	116
FIGURE 6-9. COMPARISON BETWEEN SIC (LEFT) AND PIC (RIGHT) FOR MEDIUM SIGNAL .....	117
FIGURE 6-10. COMPARISON BETWEEN SIC (LEFT) AND PIC (RIGHT) FOR MEDIUM SIGNAL .....	117
FIGURE 7-1. TIERED STATISTICAL ANALYSIS.....	120
FIGURE A-1. DISTRIBUTION OF RESULTS FROM MOE .....	123
FIGURE A-2. ILLUSTRATION OF THE UNBIASED AND CONSISTENT MOE.....	124
FIGURE B-1. HISTOGRAM OF RECEIVED SIGNAL POWER .....	126
FIGURE B-2. HISTOGRAM OF RECEIVED SIGNAL POWER .....	126
FIGURE B-3. ANTENNA PATTERN .....	127

FIGURE B-4. ANTENNA SWITCHING MECHANISM FOR AIRCRAFT.....	128
FIGURE C-1. SIC TO DECODE 4 CO-CHANNEL B-FSK SIGNALS.....	130
FIGURE C-2. SIC TO DECODE 4 COCHANNEL B-PSK SIGNALS .....	131
FIGURE C-3. SIC TO DECODE 4 COCHANNEL B-PSK SIGNALS (FOR TINY SIGNAL) .....	131

# TABLES

TABLE 2-1. AVIONIC SYSTEM PHYSICAL LAYER PARAMETERS.....	19
TABLE 2-2. HEAVY-TRAFFIC ENVIRONMENT DATA .....	28
TABLE 3-1. MESSAGE-OVERLAP COMPUTATION.....	33
TABLE 3-2. SIMULATION INPUT (HEAVY-TRAFFIC AIRCRAFT ENVIRONMENT) .....	35
TABLE 3-3. AIRCRAFT TYPES .....	36
TABLE 3-4. NUMBER OF AIRCRAFT WHICH EFFECTIVELY CONTRIBUTE TO .....	44
TABLE 3-5. REQUIRED SIRs UNDER MULTIPLE INTERFERERS .....	50
TABLE 3-6. CUMULATIVE MESSAGE-OVERLAP ANALYSIS.....	53
TABLE 4-1. SIC RECEIVER CAPABILITY FOR B-FSK AND B-PSK SIGNALS .....	91
TABLE 6-1. SYNCHRONIZATION PERFORMANCE IN THE PRESENCE OF TWO INTERFERERS .....	113
TABLE 6-2. SYNCHRONIZATION PERFORMANCE SUMMARY .....	114

# Chapter 1 : Introduction

## 1.1 Background

Multiple-user co-channel interference or multiple access interference (MAI), which is caused by many signals of the same carrier frequency overlapping one another when users in the system try to access a common communication channel, may significantly limit the capacity of any communication system, regardless of whether the system is wideband (Code Division Multiple Access [CDMA]) or narrowband [Gold71] [Bene73] [McLa75] [Tra199]. The disturbing effects of co-channel interference usually dominate and increase the noise floor, resulting in a reduction of system capacity. There has been considerable research in the area of alleviating MAI for increased wireless system capacity in the past decade. In fact, one of the key research topics in the area of improving the performance of a CDMA system is enhancing its robustness in MAI. For example, it has been shown that MAI could lead to significant performance degradation and capacity reduction, especially when facing the well-known “near-far problem”, which is when orthogonality between all users cannot be retained because higher power users can disrupt reception from lower power users. Another example is an aeronautical mobile communication system of the Federal Aviation Agency (FAA). This system is currently being engineered by the FAA and aviation community for future deployment in the National Airspace System (NAS) to enhance safety for pilots through enhanced situational awareness features offered by the system and to increase service functionality. This communication system uses a random contention channel access protocol that is somewhat similar to Aloha and slotted Aloha protocols, and thus it faces the MAI challenges and it will be studied in this dissertation.

Multi-user co-channel interference (or MAI) (or multiple access interference) poses a great challenge in increasing system capacity and improving system performance. Therefore, successful communication system design, to a great extent, requires the ability to first determine the severity of MAI and then find ways to mitigate it. This is critical, especially for safety-of-life aeronautical communication applications. Today’s communication systems and networks often handle co-channel interference (caused by

signal collisions) by either retransmitting data or allowing the system to tolerate interference up to a permissible level. These approaches waste bandwidth and limit system capacity and throughput [Abra94] [Meda99] [Abra85]. Previous studies on systems such as Aloha and slotted-Aloha have attracted world-wide research interest for many years due to their simplicity and low overhead. Researchers have derived general mathematical expressions to describe the co-channel interference effects based on certain assumptions [Kama88] [Dard00]. However, when it comes to specific systems with specific requirements such as an avionic communication system being studied in this dissertation, solutions based on general expressions or close-form mathematical derivations may no longer be valid representatives of the actual environments. An alternative solution is to use computer simulations, which can be tailored to specific systems to satisfy specific requirements [Tran94] [Woer94] [Jeru84].

This dissertation consists of two parts. The first part provides a complete analysis, using Monte Carlo computer simulations and a visualization method, to estimate the multi-user co-channel interference effects for the aeronautical mobile communication system operating in a high-density traffic environment. The system will be used as an example for interference analysis of a real-world application to illustrate the validity of the visualization method. The second part proposes that interference cancellation techniques, which can be implemented in radio receivers, be used as a potential solution to MAI. Today's avionic radio receivers can only decode signals one at a time on a single channel. This is mainly because these co-channel signals are highly correlated; thus making it difficult to differentiate and separate them. One proposed approach to alleviating MAI is to implement a radio receiver that can extract interference and allow for the successful decoding of multiple signals. This topic falls under multi-user detection (MUD), which was originally pioneered by Verdu [Verd98]. There has been significant research on MUD for CDMA signals, as thoroughly surveyed in section 1.4.2.1. However, MUD for non-spread, non-CDMA, or narrowband type of signals is not well researched, as described in section 1.4.2.2 and section 1.5. Thus, there is opportunity to perform research in this arena, which is one of the two main focuses of this research.

Throughout this dissertation, MAI and co-channel interference will be used interchangeably to refer to non-spread, non-CDMA but not necessarily narrowband signals. The main reason is because the avionic system studied in this dissertation can be thought of as a wideband system since it delivers up to 1 Mbps of data and occupies over 1 MHz of bandwidth. However, the system is neither spread spectrum, nor CDMA. One question might arise as to why non-spread, non-CDMA signal processing holds any value while most of future technological advances tend to lean toward broadband or wideband communication systems (e.g., cdma2000, WCDMA). First of all, narrowband cellular standards (e.g., GSM) are widely deployed and are expected to last beyond the next decade. Second of all, developing countries have been trying to expand their existing cellular networks using second-hand narrowband infrastructure. Third of all, the interference cancellation techniques can be extended and applied to 2G or 3G CDMA signals, or even 4G OFDM signal types on a per-sub-carrier basis. Furthermore, in some communication application, non-spread, non-CDMA signal types (sometimes referred to as narrowband signals) are often preferred due to different needs, often driven by cost, complexity and functionality tradeoffs such as the aeronautical mobile communication system studied in this dissertation. Therefore, the results of this research could have significant value for the systems mentioned above.

## **1.2 Purpose**

The purpose of this dissertation is to investigate the use of a visualization method to quantify and characterize the severity of multi-user co-channel interference effects in an aeronautical mobile environment and evaluate possible solutions to alleviating the interference based on interference cancellation techniques. A visualization method is used to evaluate the co-channel interference characteristics of complex radio frequency signals broadcasted in a heavy-traffic environment, which consists of thousands of aircraft. The interference characterization results for the avionic system provides relevant information, which leads to the development of interference cancellation receivers as possible methods to mitigate the co-channel interference effects, to improve system capacity, and to allow for better use of the scarce spectrum resources.



## 1.3 Motivation

In the area of co-channel interference assessment, the vast majority of research over the years has been performed on channel access protocols such as Aloha, slot-Aloha, TDMA, slotted TDMA, and CDMA [Abra70][ Koba77][ Gitm75][ Meda04]. However, in some communication applications, such as the aeronautical mobile communications being studied in this dissertation for example, it is desired that the protocol be moderately different to address different needs. Previously derived and general mathematical expressions would not accurately model the system. An interference assessment method and tool are needed to correctly evaluate the interference effects.

In the area of multi-user detection there has been significant research over the past decade to propose various interference cancellation techniques for CDMA signals due to the widespread 2<sup>nd</sup> generation (2G) and 3<sup>rd</sup> generation (3G) CDMA standards (e.g., IS-95, cdma2000, and WCDMA). One of the most referenced works in the area of interference cancellation techniques or multi-user detection is Verdu [Verd86] for optimal MUD. However, optimal MUD can be computationally complex, especially when attempting to perform joint detection. The detection algorithm increases exponentially with the number of users. In some applications, where implementation costs and safety-of-life are major concerns, it is more desired to have a suboptimum receiver, which can perform interference cancellation sufficiently well, while keeping costs and complexity low. In addition, interference cancellation for non-spread signals could be of great interest for other communication applications as well as the aviation system studied in this dissertation. As demand for higher capacity in the National Airspace System increases, interference cancellation could be the next research frontier, holding the key to enhancing system capacity and improving system performance. However, there is a lack of research in the area of interference cancellation for non-spread signals; thus providing opportunity for this research.

## 1.4 Previous Work

This section describes previous work that is related to the characterization of co-channel interference in several random access protocols as well as illustrating previously known interference cancellation techniques for mitigating co-channel interference.

### 1.4.1 Multiple access interference analysis

The communications protocol used in the avionic system under study in this research is somewhat similar, however not necessarily the same, as the Aloha or slotted Aloha protocols [Abra70] [Koba77] [Gitm75] [Meda04]. It differs from an Aloha protocol primarily because of the distinct message start opportunities (MSOs), where aircraft are permitted to transmit only at the beginning of each MSO. This system protocol also differs from a slotted Aloha protocol because the message sizes (either short or long) exceed the time slots. Therefore, previous work in the communications and networks literature on Aloha and slotted Aloha are useful, but not always applicable. There does not exist in the literature, to the knowledge of the authors, analysis on any system with the same characteristics as the one described in this dissertation.

### 1.4.2 Multi-User Detection (MUD)

#### 1.4.2.1 MUD FOR CDMA SIGNALS

Code Division Multiple Access (CDMA) technology has gained international acceptance and tremendous momentum over the past decade as it became the North American 2<sup>nd</sup> and 3<sup>rd</sup> generation (2G and 3G) mobile communication standards (e.g., IS-95, cdma2000) and has the potential for becoming the advanced enabling technology for 4<sup>th</sup> generation cellular standard. In fact, European and Asian 3G cellular standards also contain some forms of CDMA. Fourth-generation cellular standards will also be likely to include CDMA as the main platform for separating multiple users in the channel. Due to its popularity, a vast majority of research for communications in the past decade involves studies related to CDMA signals.

Verdu pioneered the development of an optimum detector for asynchronous binary Phase Shift Keying [Verd86]. Since then, many types of multi-user techniques and interference cancellation techniques have been investigated. Several most discussed receiver architectures in the literature are discussed below.

The conventional receiver, as shown in Figure 1-1 represents a bank of matched filters, where each filter is matched to the code sequence of the desired user. The performance then is governed by the knowledge of the desired code sequence and precise synchronization with the arriving signal to minimize MAI. In this case, the matched filter maximizes the SNR at the output of the receiver.

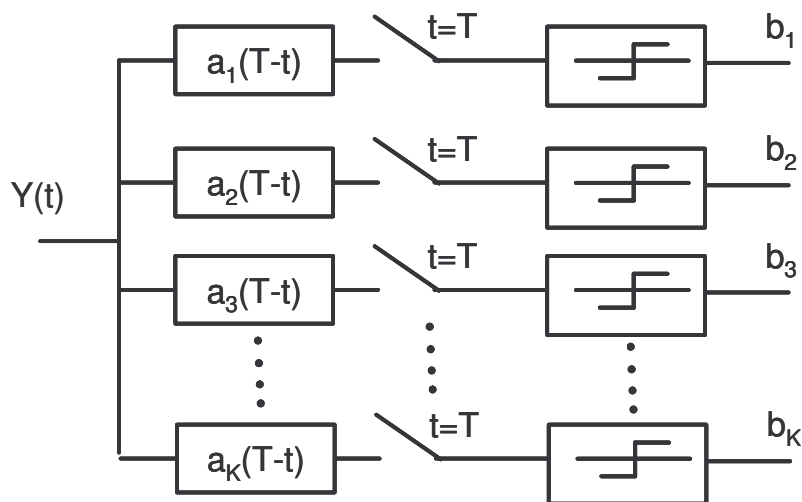


**Figure 1-1. Conventional Receiver**

The optimal receiver, shown in Figure 1-2, is for asynchronous DS-CDMA channels, and was formally introduced and derived by Verdu [Ver86] in AWGN. It is based on a maximum-likelihood sequence estimator [Forn72], which estimates digital signals by means of vector versions of the Viterbi algorithm or the Ungerboeck algorithm [Unger74], as was shown in [Ett76]. This optimal receiver requires knowledge of the code sequences, timing and received amplitudes of all users. The receiver consists of a bank of matched filters similar to those in the conventional receivers, with a Viterbi

algorithm inserted after sampling to compute the most likely path in a trellis diagram with  $2^{K-1}$  states per layer, and time varying state transitions. This optimal receiver is enormously complex but serves as a good point of reference for comparison with future developments of other suboptimal receivers.

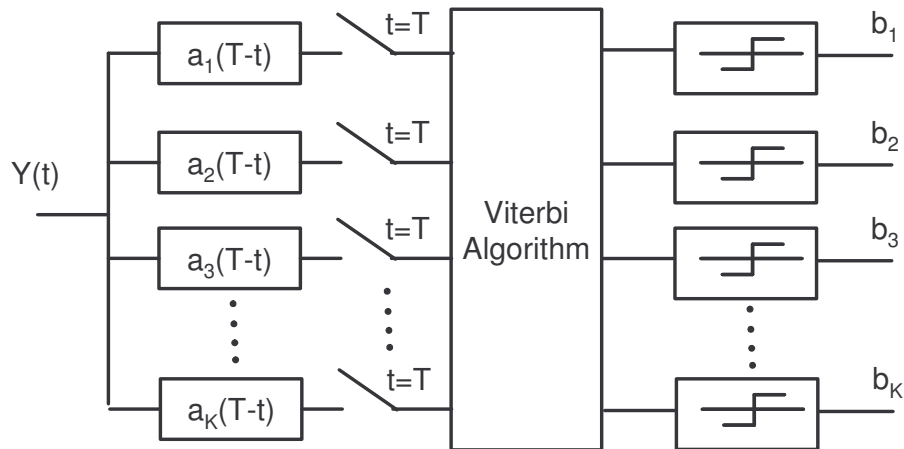


**Figure 1-2. Optimum Receiver**

Another multi-user detector is the decorrelator, as shown in Figure 1-3, initially proposed in [Schn76][Lupa89], attempts to eliminate MAI similar to the way a zero forcing equalizer eliminates Inter Symbol Interference (ISI). A linear transformation  $\mathbf{R}^{-1}$ , where  $\mathbf{R}$  is a matrix representing channel coefficients, is inserted after the sampling stage to try to cancel interference from cross correlations of all users' code sequences. Some advantageous features of the correlation receiver is that it does not require knowledge of the users' received energies and each user can be demodulated independently, and thus performs in a manner similar to matched filter detection [Verd98]

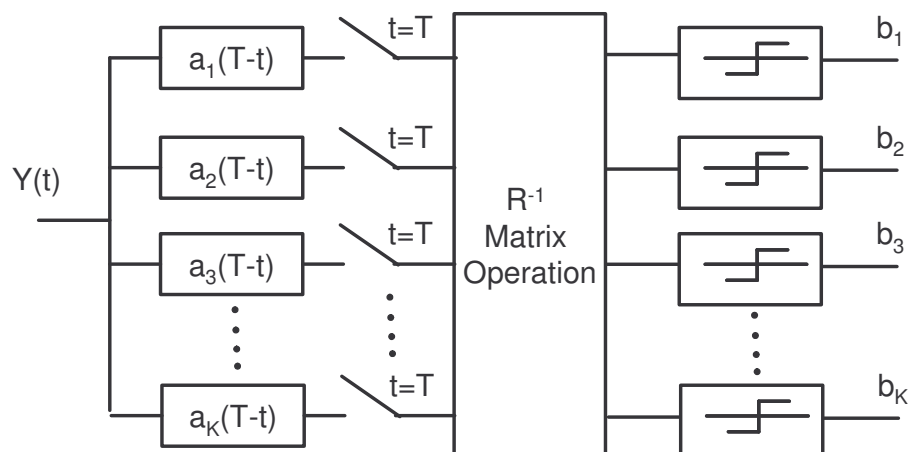


**Figure 1-3. Decorrelator Receiver**

Another receiver, known as Linear Minimum Mean-Square Error Receiver, as shown in Figure 1-4, computes and minimizes the mean-square error between the ideal noiseless MUD waveform and one reconstructed. Adaptive implementation and blind detection are possible and are shown in references [Mill96], [Hayk96] and [Honi5].

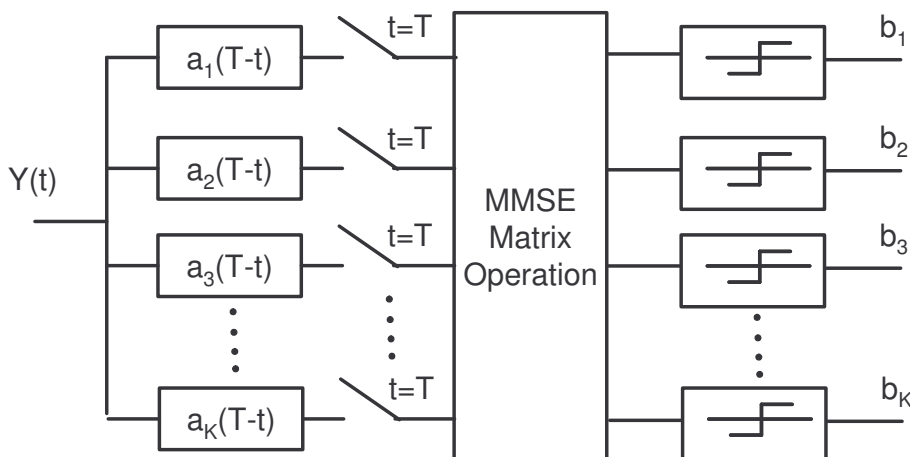


**Figure 1-4. Minimum Mean-Square Error Receiver**

Another MUD technique for receiving CDMA signals that involves interference cancellation, previously investigated by Patel [Pate94], Holtzman [Holt94], and others including authors in references [Pede], [Cho98], [Lai], and [Bueh00], is the successive

interference cancellation receiver (SIC). MAI can be achieved by first sorting signals in the order of decreasing received signal strengths, then interference cancellation can be done by removing the interference caused by signals with higher received power than the desired signal.

Another MUD technique, namely multi-stage parallel interference cancellation (PIC) was initially proposed in [Vara90][Kohn90]. Similar to SIC, where interference is removed from iteratively subtracting the large signals, PIC uses an iterative approach in which estimation, re-modulation, and cancellation of interference from other users, is performed in parallel for each user. Estimates can then be improved by computing the new decisions from the user's "reduced MAI" waveform. Several other improvements have been investigated such as adaptive PIC using partial PIC [Corr99] and the "bit inversion" technique [Huan03]. In partial PIC, partial cancellation of MAI is preferred in practical implementations of PIC to reduce bias in decision statistics, as shown in [Corr97]. The "bit inversion" method is based on the LMS algorithm to correct the bit-decision error in the previous stage before performing parallel interference cancellation. Recently, in [Oon00][Abra], a hybrid scheme to combine SIC and PIC has been proposed as a method to tradeoff between SIC and PIC to improve the long delay as experienced in the implementation of SIC and reduce complexity in PIC implementation.

#### **1.4.2.2 MUD FOR NON-CDMA SIGNALS**

There is a lack of multi-user detection research for narrowband or non-CDMA signals. This is probably due to the migration from narrowband to wideband signals in the past decade in commercial wireless communications, in which any type of wideband system includes some form of CDMA signals. Interference separation for non-CDMA signals can be difficult because the co-channel signals are highly correlated and therefore are difficult to distinguish and separate. Furthermore, code dimension is not available to help differentiate between users. To the best knowledge of the author, Janssen seems to have recently pioneered that research effort from his dual-receiver mechanism [Jans02].

Arslan also performed some study on separating co-channel signals in FDMA and TDMA signals [Arsl01].

## **1.5 Parallel Work in the Field**

To the best knowledge of the author, Janssen [Jans02] [More99] and Arslan [Arsl01] seem to be the only ones conducting similar research in the area of interference for non-spread signals. Recently, Janssen started his research effort from his dual-receiver mechanism. Arslan also performed some study on separating co-channel signals in FDMA and TDMA signals [Arsl01]. The lack of research provides opportunities to conduct research in this area for non-CDMA signals. The results would be useful for the FAA and aviation community to improve the performance of their avionic system, or possibly be applied to orthogonal frequency division multiple access (OFDM) and ultra wideband (UWB) signals since these waveforms do not contain CDMA components in them.

## **1.6 Contribution**

This research contributes to the advancement of the state of the art in communications as follows. First, the research uses a simple visualization method to quantify and characterize the multi-user co-channel interference in a complex and heavy-traffic aeronautical mobile communications. Although this method is demonstrated for use in aeronautical mobile environment, it can be used virtually in any wired or wireless RF environments which result in signal-overlaps. This work was presented at the IEEE Digital Avionic System Conference (DASC) in 2004 and was awarded “best-of-track” paper. Second, this research proposes the use of simple multi-user detection techniques, namely sequential and parallel interference cancellation, implemented for the entire receiver chain using BPSK and BFSK modulations/demodulations, to be used in aeronautical mobile communications to substantially improve performance and increase system capacity. These techniques are simpler to implement compared to other MUD techniques currently in research. This solution offers great benefits and costs less. These two important features would be highly desirable, especially in the aeronautical

environment in which airline industries are experiencing tremendous financial distress. The contribution details are further elaborated in Chapter 7.

## **1.7 Organization of Dissertation**

This dissertation is organized as follows.

This chapter provides an introduction of the research, and the reasons and motivation for performing it. In addition, this chapter provides a brief description of literature research on the two main topics, namely co-channel interference modeling, simulation and analysis, and multi-user detection for both wideband CDMA-type signals and non-CDMA type of signals (could be wideband or narrowband, as long as the transmission and reception of signals do not involve spreading codes [or signature codes]). This chapter also highlights the contribution of this research to the advance the state of the art.

Chapter 2 provides a complete description of a practical avionic communication system that is being considered for future FAA National Airspace Operations. Chapter 2 also provides a detailed description of the worst-case high-density traffic environment in which this avionic system is required to operate beyond the year 2020. The avionic system and the traffic environment form the basis of the rest of the research, which focuses on interference analysis and multi-user detection.

Chapter 3 proposes a graphical approach, effective for quantifying and analyzing the effects of co-channel interference when an aircraft equipped with this avionic communication system acts as a victim receiver, being bombarded with thousands of RF transmissions from thousands of other aircraft in the high-density traffic environment.

Chapter 4 proposes an approach to solving the interference effects as described in Chapter 3 by using a Sequential (Successive) Interference Cancellation (SIC). A SIC receiver structure is shown, followed by complete analytical and simulated performance results.



Chapter 5 proposes another approach to solving the interference effects by utilizing a Parallel Interference Cancellation (PIC) technique. A receiver structure implemented using PIC is shown, followed by various performance results.

Chapter 6 provides a practical implementation of SIC and PIC that we propose to show how they can be inserted into a typical communications receiver architecture. This chapter also provides a performance comparison between SIC and PIC.

Finally, Chapter 7 summarizes the entire research, emphasizes key research findings and provides direction for future research.

# **Chapter 2 : Aeronautical Mobile Communication System Operating in a Heavy-Traffic Environment**

This chapter provides descriptions of the aeronautical mobile communication system and the heavy-traffic environment in which it is envisioned to operate. This communication system consists of ground radios and avionic radios. However, this dissertation studies the air-to-air transmissions which involve only avionic radios. The FAA plans to deploy this system in the National Airspace System in the near future in order to enhance safety and efficiency in airspace operations and to allow for better pilots' situational awareness. This system will allow pilots to conduct safe flight operations without having to repeatedly look out the cockpit windows to monitor nearby aircraft. That could become dangerous especially in inclement or foggy weather conditions. Using this system, pilots will have access to information about other aircraft displayed in text or graphical images, as shown in Figure 2-1. It is envisioned that all aircraft equipped with this multi-purpose aeronautical data-link avionic system will continuously broadcast information regarding their position, velocity, and other information. This system will also enable in the future the transmission of flight information, traffic information, weather data, advisories, and ranging and positioning information. The avionic radio and some of its functionalities are shown in Figure 2-2 and 2-3.

## **2.1 Overview**

The avionic system contains many parameters, encompassing all layers of the open standards interconnect (OSI) communications stack. However, this chapter selects the system parameters, mostly in the physical and data-link layers, that are relevant to the interference analysis. These parameters, such as the type of modulation, coding, message-lengths, and channel access protocols, have been scrutinized and down-selected from research and development efforts by government, industry and academic

organizations. In fact, these system parameters have been adopted as minimum operational performance standards [RTCA02]. Further detailed descriptions and technical papers developed leading to the derivation of these system parameters can be found in reference [MOPS02].



**Figure 2-1. Aircraft position, velocity, weather, traffic, advisory information display in the cockpit using the avionic system [Mood03]**



**Figure 2-2. The Avionic Radio and Display Panel [UPS03]**

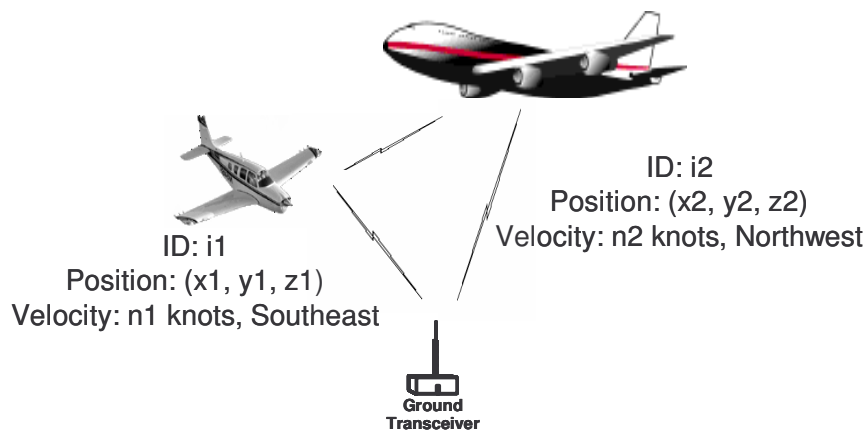


Figure 2-3. Various types of information display using the avionic system [UPS03]

## 2.2 Avionic Communication System Description

The avionic communication system is a wideband multi-purpose data link intended to operate globally on a single channel, currently designated to operate at 978 MHz, with a channel signaling rate of about 1 Mbps using a binary Frequency Shift Keying modulation and demodulation scheme with raised-cosine filter [Mood03][Dieu01]. This system provides the data-link capabilities for both pilots and air traffic controllers to access accurate data about each aircraft's location and velocity, as shown in Figures 2-3 and 2-4 and in references [Zeit02] [CAPS00]. The location and velocity is broken down into horizontal position and velocity and vertical position and velocity. The transmissions are governed by a random channel contention access technique. This technique, which is

somewhat similar to slotted Aloha as shown in references [RTCA02], [MOPS02], and [Rom90], allows each aircraft to broadcast surveillance information once per second (1 frame). As shown in Figure 2, there are 4,000 unique MSOs, for either the aircraft or a ground station to select in a pseudo-random manner. Therefore MSOs are equally spaced at 250 microseconds ( $\mu s$ ). The total 4,000 available MSOs are used in the following way: 3,200 available MSOs are reserved for air-to-air broadcast services for which each aircraft radio selects an MSO from the 3,200 in which to transmit; 48 MSOs are reserved for guard time; and, the remaining 752 MSOs are used for ground-to-air transmissions [MOPS02] [RTCA02].



**Figure 2-4. The Avionic System Operational Concept**

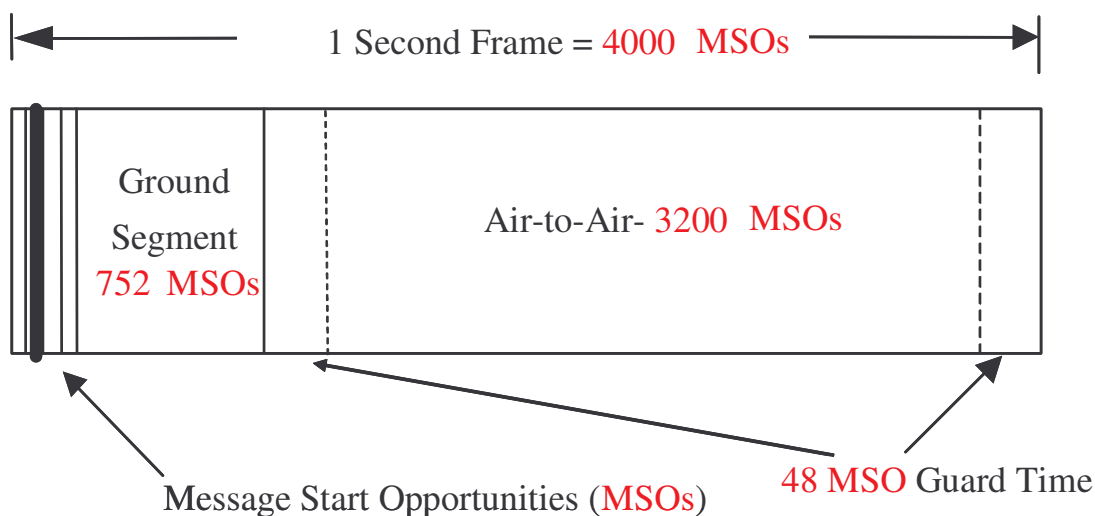


**Figure 2-5. Message Frame**

Airborne transmissions are in bursts of either  $265 \mu s$  (short message format) or  $403 \mu s$  (long message format). An RF signal representing a short message is captured from the avionic radio prototype and is shown in Figure 2-6. The signal's transient ramp-up and ramp-down is governed by criteria shown in Figure 2-7. A sample ramp-up time is shown in Figure 2-8. The ramping time allows an RF signal to build up enough energy for the signal demodulation process and to begin to trigger the signal de-correlation which consists of the first 36 symbols after 8 symbols of ramp time. Both the short and the long message extend over an MSO length. The excess time (i.e., the amount of time beyond  $250 \mu s$ ) is  $15 \mu s$  for short and  $153 \mu s$  for long messages. These excess times are one of several potential contributors to co-channel interference at the victim receiving aircraft. Other potential contributors are the random access protocol, the co-channel effect, and various propagation delays of each aircraft transmission. This co-channel interference issue is referred to as "message-overlap" in this paper because each transmission represents an entire message.

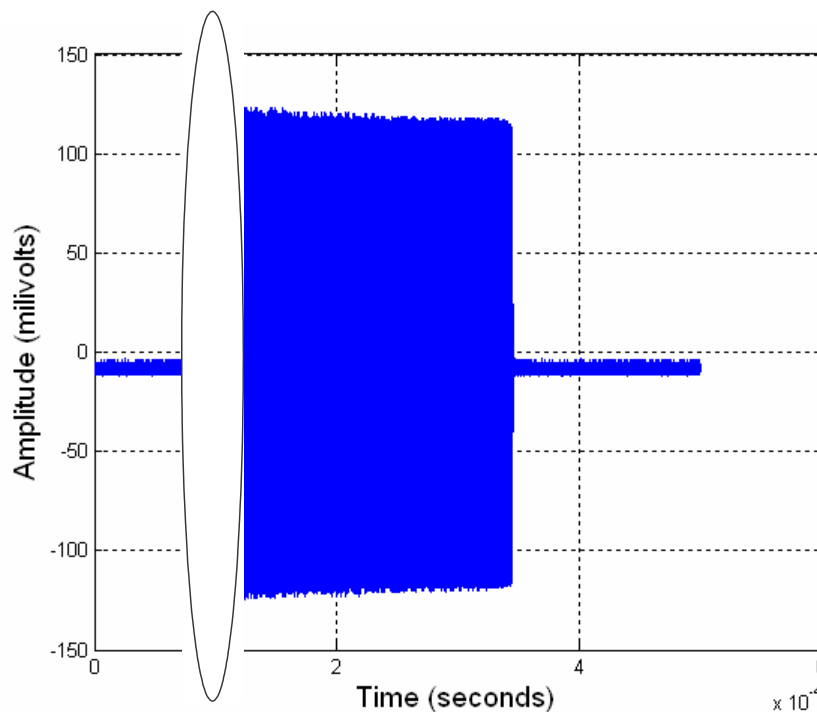


**Figure 2-6. Measured RF Signal of the Avionic Communication System**

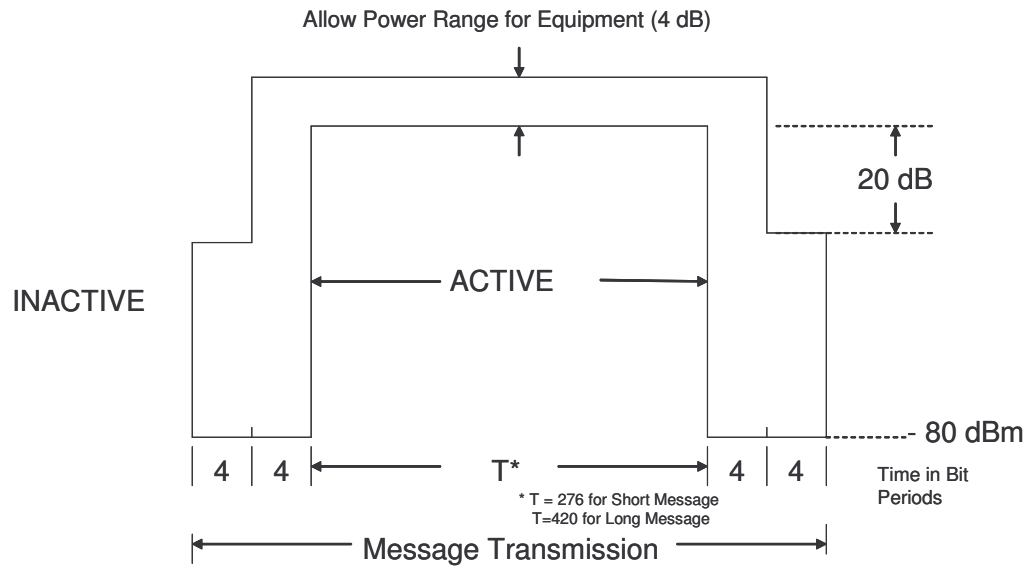


Figure 2-7. RF Signal Requirements [RTCA02]

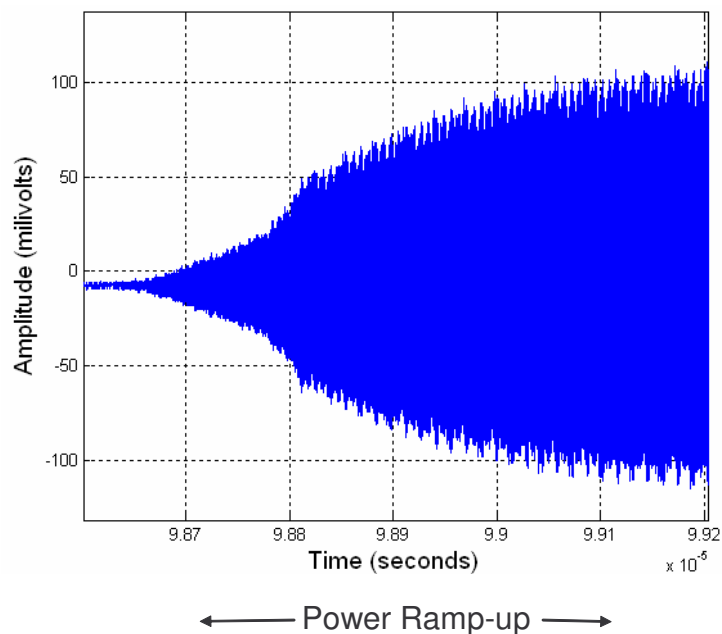


Figure 2-8. Power Ramp-up of the RF Signal

The avionic system parameters used for the receiver model are summarized in Table 2-1. These parameters have been developed through an RTCA standards committee and are shown in reference [RTCA02]. As shown in Table 2-1, the avionic system operates at 978 MHz with nominal signaling rate  $R_b=1.041667$  Mbps, thus

making each bit period 0.96 micro-second. Data is modulated using binary Frequency Shift Keying (FSK) with modulation index  $h=0.6$ , which implies that the frequency separation between binary 1 and binary 0 is  $\Delta f=h \cdot R_b$ , or  $\pm 312.5$  kHz. The frequency deviation will apply at the optimum sampling points for the bit interval. A  $\pm 3$  period raised-cosine pulse-shaping filter with roll-off rate  $r=0.5$  is required to meet the FCC spectral containment requirement. A 48-bit Reed-Solomon code is applied to the raw data to enhance message protection against noise.

**Table 2-1. Avionic System Physical Layer Parameters**

<b>System Parameters</b>	<b>Avionic System Values</b>
<b>Frequency Band</b>	<b>978 MHz</b>
<b>Bit Rate</b>	<b>1 Mbps</b>
<b>Modulation</b>	<b>Binary FSK, roll-off rate =0.5    <math>\pm 312</math> KHz</b>
<b>Parity</b>	<b>Reed-Solomon FEC</b>
<b>Receiver Minimum Threshold Level</b>	<b>-93dBm</b>
<b>Channel</b>	<b>1 channel</b>
<b>Transmission</b>	<b>1 burst per second</b>

The avionic transmit spectrum is required to be contained within the spectral mask shown in Figure 2.2 to minimize out-of-band interference.



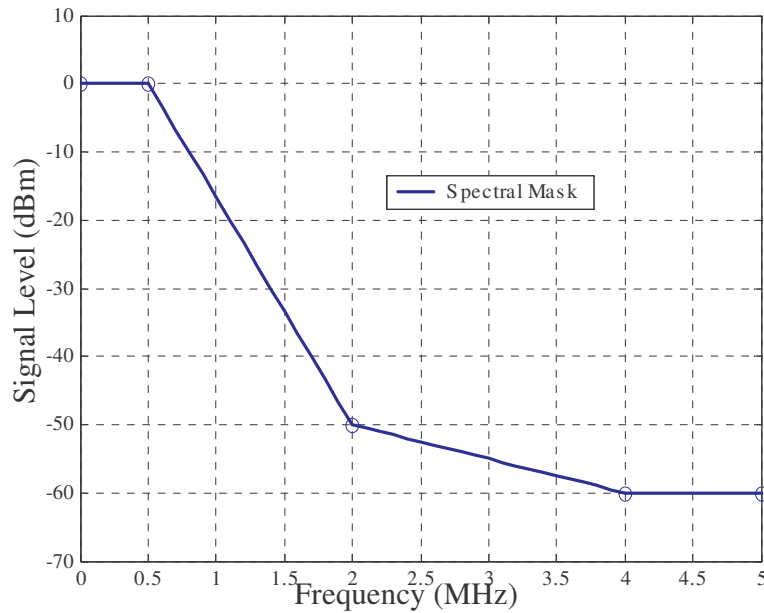


**Figure 2-9. Required transmit spectral mask**

A  $\pm 3$  symbol period Finite Impulse Response (FIR) raised-cosine pulse shaping filter, truncated by a rectangular window, with roll-off factor of 0.5 was used to contain the signal with the required spectral mask. The resulting impulse response in the time domain is shown in Figure 2-10 and the corresponding impulse response in the frequency domain is shown in Figure 2-11.

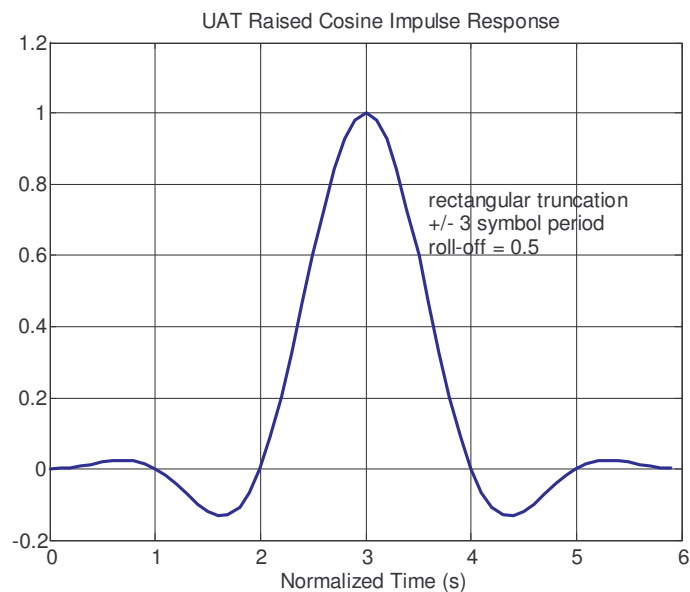


**Figure 2-10. Raised cosine impulse response in time domain**

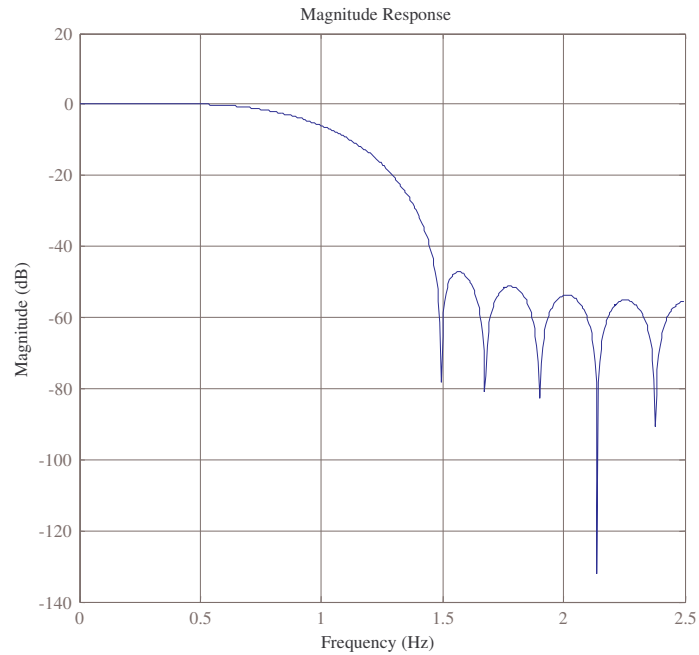


**Figure 2-11. Raised cosine impulse response in frequency domain**

As simulated transmit spectrum of the avionic system is shown in Figure 2-12 using the parameters in Table 2-1 and a baseband sampling rate of  $6 \times R_b$ . It can be seen that the spectrum meets FCC requirements and is well contained within the spectral mask.

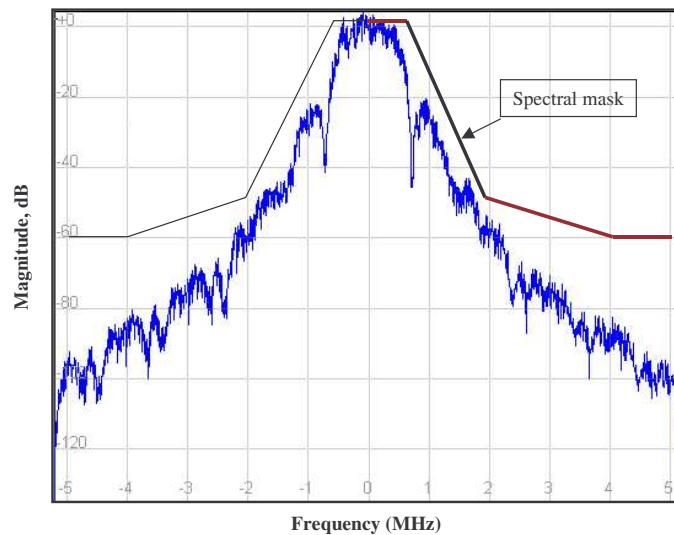


**Figure 2-12. Transmit spectrum complies with spectral mask requirements**

## 2.3 Heavy-traffic aeronautical environment description

The aviation communication system described above is expected to operate in a heavy-traffic environment in the future. A worst-case future traffic environment model was created by John Hopkins University- Applied Physics Lab based on historical traffic data and future aircraft growth projections in the Los Angeles region [MOPS02] [Bach01]. This traffic data was adopted for analysis by the RTCA standards committee [RTCA02]. This environment, which extends to a maximum radius of 400 nautical miles (NM) from the Los Angeles Airport (LAX), contains approximately three thousand aircraft as shown in Figure 2-13 [Mont03]. Specifically, in this environment about 44% of the aircraft are in the core, which is a circular region of radius 225 NM with LAX at its center, about 48% are in the annular region between 225-400 NM from LAX and about 8% are on the ground. The data contains information for each aircraft such as aircraft identification number (ID), position, and velocity. Vertical velocity is not considered since it would have negligible impact on the results.

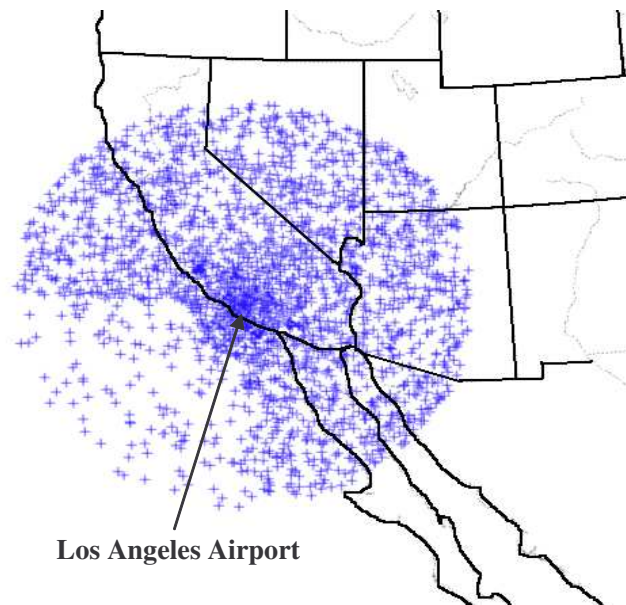


**Figure 2-13. Heavy-Traffic Environment (Plan View)**

The distribution includes aircraft on the surface at airports and all aircraft up to flight level of 40,000 feet, as shown in Figure 2-14 and 2-15. If an aircraft is to be

selected for interference analysis, one could select aircraft position anywhere in the environment. However, one good choice would be right above LAX because at this aircraft position the surrounding environment is denser than other areas, therefore allowing more conservative analysis. Figure 2-16 illustrates a victim aircraft positioned above LAX and receiving signals transmitted from other nearby aircraft.

Note that the units used in this dissertation are feet for altitude, nautical miles (NM) for range, and knots for speed.

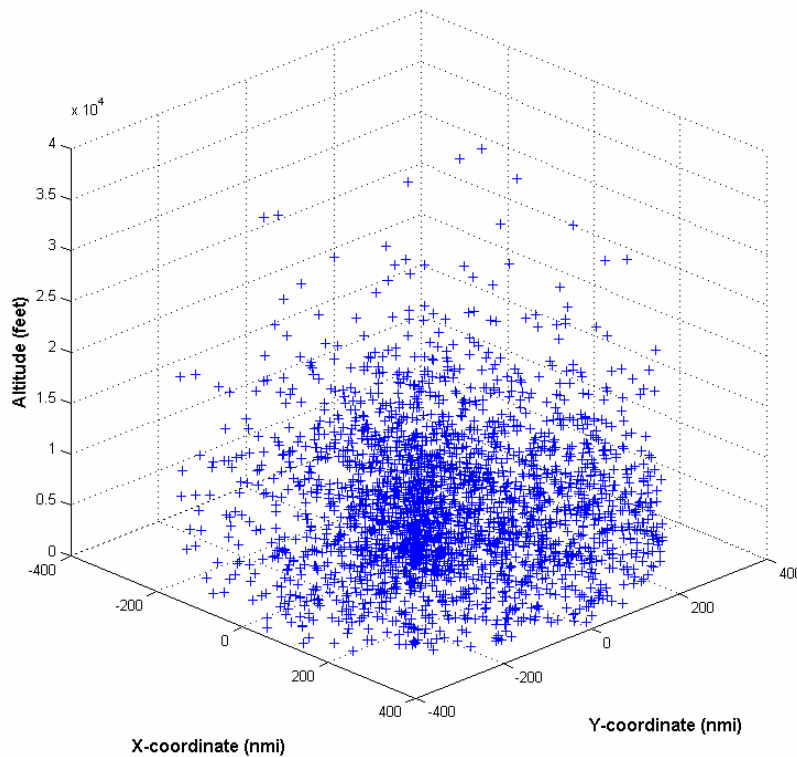


**Figure 2-14. Heavy-Traffic Environment (3-D)**

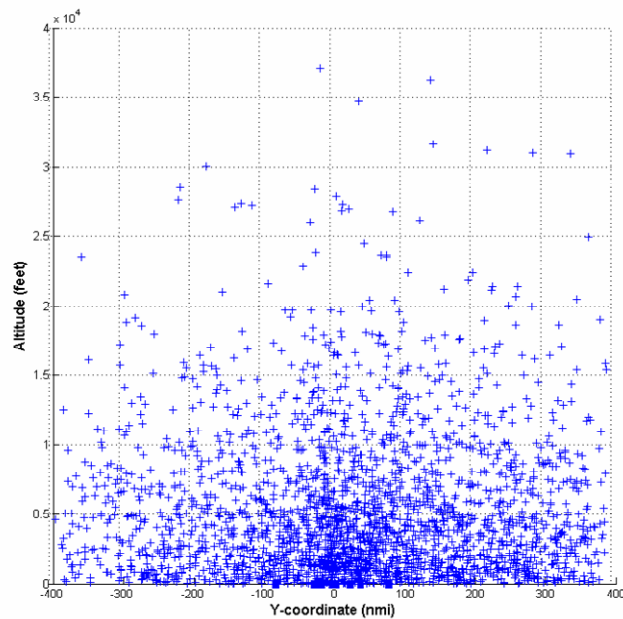


Figure 2-15. Heavy-Traffic Environment (Side View)

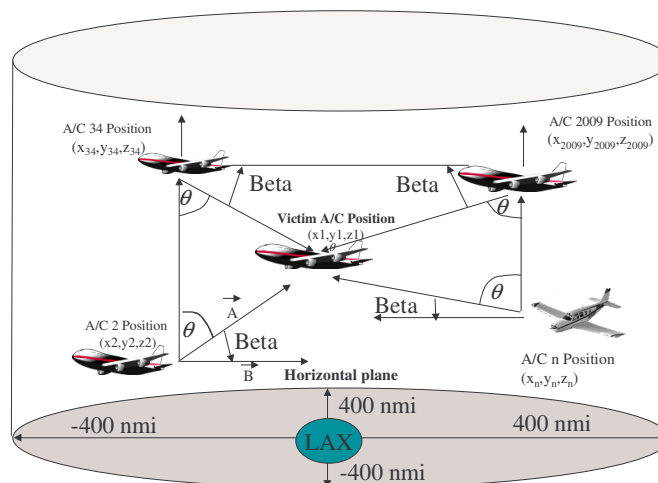
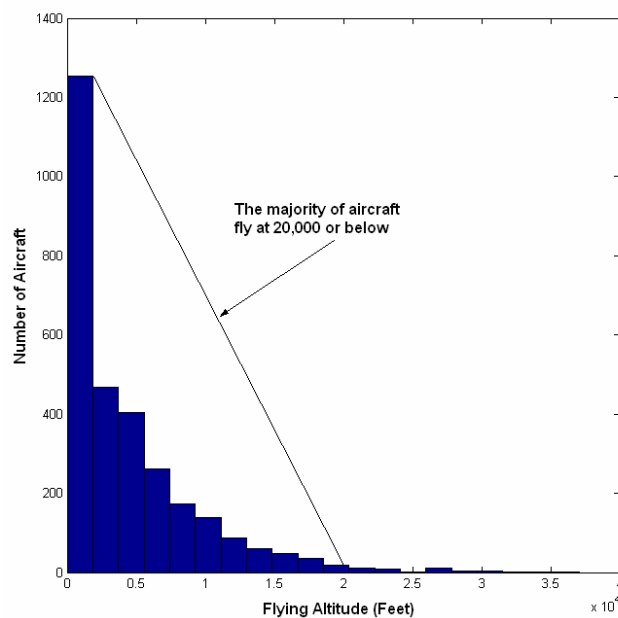


Figure 2-16. Victim aircraft in heavy-traffic environment

Several assumptions were used to create the traffic data. Further details can be found in Appendix K of the standards document [MOPS02].

- o Assumptions for density of airborne aircraft:

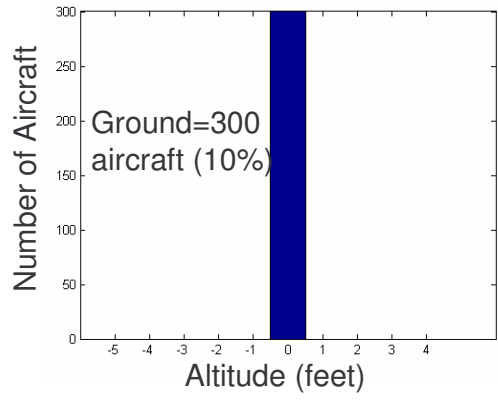
- Constant range from center of the area (Los Angeles Airport) out to 225 nautical miles (5.25 aircraft/NM)
- Constant in area from 225 NM to 400 NM (0.00375 aircraft/NM<sup>2</sup>)
- Fixed number of aircraft on the ground (within a circle of radius 5 NM at each airport), divided among Los Angeles, San Diego, Long Beach, and five other smaller airports, totalling 225 aircraft. Half of these aircraft are assumed moving at 5 knots, while the other half were stationary.
- The altitude distribution of airborne aircraft is assumed to be exponential, with mean altitude around 5,500 feet. Therefore, most aircraft fly below 20,000 feet as shown in Figure 2-17.



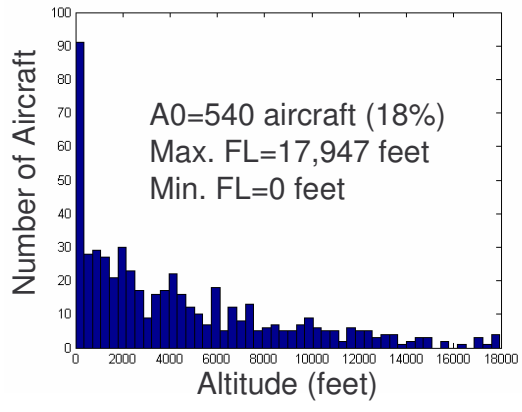
**Figure 2-17. Aircraft flying below 20,000 feet**

- Each aircraft is assigned a velocity, depending on its flying altitude. Aircraft flying below 25,000 feet have velocities that are uniformly distributed over a band, that depends on altitude, where each aircraft's velocity is within 30 percent of some nominal velocity. These nominal velocities are shown below. For example, an aircraft flying between 3,000 and 10,000 feet would have a velocity within 30 percent of 200 knots.

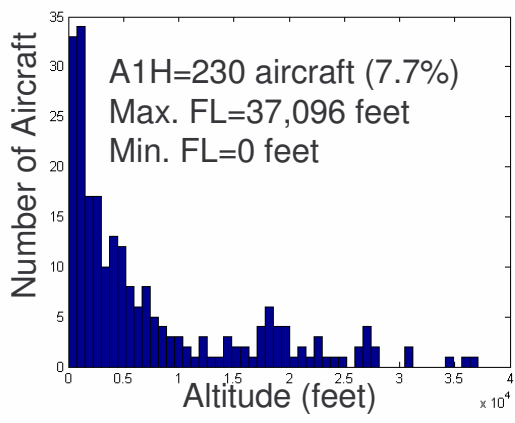
- 0-30,000 feet altitude      130 knots
  - 3,000-10,000 feet          200 knots
  - 10,000-25,000 feet        300 knots
  - 25,000 feet – up            450 knots
- All aircraft are assumed to be moving in random directions
  - Different airborne classes (or types) equipped with the avionic equipment are expected to fly at different designated altitudes. These aircraft classes include A0, A1L (low), A1H (high), A2, A3 and those on the ground. The distributions of these aircraft are shown below.



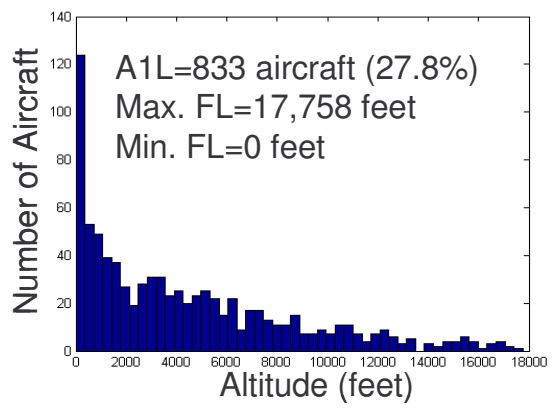
(a)



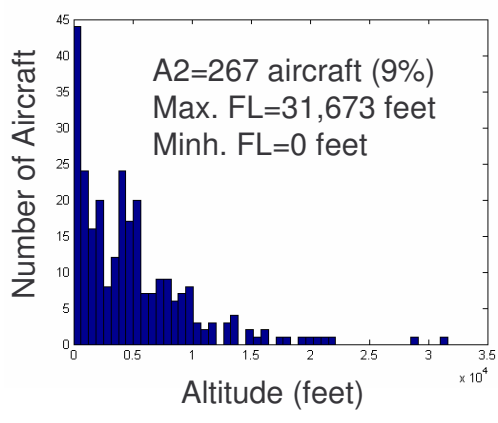
(b)



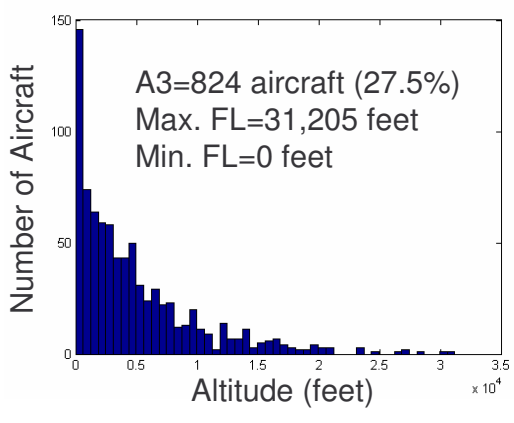
(c)



(d)



(e)



(f)

**Figure 2-18. Aircraft Distribution in heavy –traffic environment depending on aircraft types**



After taking all the previous assumptions into account, the traffic data is generated and is shown below in Table 2-2. Aircraft ID shows identification numbers of the 2,994 aircraft in the environment. X and Y coordinates (in NM) and altitude (in feet) show the position of the aircraft using Cartesian coordinates with respect to LAX. Position can be converted to represent latitude, longitude and altitude to represent real positions.

This set of data and the avionic system parameters shown in the previous section will be used in Chapter 3 to quantify the co-channel interference effects impinging on the avionic system by operating in the heavy-traffic environment.

**Table 2-2. Heavy-traffic environment data**

Aircraft ID	X-Coordinate (nmi)	Y-Coordinate (nmi)	Altitude (feet)	Velocity-X direction (knots)	Velocity- Y direction (knots)	Transmit Power (dBm)	Message Length (seconds)
1	202.662	73.1711	4671.83	208.695	1.80215	54	4.03E-04
2	48.6307	60.541	9107.32	-86.8018	-222.029	54	4.03E-04
3	72.3484	-57.5201	3416.67	-11.6691	236.908	54	4.03E-04
4	-169.316	147.022	9553.72	-97.5004	167.734	42.5	2.56E-04
5	87.0183	-68.3116	4769.96	-194.264	-153.519	54	4.03E-04
6	62.4933	-36.8638	1730.85	-11.8113	-101.15	54	4.03E-04
7	91.2437	-161.707	783.043	94.5167	-94.7886	42.5	2.56E-04
8	56.4462	216.787	8128.29	-202.395	131.058	42.5	2.56E-04
9	109.669	177.395	682.99	102.096	-87.7992	42.5	2.56E-04
10	44.5925	-151.794	2936.82	-0.454252	148.359	42.5	2.56E-04
11	-7.55854	-8.86014	8705.3	24.5624	-164.743	42.5	2.56E-04
12	-16.7701	-87.209	5033.91	-211.742	114.73	54	4.03E-04
13	-60.6408	135.092	6623.54	-67.5871	-208.774	54	4.03E-04
14	101.212	34.3136	1017	71.5541	-125.431	54	4.03E-04
15	90.4922	82.7782	6616.17	-0.235555	181.72	54	4.03E-04
16	-64.2316	75.9552	17263.2	262.12	-38.1454	54	4.03E-04
17	66.5074	36.5614	774.938	130.66	-31.8549	42.5	2.56E-04
18	100.577	-86.9085	10111.9	109.825	340.659	42.5	2.56E-04
19	-23.8546	-22.6085	348.494	-85.6047	-44.9444	42.5	2.56E-04
⋮	⋮	⋮	⋮	⋮	⋮	⋮	⋮
2994	Approximately 3,000 aircraft						

## 2.4 Summary

This chapter describes the avionic system and the heavy-traffic environment in which it is envisioned to operate until the year 2020. The avionic system will provide

aeronautical data-link capabilities such as aircraft position and velocity, traffic, weather, and advisory information. The information will help enhance pilots' situational awareness by giving pilots access to information about other aircraft in the environment, advisory data, and flight routes. This avionic system uses binary FSK modulation/demodulation with a channel rate of about 1 Mbps. Each aircraft equipped with this system will access the RF channel by a random contention access protocol somewhat similar to slotted-Aloha, except that the message lengths are longer than slot lengths.

This chapter also describes the worst-case traffic scenario around Los Angeles airport. The environmental model has been adopted by the standards development committee in order to form the common baseline for environmental modeling and simulation. The environment contains three thousand aircraft, from ground to flight level 40,000 feet. The environment data consists of all possible types of commercial aircraft, their locations, velocity vectors, as well as transmit power and message lengths that these aircraft are allowed to transmit.

It is important to understand the avionic system and the heavy-traffic environment it is expected to operate within. This chapter sets the stage for detailed analysis on characterizing, in Chapter 3, the multi-user co-channel interference effects of the system caused by random transmissions of thousands of aircraft in this heavy-traffic environment; and on developing methods to mitigate the interference so that system performance, capacity and throughput can be improved, as will be shown in Chapters 4 and 5.

## Chapter 3 : Characterization of Multiple Access Interference in the Heavy-Traffic Environment

Multiple access co-channel interference is caused by the overlaps (collisions) of RF signals that operate at the same carrier frequency. Signal overlaps occur when many users try to access a common communication channel and they happen to “step” on one another. Co-channel interference is experienced in almost all communication systems, such as the ones that exhibit Aloha, slotted Aloha, slotted TDMA, carrier sense multiple access (CSMA) [Gold71][Bene73][McLa75][Tral99]. The disturbing effects of co-channel interference usually dominate and increase the noise floor, resulting in a reduction of system capacity. Therefore, successful communication system design, to a great extent, requires the ability to understand and quantify the effects of co-channel interference, especially in safety-of-life aeronautical applications.

Today, many Aloha and Aloha-like systems operate based on their ability to tolerate co-channel interference, but at a cost of capacity reduction [Abra94][Meda99][Abra85]. Previous studies on Aloha and slotted Aloha protocols have attracted world-wide research interest for many years due to their simplicity and low overhead. Researchers have derived general mathematical expressions to describe the co-channel interference effects based on certain assumptions [Kama88][Dard00]. However, when it comes to specific systems with specific requirements such as an avionic communication system being studied in this dissertation, solutions based on general expressions or close-form mathematical derivations may no longer be valid representatives of the actual environments [Mood02][Dieu01]. An alternative solution is to use computer simulations, which can be tailored to specific systems to satisfy specific requirements [Trant94][Woer94][Jeru84].

This chapter provides a complete analysis, using Monte Carlo computer simulations and a visualization method, to quantify and estimate the co-channel interference effects impinging upon a victim aircraft receiver operating in the heavy-traffic environment for an aviation system whose random contention channel access protocol is somewhat similar to Aloha and slotted Aloha protocols.

### 3.1 Method for evaluating multiple access interference

An algorithm called Message-Overlap Estimator is developed for the computer simulation engine, which computes the message-overlap statistics for the entire population of 2,994 aircraft in the high-density traffic environment [MOPS02] [Bach2001] [RTCA02]. Note that the terms message-overlap and signal-overlap will be used interchangeably throughout this dissertation. The proof of concept for the MOE algorithm is illustrated below.

Assume a traffic environment that only contains nine aircraft: eight aircraft equipped with the avionic system would be transmitting eight messages per second and one “victim” aircraft would be receiving. These messages are transmitted according to the random access protocol described in chapter 2. Figure 3-1 illustrates the positions in time of the messages (from the eight aircraft) that arrive at the 9th aircraft.

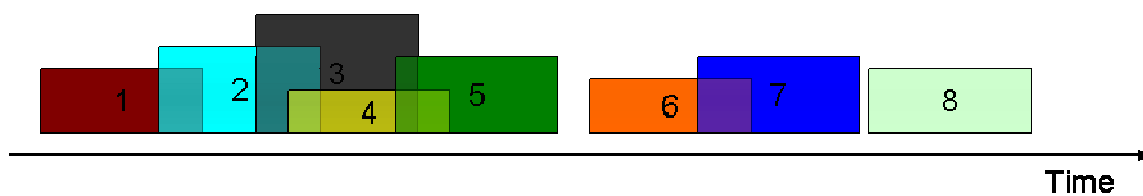


**Figure 3-1. Message-Overlaps Example**

A graph, based on Figure 3-1, can be used as a visual aid to help visualize the message-overlaps for the MOE algorithm and is shown in Figure 3-2 [Merr01]. The nodes or vertices of the graph are the messages from the individual aircraft, and the edges or arcs indicate message overlaps. Thus, two messages overlap if their representative vertices are connected by an arc. This graph defines all the possible overlaps of the

messages transmitted from eight aircraft. For example, message number two overlaps with messages number one, three, and four, leading to three arcs connected to message number two. Message number eight does not overlap with any other messages so there is no connection to it.

The concept shown in Figure 3-2 can be converted to an eight-by-eight matrix, in which ones represent the overlaps, and zeros represent no overlaps, as illustrated in Figure 3-3. This matrix is referred to as the adjacency matrix. The sum of each row  $i$  represents the number of overlaps for message  $i$  (e.g., message number five is overlapped by two messages -- numbers three and four).

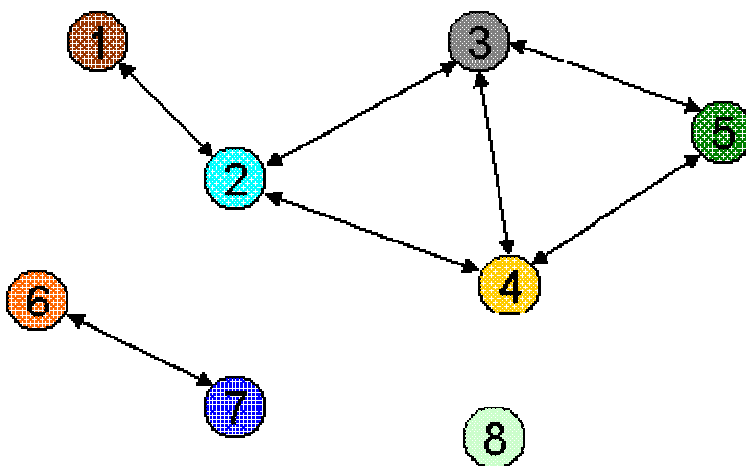


Figure 3-2. Message-Overlaps Concept Using Visual Representation

		Message Number								
		1	2	3	4	5	6	7	8	# overlaps
Message Number	1	0	1	0	0	0	0	0	0	= 1
	2	1	0	1	1	0	0	0	0	= 3
	3	0	1	0	1	1	0	0	0	= 3
	4	0	1	1	0	1	0	0	0	= 3
	5	0	0	1	1	0	0	0	0	= 2
	6	0	0	0	0	0	0	1	0	= 1
	7	0	0	0	0	0	1	0	0	= 1
	8	0	0	0	0	0	0	0	0	= 0

Figure 3-3. Square Matrix Conversion

The final step is to generate a table of message-overlap statistics, shown in Table 3-1, to compute the number of times (frequency of occurrence) the overlaps occur (zero to six overlaps in this case).

**Table 3-1. Message-Overlap Computation**

Number of Overlaps	Frequency of Occurrences
0	1
1	3
2	1
3	3
4	0
5	0
6	0

This concept can now be extended to handle the complex interactions of thousands of radio frequency signals in the high-density traffic environment to compute the message-overlap statistics. In this paper, all simulations are set up to generate approximately seventeen minutes of real-time data, in which one second of data represents an adjacency matrix of 2,994 x 2,994 elements. Thus, the message overlap computation involves a total of one thousand 2,994 x 2,994 matrix elements. Seventeen minutes (or one thousand simulation trials) of real-time data is chosen so that highly accurate results can be achieved, as described in the Appendix A.

## 3.2 Simulation

A simulation model is developed to analyze the message-overlap statistics (at the front-end of a receiver). Figure 3-4 shows a block diagram of the simulation. This model consists of simulation input, simulation engine, and simulation output. The simulation engine is coded using Matlab.

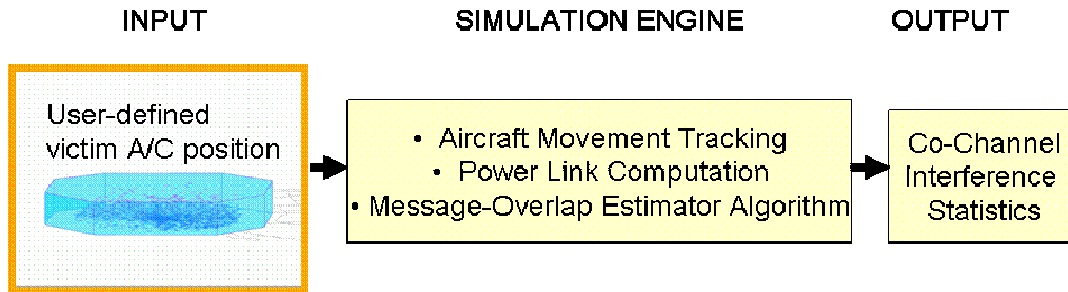


**Figure 3-4. Simulation Setup**

### 3.2.1 Assumptions

The following assumptions are used in the simulation:

- The traffic environment is dynamic (aircraft are flying) and the environment contains 2,994 aircraft.
- A receiving aircraft is assumed to be at 40,000 feet above LAX airport to represent the worst case because this aircraft would have a higher chance (less limited by the radio horizon) of receiving more messages from other aircraft in the environment.
- This study focuses on the air-to-air communication link (air-to-ground and ground-to-air can be evaluated in the same manner).
- Forward error coding and synchronization are not accounted for in this study.

### 3.2.2 Data input

The input provides the traffic data in the environment for the simulation. A sample of this data is shown in Table 3-2. This set of data describes the environment by providing information for each aircraft including aircraft ID, position, velocity vector (speed and direction), aircraft types (which determine the permitted transmit powers and flying altitudes), and the message format (either short or long) that an aircraft is transmitting. A description of aircraft types are provided in Table 3-3 to illustrate the mixed equipage of aircraft in the environment, in which aircraft are expected to fly at certain altitudes and transmit at certain powers depending on their types. This data setup

will be used to analyze the most-likely scenario, which is described in detail in the next section.

The input also requires the position and speed (velocity vector) of a receiving “victim” aircraft, which is assumed to be 40,000 feet and 400 knots, respectively. The altitude and speed of the “victim” receiving aircraft represent realistic values for commercial aircraft.

**Table 3-2. Simulation Input (heavy-traffic aircraft environment)**

Aircraft ID	X-Coordinate (nmi)	Y-Coordinate (nmi)	Z-Coordinate (Altitude) (feet)	Velocity in X Direction	Velocity in Y Direction	Aircraft Types	Transmit Power (dBm)	Message Lengths (seconds)
1	202.662	73.1711	4671.83	208.695	1.80215	3	54	4.03E-04
2	48.6307	60.541	9107.32	-86.8018	-222.029	3	54	4.03E-04
3	72.3484	-57.5201	3416.67	-11.6691	236.908	3	54	4.03E-04
4	-169.316	147.022	9553.72	-97.5004	167.734	-1	42.5	2.56E-04
5	87.0183	-68.3116	4769.96	-194.264	-153.519	3	54	4.03E-04
6	62.4933	-36.8638	1730.85	-11.8113	-101.15	3	54	4.03E-04
7	91.2437	-161.707	783.043	94.5167	-94.7886	0	42.5	2.56E-04
8	56.4462	216.787	8128.29	-202.395	131.058	-1	42.5	2.56E-04
9	109.669	177.395	682.99	102.096	-87.7992	0	42.5	2.56E-04
10	44.5925	-151.794	2936.82	-0.454252	148.359	-1	42.5	2.56E-04
11	-7.55854	-8.86014	8705.3	24.5624	-164.743	-1	42.5	2.56E-04
12	-16.7701	-87.209	5033.91	-211.742	114.73	3	54	4.03E-04
13	-60.6408	135.092	6623.54	-67.5871	-208.774	3	54	4.03E-04
14	101.212	34.3136	1017	71.5541	-125.431	3	54	4.03E-04
.	.	.	.	.	.	.	.	.
.	.	.	.	.	.	.	.	.
2994	-34.9291	79.9581	0	0	0	4	32	2.56E-04



**Table 3-3. Aircraft types**

<b>Aircraft Types</b>	<b>Flight Levels</b>	<b>Percentage (%) of equipage</b>	<b>Maximum Transmitter Power</b>	<b>Message Type (short or long ADS-B)</b>	<b>Required Range (nautical miles)</b>
<b>0</b>	0-17,947 feet	18%	42.5 dBm	Short	10 nmi
<b>-1</b>	0-17,758 feet	7.7%	42.5 dBm	Short	20 nmi
<b>1</b>	0-37,096 feet	27.8%	46 dBm	Short	20 nmi
<b>2</b>	0-31,673 feet	9%	46 dBm	Short, Long	40 nmi
<b>3</b>	0-31,205 feet	27.5%	54 dBm	Short, Long	90 nmi
<b>4</b>	On Airport Ground	10%	32 dBm	Short	Airport Area

### 3.2.3 Simulation engine

The simulation engine contains three features: aircraft movement tracking, power-link computation, and MOE algorithm, as shown in Figure 3-4. The aircraft movement tracking feature calculates and updates the aircraft positions in real-time, with one second increments. The power-link computation calculates the line-of-sight signal-in-space attenuation and received power at the receiving aircraft antenna. The main module in the simulation engine is the MOE algorithm, whose concept of operation is described in the previous section. This engine is responsible for computing the message-overlap statistics for the entire population of 2,994 aircraft in the environment based on the input data [MOPS02]. This simulation engine is configured to perform two separate case studies:

CASE I: Determine the worst-case estimates of co-channel interference

CASE II: Determine the realistic (or actual) estimates of co-channel interference

Each of the two cases is analyzed in detail under three scenarios, namely the worst-case, the most-likely-case and the best-case scenarios, depending on the message-length requirements. The worst-case scenario is represented when all aircraft in the environment transmit long messages. The best-case scenario is represented when all

aircraft transmit short messages. The most-likely-case scenario is represented when a mixture of short (63.5% of the total aircraft in the environment) and long (36.5% of the total aircraft) messages, depending on aircraft types, are transmitted. The co-channel interference is specified in terms of message-overlap statistics.

### **3.2.4 CASE I: Worst-case estimates of interference**

In CASE I, it is desired that all interferences caused by overlaps are accounted for, regardless of whether they might or might not cause harmful interference. Harmful interference is defined to be interference above certain thresholds, which is the subject of study in CASE II. Therefore CASE 1 represents a worst-case analysis and serves to provide an upper-bound. Simulations are conducted based on the input data shown in Tables II and III, and the assumptions stated previously. Since propagation and receiver characteristics are not considered in CASE I, the transmit power column (highlighted) in Table II is disabled and is not included in the simulations.

Approximately seventeen minutes of real-time data are captured so that the results of one thousand simulation trials can be analyzed. Figures 3-5, 3-6, and 3-7 show the message-overlap results for CASE 1 under the three scenarios, the worst, the most-likely and the best scenarios, respectively. Note that each “bar” in the graphs is made up of one thousand “vertical lines”. Each “vertical line” represents the result of one simulation trial. The dotted line represents the final result, which is an average over one thousand simulation trials.

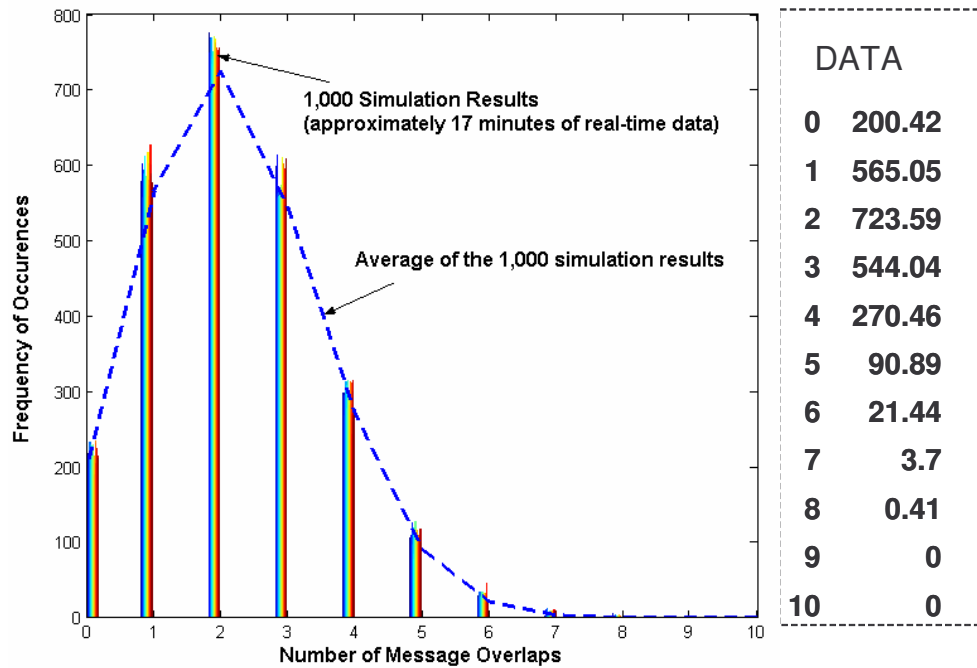


Figure 3-5. Worst-Case Scenario for CASE I

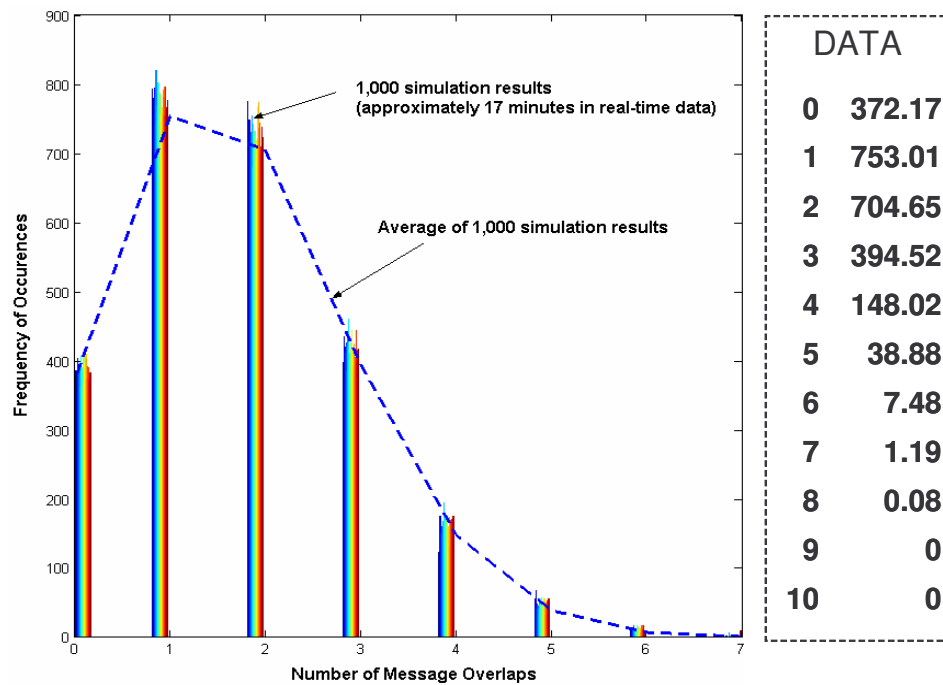
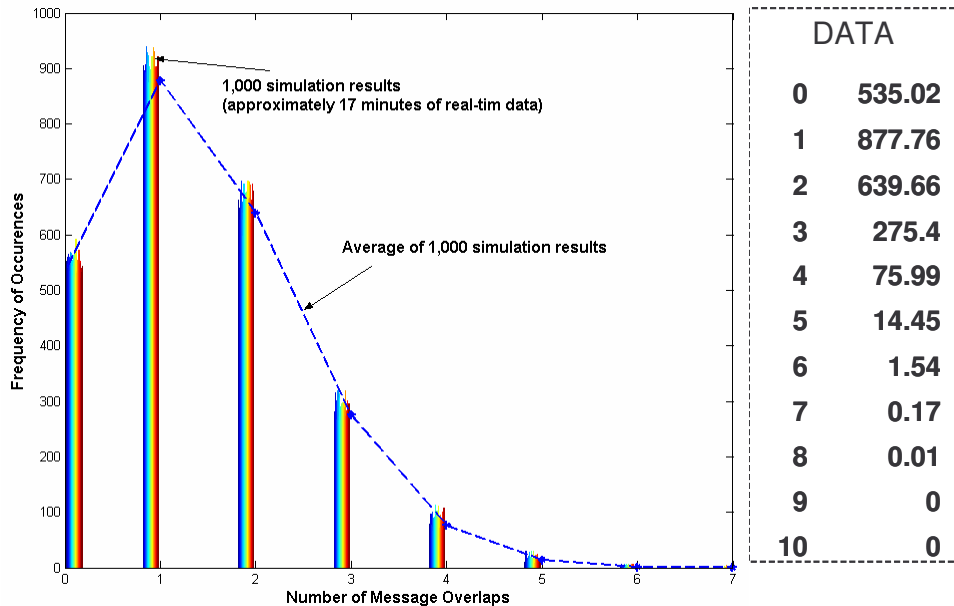


Figure 3-6. Most-Likely Scenario for CASE 1



**Figure 3-7. Best-Case Overlap Statistics**

The results shown in Figures 3-5, 3-6 and 3-7 are then normalized so that they can be represented by a known type of discrete statistical distribution. The normalized results for message overlaps are shown in Figure 3-8, which illustrates the possibilities of message overlaps from zero overlaps to seven overlaps. It can be observed that in the worst-case scenario, in which all aircraft are assumed to transmit long messages, the plot extends to the right, resulting in a higher potential for message overlaps whereas the plot extends further to the left for the best-case scenario. The most-likely scenario is in between these scenarios [Wils02].

The Poisson distribution is selected because it provides the best fit of the data, as compared to other discrete distributions. Besides, the Poisson distribution is appropriate for applications that involve the counting number of times a random event (message-overlap in this case) occur in a given time (1 second in this case). Recall that the Poisson distribution  $p(k : n, p) = \frac{\lambda^k}{k!} e^{-\lambda}$  [Star94], where  $k$  is the number of message-overlaps and  $\lambda$  represents both the mean and variance of the distribution that is being estimated. The results obtained from Poisson estimates, in terms of means (variances) are 2.37, 1.88 and

1.5 for the worst-case, the most-likely and the best-case scenarios for the Case I study, respectively. These results are shown in Figure 3-8.

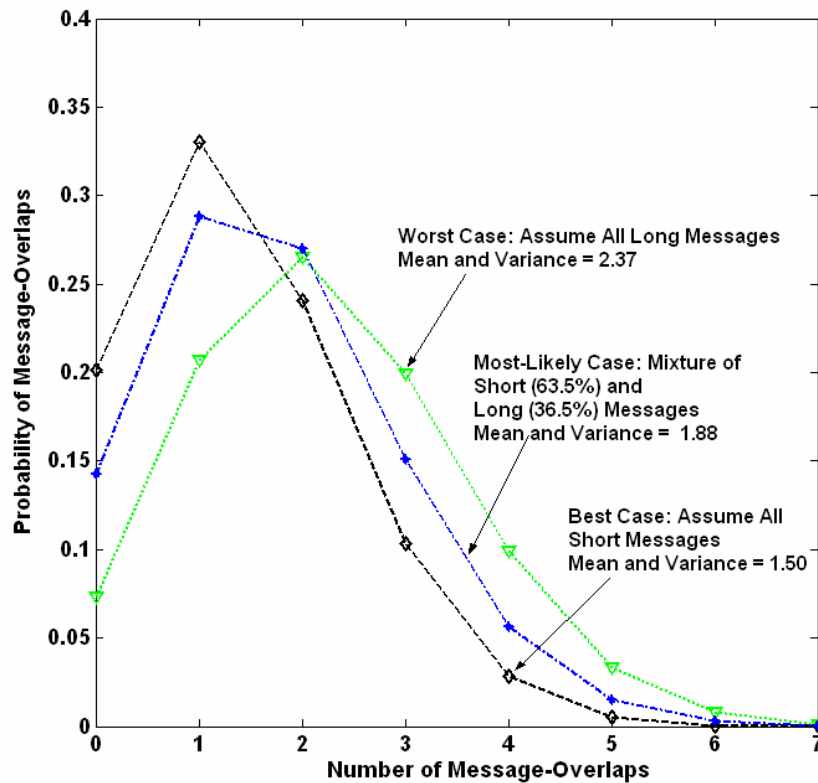


Figure 3-8. Aggregate Message-Overlap Statistics for CASE I

### 3.2.5 CASE II: Realistic estimates of interference

In CASE II, it is desired to only account for co-channel interference which causes *harmful* interference, in other words, interference above certain thresholds. Therefore, these *effective* message overlaps found in CASE II are actually subsets of CASE I. In order to account for effective overlaps, several key factors are considered so that interference thresholds can be determined. These factors include propagation attenuation, minimum signal-to-noise ratio (SNR) required for successful message decoding, maximum signal-to-interference (SIR) that the system can tolerate, the severity of the overlaps and placement of these overlaps. These factors are computed and converted into threshold conditions, which are then added into the computer simulation engine. Thus, a

message can be successfully decoded only if all the threshold conditions are satisfied. This entire section describes how these conditions are determined.

Propagation attenuation is computed using a line-of-sight power-link calculation. Note that implementation-specific factors such as antenna gain variations, receiver sensitivity fluctuations for different aircraft types, and antenna diversity are not considered. However, enhancements to the model can be made to account for antenna gain variations and antenna diversity using an antenna-switching technique, as shown in Appendix B. Assuming that the input data is from Table II, with the transmit power column enabled, the received power distributions for a “victim” aircraft located at 10,000, 20,000, 30,000, and 40,000 feet, are shown in Figures 3-9 through 3-12. The received power histograms depict the potential interference and the severity of the interference caused by messages transmitted from other aircraft in the environment. The receiver sensitivity is assumed to be -93 dBm.

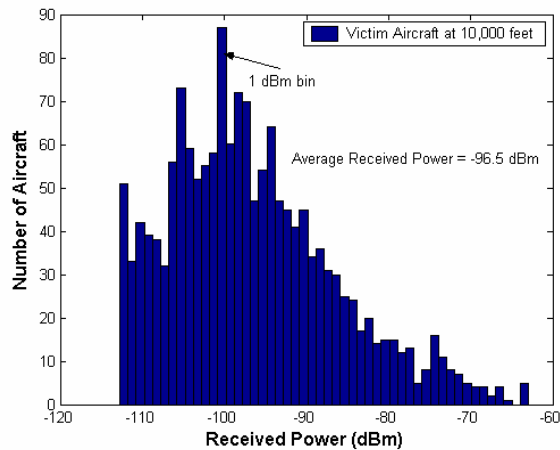


**Figure 3-9. Received Power Histogram when Victim Aircraft is at 10,000 Feet**

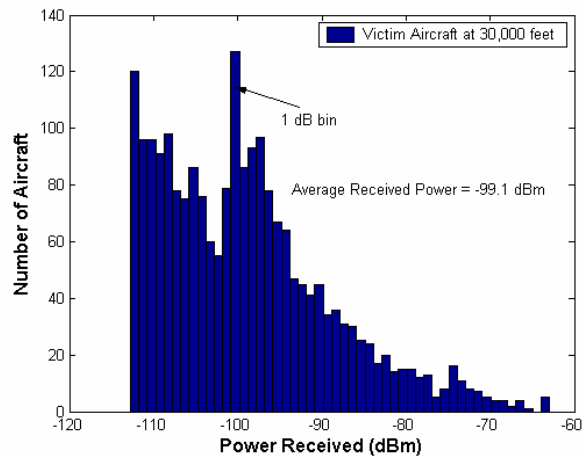


**Figure 3-11. Received Power Histogram when Victim Aircraft is at 30,000 Feet**

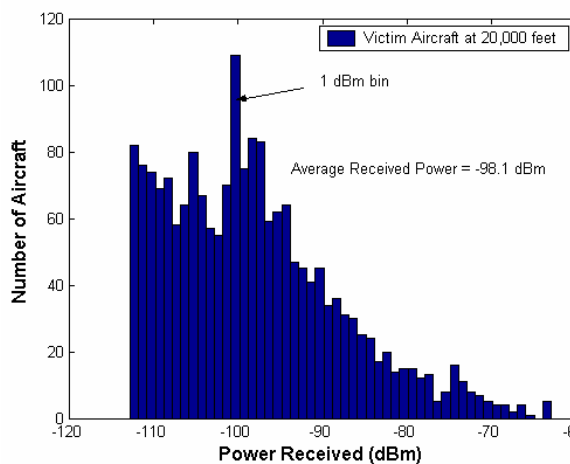


**Figure 3-10. Received Power Histogram when Victim Aircraft is at 20,000 Feet**

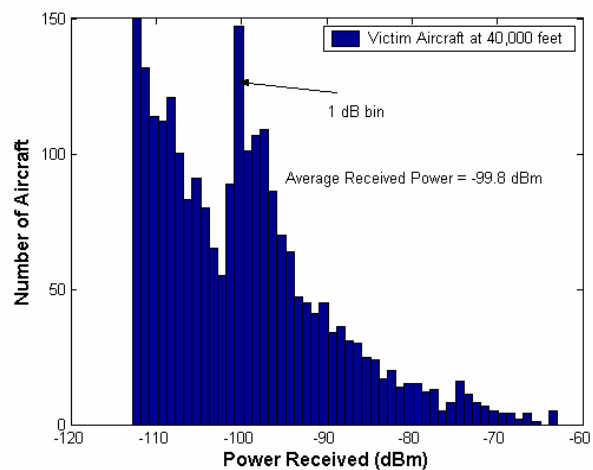


**Figure 3-12. Received Power Histogram when Victim Aircraft is at 40,000 Feet**

It is important to note that the total number of aircraft shown in Figures 4, 5, 6, and 7 are not the same because the communications link among aircraft is limited by the radio horizon, which is a function of the altitude of the victim aircraft. In fact, the total number of aircraft shown in Figures 3-9 through 3-12 is 1586, 1904, 2166, and 2420, respectively. The maximum communications range can be determined based on the positions of the victim aircraft with respect to other aircraft and is governed by the results in Figure 3-13 assuming 4/3 earth radius to calculate for radio line of site [FAA98]

$$RLOS(nmi) = 1.23 \left( \sqrt{h_1} + \sqrt{h_2} \right) \quad \text{Eq. 3.1}$$

where  $h_1$  represents the position of the victim aircraft (in feet) and  $h_2$  represents the position of any other aircraft in the environment (also in feet).

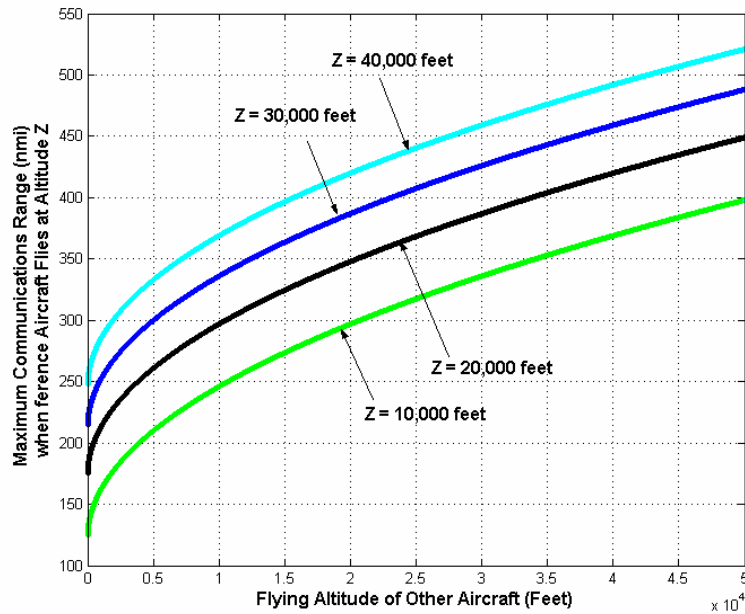


**Figure 3-13. Maximum Communications Range**

Figure 18 shows the side view of the operating environment and the bounds in which a victim aircraft can communicate with other aircraft without being limited by the radio horizon. Examples are shown for victim aircraft positioned at 5,000, 10,000, 20,000, 30,000, and 40,000 feet. This implies that the maximum number of aircraft that contribute to the message-overlap statistics never reaches the total 2,994 aircraft in the environment. In fact, at most 80.8% (or 2420 aircraft) would contribute to the computation of message overlaps, as shown in Table 3-4. Since most general aviation and commercial aircraft fly below 40,000 feet, flight levels above 40,000 are not considered in this study.



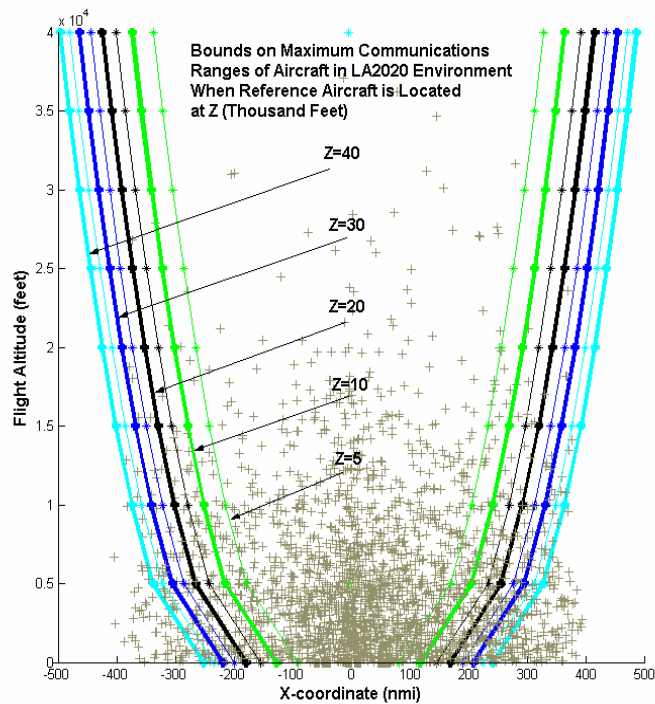


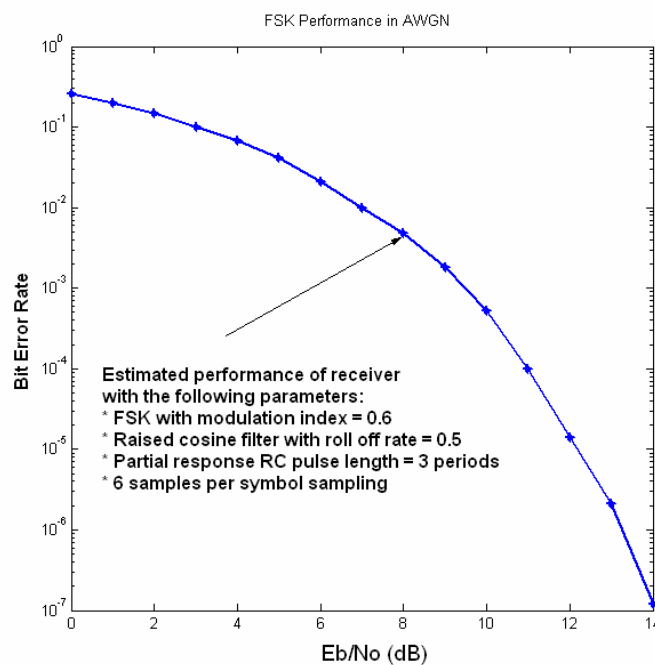
Figure 3-14. Aircraft Contained within Maximum Communications Range

Table 3-4. Number of aircraft which effectively contribute to the message-overlap statistical analysis

Reference Aircraft Flying Level (Thousand Feet)	Maximum Number of Aircraft whose Transmissions are Received by the Reference Aircraft	Percentage (%) out of the 2994 aircraft in LA Basin Environment
5	1290	43.1%
10	1586	53.0%
15	1748	58.4%
20	1904	63.6%
25	2030	67.8%
30	2166	72.3%
35	2286	76.4%
40	2420	80.8%
60	2748	91.8%
80	2955	98.7%
100	2993	Approx. 100%

Another factor included into the MOE is the minimum signal-to-noise ratio ( $E_b/N_o$  in this case) required for successful message decoding. The receiver performance, which is estimated using Matlab/Simulink, is shown in Figure 3-15 [Wils02] [Jeru92]. The estimate is made based on the following assumptions:

- Binary Frequency Shift Keying Modulation and Demodulation are used with modulation index equal 0.6
- The transmitter contains a raised cosine filter with a roll-off rate of 0.5
- The raised cosine pulse is truncated to  $\pm 3$  symbol periods
- The baseband transmit bandwidth is 1.56 MHz
- The sampling rate is at 6 samples/symbol



**Figure 3-15. Receiver Performance**

The bit error rate performance is converted to another figure of merit called message success rate, shown in Figure 3-16. The system is designed to operate above an MSR threshold, at which all the messages are successfully decoded if the following conditions are true:

1. The received power is above a receiver sensitivity of  $-93$  dBm at the antenna

2. The required  $E_b/N_o$  is 90% MSR, which is approximately 10.85 dB of the power of the message of interest

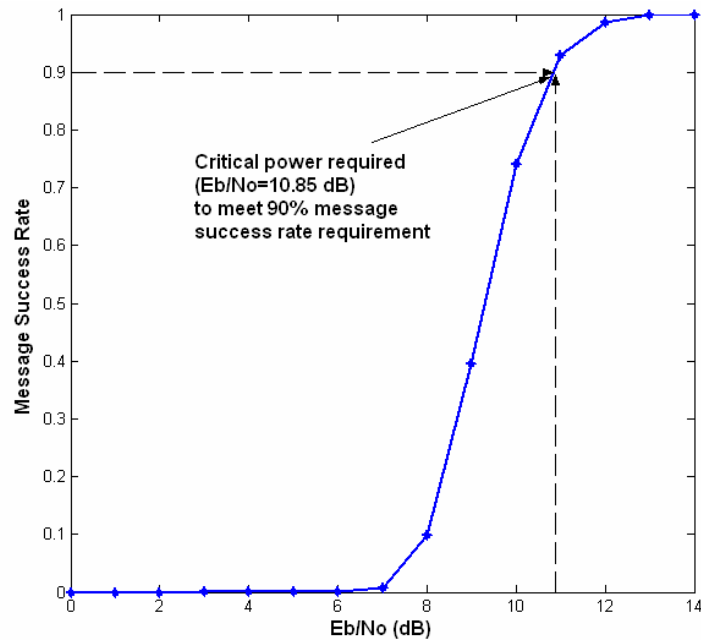


**Figure 3-16. Message Success Rate**

The last factor to consider is the signal-to-interference ratio required for successful decoding of messages. In the case of one co-channel interferer (two overlapped messages), the performance of the system is governed by the curves in Figures 3-17 and 3-18, which yields an SIR value of 4.4 dB for a 90% MSR requirement. In the case of two co-channel interferers (three overlapped messages), the system performance is governed by the curves in Figures 3-19 and 3-20, which results in an estimated SIR value at about 9.5 dB.

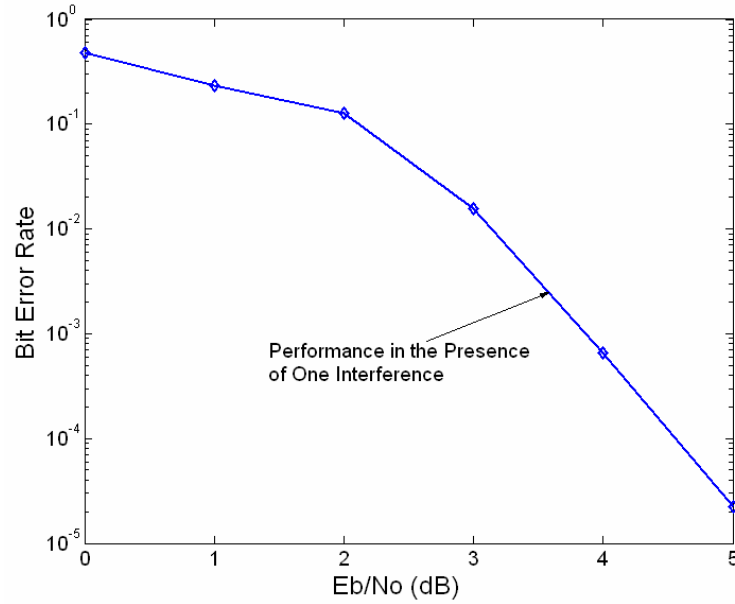


**Figure 3-17. BER Performance in the Presence of One Interferer**

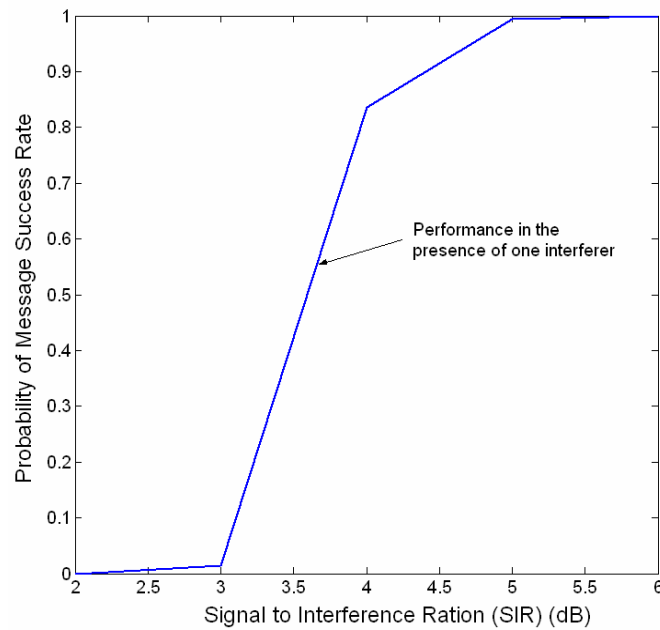


**Figure 3-18. MSR Performance in the Presence of One Interferer**

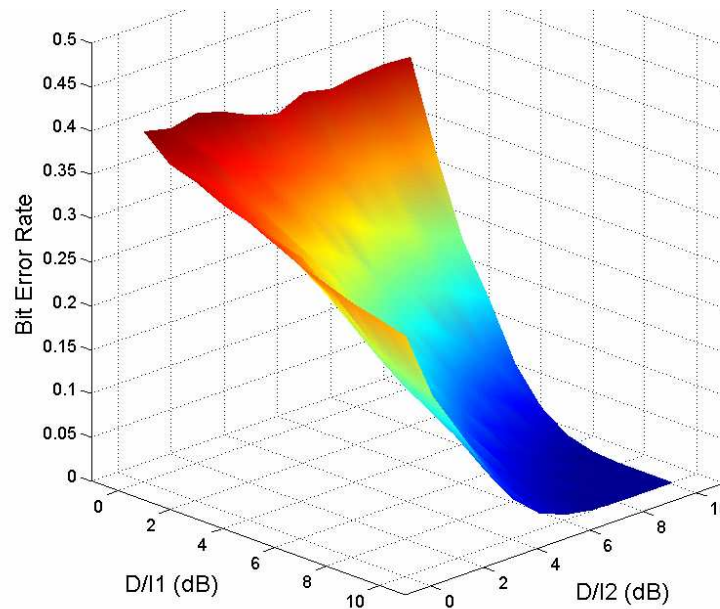


**Figure 3-19. BER Performance in the Presence of Two Interferers (linear scale)**

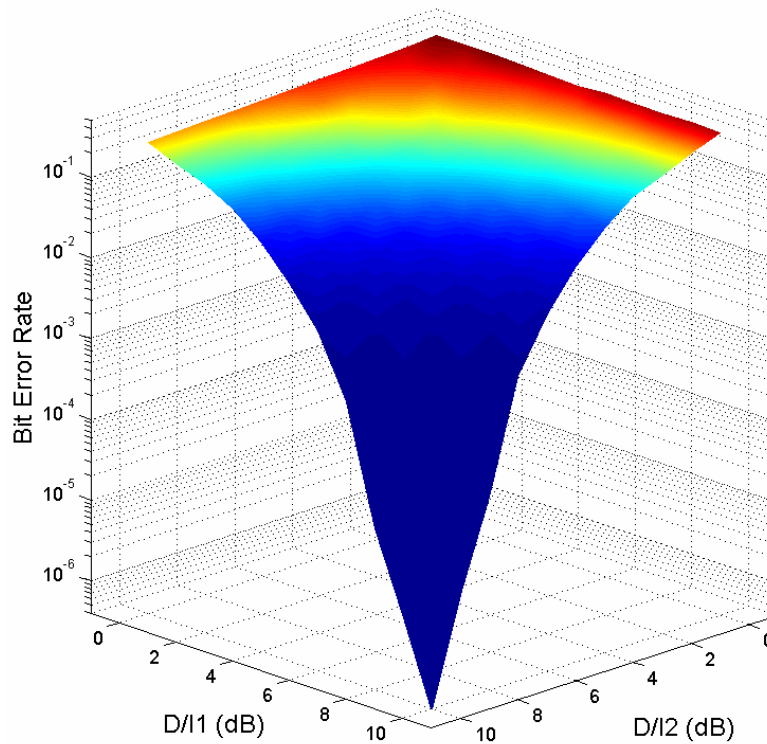


**Figure 3-20. BER Performance in the Presence of Two Interferers (log scale)**

It can be observed that the required SIR is increasing as the number of co-channel interferers increases. Therefore, the SIR conditions to use in the simulation are

dependent on the number of co-channel interferers, or message overlaps, as shown in Figures 3-21 and 3-22. If the requirement is to operate at 90% MSR, then the required SIRs for up to seven interferers are tabulated and shown in Table 3-5. These required SIRs are the threshold conditions that are used in the MOE engine to distinguish between harmful and non-harmful interference.

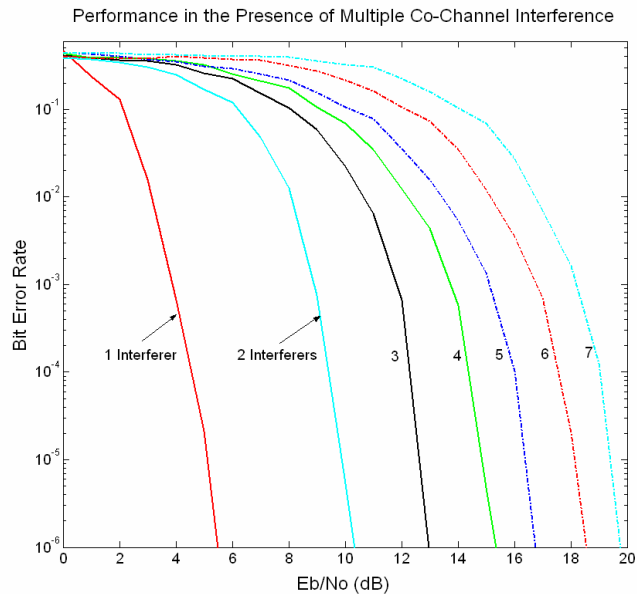


**Figure 3-21. BER Performance in the Presence of Multiple Interferers**

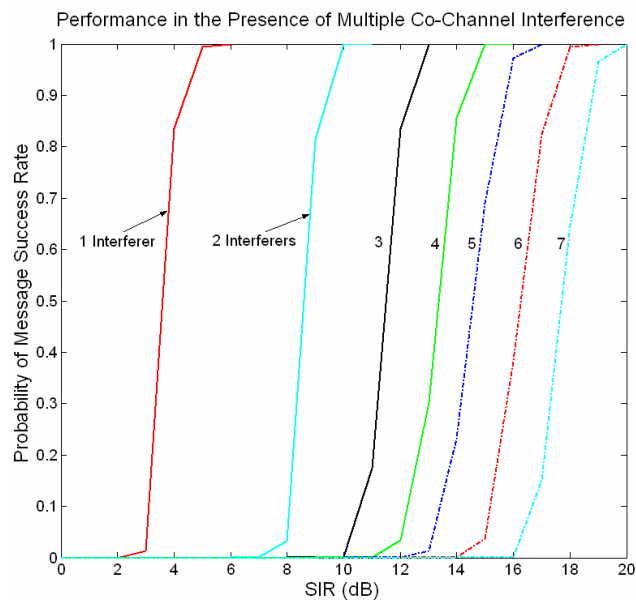


**Figure 3-22. MSR Performance in the Presence of Multiple Interferers**

**Table 3-5. Required SIRs under multiple interferers**

Number of Co-Channel Interferers	Required SIR to Obtain 90% MSR	Note
1	4.4 dB	2 overlapped messages
2	9.5 dB	3 overlapped messages
3	12.4 dB	4 overlapped messages
4	14.3 dB	5 overlapped messages
5	15.7 dB	6 overlapped messages
6	17.5 dB	7 overlapped messages
7	18.8 dB	8 overlapped messages

After all the threshold conditions described above are inserted into the simulation engine, the results are obtained by performing one thousand simulation trials to represent an approximately seventeen minutes of real-time data. The message-overlap results for CASE II are shown in Figure 3-23.

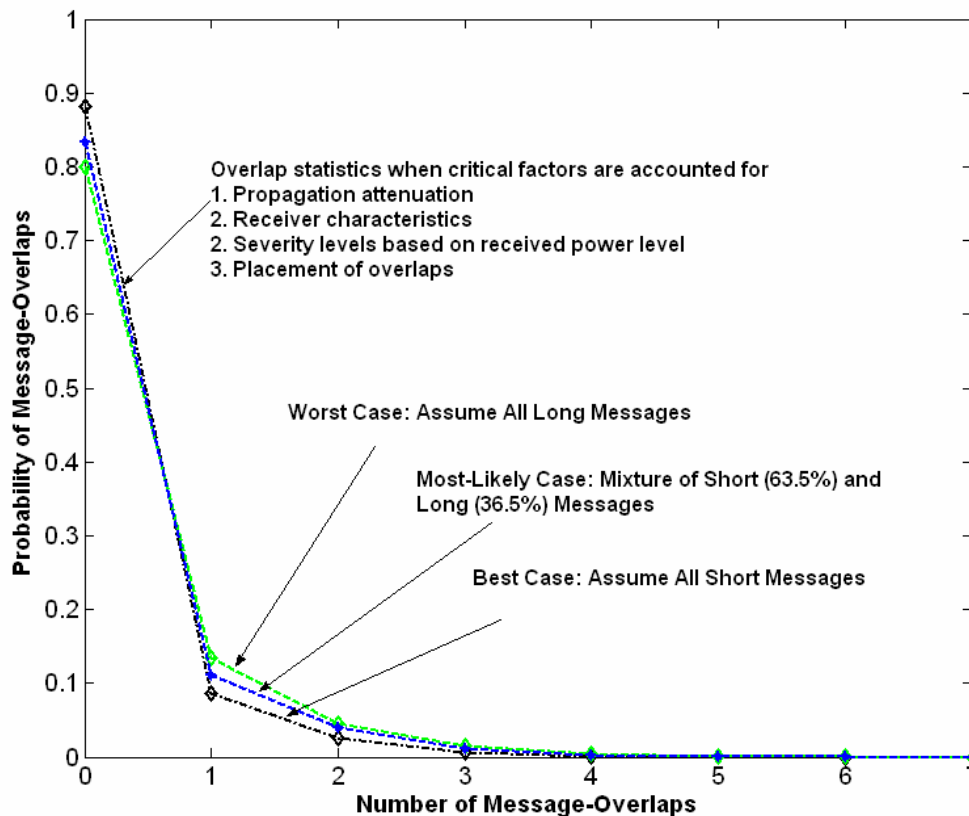


**Figure 3-23. Aggregate Message-Overlap Statistics for CASE II**

The Poisson distribution is again selected to curve fit the data because it provides the best estimates as compared to other discrete distributions. The results obtained from the Poisson estimates, in terms of means (variances) are 0.12, 0.17, and 0.21 for the best-case, most-likely-case, and worst-case scenarios, respectively.

### 3.3 Results and interpretation

The results of the CASE I and CASE II studies are plotted in the same graph in Figure 3-24. These results show that, after accounting for propagation attenuation, minimum signal-to-noise ratio (SNR) required for successful decoding, severity level and placement of the overlaps, the Poisson distribution still provides a good fit for the results. It can be observed that the overlaps that do not effectively cause interference are not computed, therefore increasing the probability of no overlaps and lowering the probability of other overlaps.

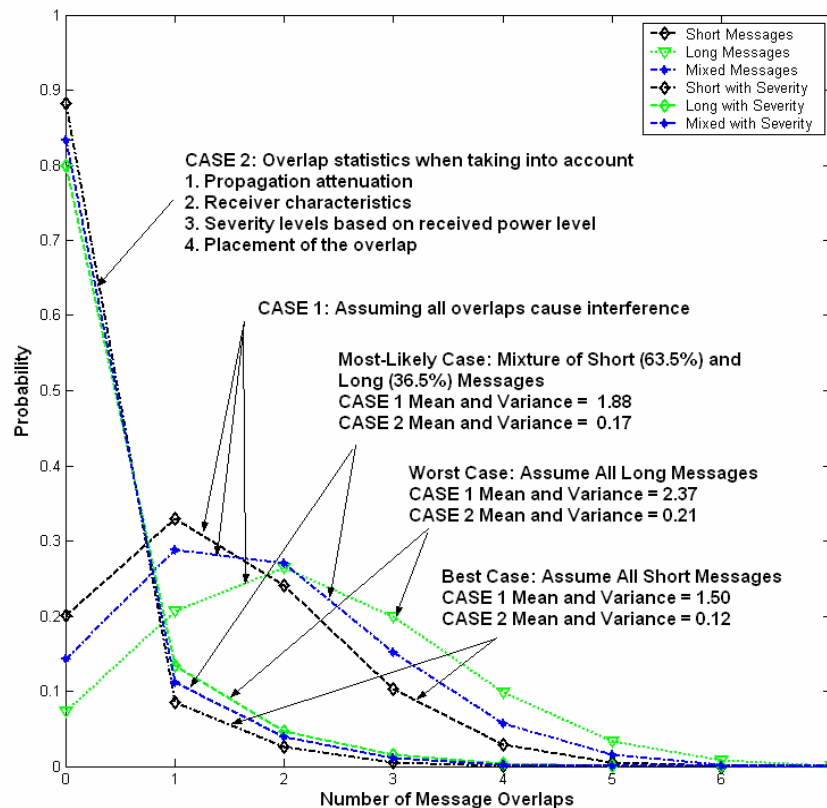


Figure 3-24. Message-Overlaps Results for CASE I and CASE II



These simulation results characterize the co-channel interference in terms of message-overlap statistics, which are based on the Poisson statistical distribution. Furthermore, the cumulative message-overlap statistics provide useful information about receiver characteristics. It can be implied from Figure 28 that co-channel interference is a problem for signal reception in this high-density environment, assuming that the “victim” aircraft is required to decode all messages in the entire operating system. Today’s receivers, which tend to decode one message at a time, cannot be used to decode multiple overlapped messages simultaneously.

An approach to improve the system performance is to design a type of multi-user or multi-message detection scheme in a receiver that would allow for the simultaneous decoding of multiple co-channel messages. Table VI shows, in terms of percent, the number of messages that are decoded correctly if the victim aircraft receiver can handle  $N+1$  overlaps.  $N$  is from 1 to 6, and the extra “1” accounts for the originally desired signal. As an example in Table 3-6 and the assumptions listed previously, to obtain a 95% success rate, this special receiver should be designed to handle five overlapping messages (corresponding to four overlaps shown in Table 3-6) for CASE I and three overlaps (corresponding to two overlaps shown in Table 3-6) for CASE II. One overlap shown in the table corresponds to two messages overlapping each other. So, two overlaps in the table represent three messages overlapping one another, and so on. The results show a significant decrease of the number of overlaps the special receiver could be designed to handle when critical factors are accounted for. This reduction is envisioned to reduce significantly signal processing and computational complexity for practical implementation.

**Table 3-6. Cumulative message-overlap analysis**

N overlaps a receiver could handle	CASE 1			CASE 2		
	Best-Case Scenario	Most-Likely Scenario	Worst-Case Scenario	Best-Case Scenario	Most-Likely Scenario	Worst-Case Scenario
0	22.1%	15.4%	8.3%	88.1%	83.4%	80.0%
1	58.4%	46.5%	31.6%	96.7%	94.5%	93.4%
2	84.8%	75.6%	61.5%	99.4%	98.5%	97.6%
3	96.2%	91.9%	84.0%	99.9%	99.7%	99.5%
4	99.3%	98.0%	95.2%	100.0%	99.9%	99.9%
5	99.9%	99.6%	98.9%	100.0%	100.0%	100.0%
6	100.0%	99.9%	99.8%	100.0%	100.0%	100.0%

### 3.4 Conclusion and Recommendation

A simulation model is developed to analyze the complex multi-user co-channel interference problem impinging on an aeronautical communication system, which operates in a heavy-traffic aeronautical mobile environment containing three thousand aircraft. We show, using Monte Carlo simulation model implemented based on the visualization method, that the co-channel interference for this aviation system can be best estimated using the statistical Poisson distribution.

Two case studies are conducted. CASE I provides the worst-case estimates of the interference. In CASE I, all interference caused by signal-overlaps are accounted for, regardless of whether they might or might not cause harmful interference. This is the absolute worst case that can happen to the system. In CASE II, realistic estimates of the interference are provided by taking into account only those signal-overlaps that actually cause harmful interference. Each case is subdivided into three scenarios to accurately represent the signal durations (or message lengths). The best, the worst and the most-likely scenarios are used to provide bounds on the simulation results. The best-scenario assumes that all aircraft transmit only short messages, which is a realistic assumption for the initial operation of the system. The worst-scenario assumes that all aircraft would transmit long messages. It is expected that future operation of this system would be most likely to fit the most-likely scenario, which assumes that aircraft are allowed to transmit a mixture of short and long messages, depending on the aircraft types. We found that

CASE I yields Poisson means (variances) equal to 1.5, 1.88 and 2.37 for the best, most-likely, and worst scenarios, respectively. CASE II yields Poisson means (variances) equal to 0.12, 0.17 and 0.21 for the best, most-likely and worst scenarios, respectively.

Based on these results, we conclude with one key finding that co-channel interference, which is specified in terms of signal-overlaps, could result from up to *eight* overlaps. However, high-quality communications, up to 98.5% success rate in signal detection, could be achieved by eliminating the interference of just *three* overlaps. This important finding is the motivation for further research in interference cancellation techniques to mitigate the interference, which will be described in Chapters 4 and 5.

### 3.5 Acknowledgement

This chapter, in part, is a reprint of the material that appears in the following conference and journal publications, in which the dissertation author was the primary author for these papers.

- M. Nguyen, A. Zaghoul, “Extension on Characterizing Packet Interference in a High-Density Traffic Environment,” in *Proceedings of twenty-third IEEE Conference on Digital Avionics Systems*, Salt Lake City, Utah, October 24-28, 2004.
- M. Nguyen, A. Zaghoul, “A Method for Characterizing Packet Interference in a High-Density Traffic Environment,” in *Proceedings of sixtieth IEEE Conference on Vehicular Technology*, Los Angeles, California, September 26-29, 2004.
- M. Nguyen, A. Zaghoul, “On the Characterization of Co-Channel Interference in an Aeronautical Mobile Environment,” paper accepted in April 2005, to be published in the *IEEE Transactions of Vehicular Technology*.

Also, it is important to note that the communications protocol used in this avionic system is somewhat similar, however not necessarily the same, as the Aloha or slotted

Aloha protocols [Abra70][Koba77][Gitm75][Meda04]. It differs from an Aloha protocol primarily because of the distinct MSOs, where aircraft are permitted to transmit only at the beginning of each MSO. This system protocol also differs from a slotted Aloha protocol because the message sizes (either short or long) exceed the time slots.

Therefore, previous work in the communications and networks literature on Aloha and slotted Aloha are useful, but not always applicable. There does not exist in the literature, to the knowledge of the authors, analysis on any system with the same characteristics as the one described in this paper.

## Chapter 4 : Sequential Interference Cancellation (SIC) Receiver

Co-channel interference degrades communication system performance and limits system capacity and throughput. Today's communication systems and networks often handle co-channel interference (caused by signal collisions) by either retransmitting data or allowing the system to tolerate interference up to a permissible level. These approaches waste bandwidth and limit system capacity. Retransmissions tie up the communication link that can be used to transmit more data, or make this link available for other users in the system. Tolerating interference lowers the capacity and system performance.

One approach to alleviating co-channel interference is to implement a radio receiver that can extract interference and allow for the successful decoding of multiple signals (assuming all signal overlaps or collisions are desired signals). However, most of today's conventional single-user radio receivers can only decode signals one at a time on a single channel. This is mainly because these co-channel signals (especially the non-CDMA and non-spread signal types) are highly correlated; thus making it difficult to differentiate and separate them.

The limitation of a single-user conventional receiver is depicted in Figure 4-1, which illustrates how today's avionic radio receivers attempt to decode *two* overlapping co-channel signals  $S_1$  and  $S_2$ . The performance graph shows that only one signal can be decoded successfully at any given time. For example, when signal  $S_1$  dominates signal  $S_2$  ( $S_1/S_2 > 0$ ), signal  $S_1$  can be decoded with low probability of error while signal  $S_2$  is totally corrupted ( $BER_{S_2} \approx 0.5$ ). Similarly, when signal  $S_2$  dominates signal  $S_1$ , signal  $S_2$  can be successfully decoded while signal  $S_1$  is corrupted ( $BER_{S_1} \approx 0.5$ ) and unrecoverable.

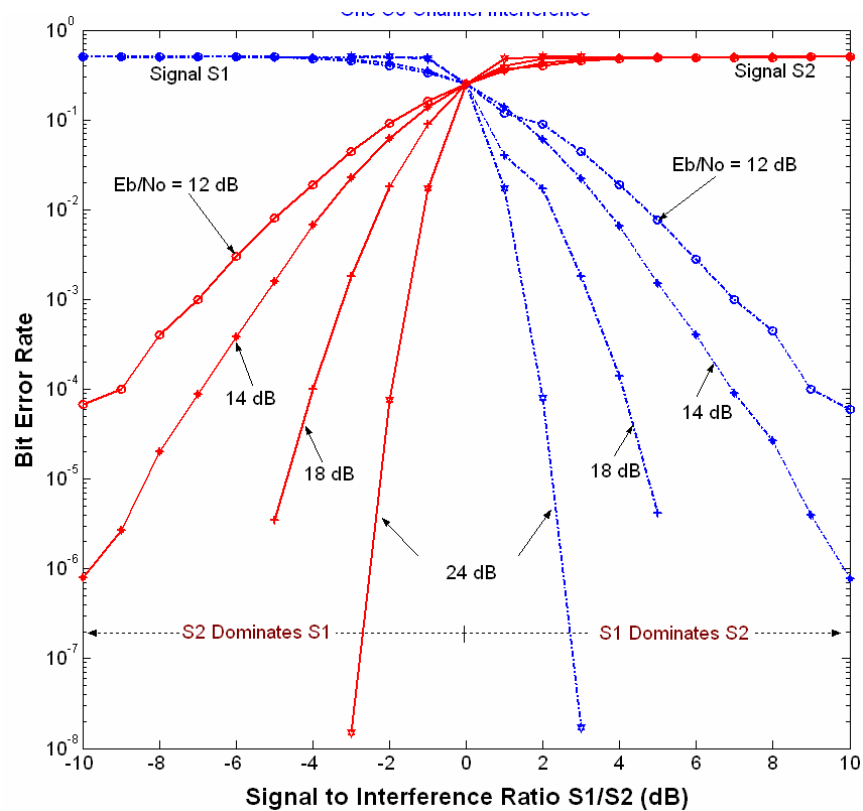


**Figure 4-1. Limitation of today's radio receivers.**

In an interference analysis for an aeronautical mobile communication system operating in a heavy-traffic environment shown in Chapter 3 and references [MOPS02] [Wils02] and [Nguy05], it was determined that a victim aircraft (A/C) receiver, whose position is assumed above Los Angeles Airport, could experience an amount of interference caused by *eight* co-channel signal overlaps (collisions of up to *eight* signals) [Nguy04a]. However, the statistical analysis concluded that high-quality communications could be achieved if there existed a receiver that could decode successfully *three* overlapping co-channel signals, as also described in references [Wils02], [Nguy04a], [Nguy04b] and [Nguy05].

This chapter extends the results of Chapter 3 to propose an effective interference cancellation technique, namely the sequential (successive) interference cancellation (SIC), that can be used to solve the co-channel interference problem [Webe80] [Reed97]. This SIC technique sequentially extracts co-channel interference and linearly decodes

multiple co-channel signals so that data retransmissions or tolerance to collisions is not needed. As a result, this would lead to efficient use of the scarce spectrum resources and achieve higher system capacity and throughput. A communication receiver implemented based on this interference cancellation technique cancels undesired co-channel signals (interference) so that desired signals can be totally recovered [More98] [Jans95] [Jans02]. This technique performs well even in situations when the desired signals are completely buried inside much stronger interferers, as experienced by the avionic communication system operating in the heavy-traffic environment.

A radio receiver architecture with interference cancellation capability and its performance characteristics will be shown in this chapter using binary Frequency Shift Keying (FSK) and binary Phase Shift Keying (PSK) modulation and demodulation methods.

## 4.1 SIC receiver structure

A communication receiver architecture that is capable of performing interference cancellation is shown in Figure 4-2. We assume that all co-channel signals in the collisions are desired signals and therefore all will be decoded eventually. However, while attempting to decode one signal (desired signal), other signals will be treated as interferers because their presence increases the noise floor of the desired signal. The proposed interference cancellation receiver works as follows. Multiple overlapped co-channel signals  $S_1, S_2, S_3, \dots, S_N$  arrive at the radio receiver. After arranging these signals from strongest to weakest in terms of their received power levels (a signal sorter), these signals are fed into Demodulator\_1, which demodulates the strongest signal, in the presence of interference of other weaker signals. After recovering the strongest signal ( $d_1(t)$ ), the resultant bit streams are re-modulated (Remodulator\_1) and subtracted from the sum of all incoming signals  $S_1 + S_2 + S_3 + \dots + S_N$ . So, if there is a sufficient separation between  $S_1$  and the rest of the signals, and correct compensations in amplitude, phase, frequency deviations and delay ( $\tau$ ) are accounted for, then the subtraction of  $S_1$  is perfect and  $S_1$  is completely removed from the list of incoming signals. Then the

resulting  $S_2, S_3, \dots, S_N$  are fed into Demodulator\_2 and the same process is repeated in subsequent stages. This iterative interference cancellation process loops back and extracts out the strongest signal among all signals before proceeding to the next stage. By the time  $S_N$  is reached, all the preceding stronger signals have already been canceled out. This “onion peeling” interference cancellation technique not only allows the receiver to decode strong signals, but weak ones will be successfully recovered as well.

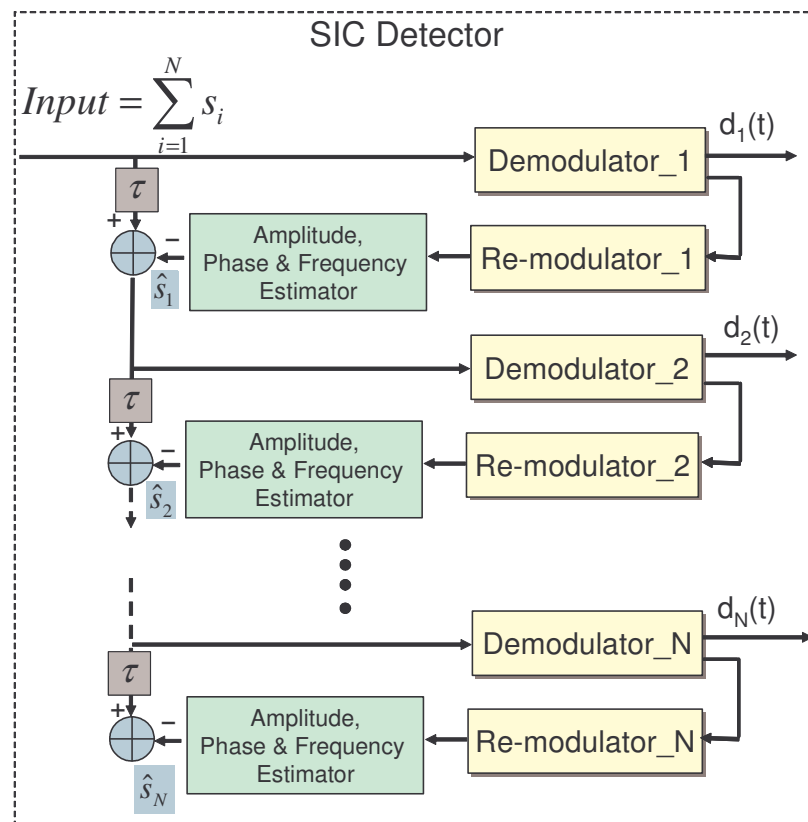


**Figure 4-2. Interference cancellation radio receiver architecture.**

In this section, we will use computer simulation based on the Monte Carlo technique to show how the interference cancellation receiver can decode multiple overlapping co-channel signals simultaneously for the following two cases:

- *Case 1:* Interference cancellation receiver capable of decoding *two* co-channel signals



- a. Binary FSK signals
  - b. Binary PSK signals
- *Case 2*: Interference cancellation receiver capable of decoding *three* co-channel signals
  - a. Binary FSK signals
  - b. Binary PSK signals

## 4.2 Simulation Assumptions

This interference cancellation technique can handle more than *three* interfering signals. However, solving the co-channel interference up to three overlapping signals was determined in Chapter 3 to be sufficient to achieve high-quality communications, especially for the avionic communication system [Nguy04a][Nguy04b][Nguy05]. A simulation model is developed using Matlab/Simulink based on the following assumptions:

- Non-spread signaling scheme (CDMA signals are not yet considered)
- System is synchronous in order to analyze a worst-case lower-bound performance. (Note: An asynchronous system would be expected to perform better since signals do not overlap one another entirely);
- All co-channel signals are desired signals with similar signaling formats: modulation, carrier frequency and message formats are exactly the same (although information bits are different);
- The channels are ideal with additive white Gaussian noise (AWGN);
- Perfect cancellation of the larger signals provided by ideal recovery of system parameters: amplitude, frequency and phase have been correctly estimated before subtraction. Therefore, after subtraction, the smaller signals are only corrupted by AWGN;
- The information bits are uniformly distributed with equally probability of 0's and 1's.

## 4.3 SIC based on B-FSK De/modulation

### 4.3.1 Analytical performance evaluation

This section provides complete analytical bit error rate equations that describe the performance of two overlapping co-channel B-FSK signals. Specifically, the probability of error for the large signal,  $P_{e_{large,B-FSK}}$ , and the probability of error for the small signal,  $P_{e_{small,B-FSK}}$  will be derived.

The received signal  $r_{composite}(t)$ , as shown in equations 4.1 and 4.2, at the input of the receiver consists of the sum of two signals and noise  $n(t)$ .  $s_{large}$  represents the large signal and  $s_{small}$  the small signal. The subscripts *large* and *small* refer to the parameters belonging to either the large signal or the small signal.

$$r_{composite}(t) = s_{large}(t) + s_{small}(t) + n(t) = \text{Re}\{R_{large}(t) \times e^{j2\pi f_c t}\} + \text{Re}\{R_{small}(t) \times e^{j2\pi f_c t}\} \quad \text{Eq. 4.1}$$

$$= A_{large} a_{large}(t) \cos(2\pi f_c t + \theta_{large}) + A_{small} a_{small}(t) \cos(2\pi f_c t + \theta_{small}(t)) \quad \text{Eq. 4.2}$$

$s_{large}$  and  $s_{small}$  are co-channel signals. By definition, they occupy the same frequency band, have the same modulation/demodulation and message formats.  $A_{large}$  or  $A_{small}$  represents signal amplitude that could take on any real value,  $f_c$  represents the common carrier frequency of the two signals and  $\theta_{large,small}$  represents two different phases of the signals when they arrive at the receiver.  $a_{large}(t)$  or  $a_{small}(t)$  denotes the random data sequences of a bipolar rectangular pulse shape having symbol duration  $T_b$ . The probability of occurrence for bipolar pulses  $\{-1,1\}$  are equal. Any frequency difference between the two signals are assumed very small compared to the symbol error rate, and therefore can be accounted for in  $\theta_{small}(t)$ , a time dependent phase change.

#### A. Decoding the large signal

When two signals overlap asynchronously, the large signal  $s_{large}$  is interfered by two adjacent symbols from the small signal  $s_{small}$  at most, as shown in Figure 4-3. The

subscripts  $m$  and  $n$  denote the  $m^{th}$  and  $n^{th}$  symbols,  $\Delta T_b$  denotes the displacement of the overlap of the small signal as compared to the large signal.

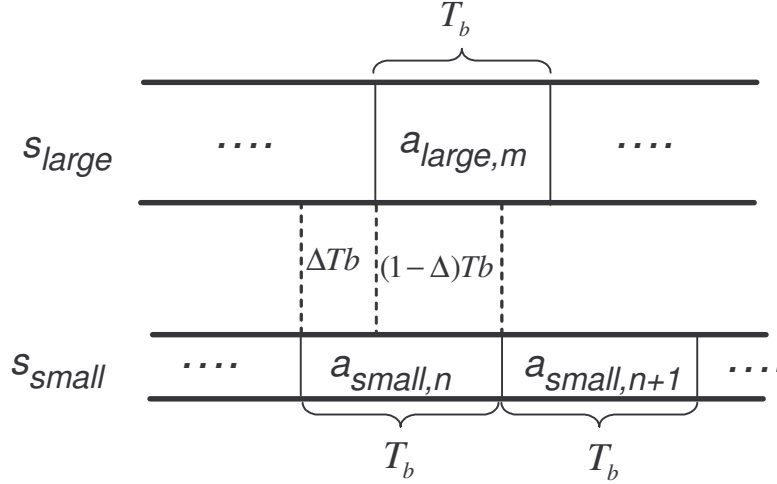


**Figure 4-3. Detecting the large signal in the presence of interference from the small signal**

We assume perfect frequency lock and phase lock with respect to the large signal. The received signal,  $r_{large}(t)$  shown in equation 4.3, which is a component of  $r_{composite}(t)$ , and represents the signal after phase acquisition with reference  $\theta_{large}$  then becomes:

$$r_{large}(t) = A_{large} a_{large}(t) + A_{small} a_{small}(t) \cos((\theta_{large} - \theta_{small})t) + n(t) \quad \text{Eq. 4.3}$$

When  $r_{large}(t)$  is detected with a matched filter, the output becomes:

$$\hat{d}_{large} = \frac{1}{T_b} \int_{t-(m-1)T_b}^{t-mT_b} A_{large} a_{large}(x) + A_{small} a_{small}(x) \cos(\theta_{large} - \theta_{small}) dx \quad \text{Eq. 4.4}$$

$$= \frac{1}{T_b} \left[ A_{large} a_{large,m} T_b + A_{small} (\Delta T_b a_{small,n} + (1 - \Delta) T_b a_{small,n+1}) \cos(\theta_{large} - \theta_{small}) \right] \quad \text{Eq. 4.5}$$

$$= A_{large} \left[ a_{large,m} + \frac{(\Delta T_b a_{small,n} + (1 - \Delta) T_b a_{small,n+1}) \cos(\theta_{large} - \theta_{small})}{A_{large} / A_{small}} \right] \quad \text{Eq. 4.6}$$

$$= A_{l\text{arge},m} \left[ a_{l\text{arge},m} + \frac{(|\Delta| a_{small,n} + (1-|\Delta|) a_{small,n+1}) \cos(\theta_{l\text{arge}} - \theta_{small})}{\sqrt{SIR_{l\text{arge}}}} \right] \quad \text{Eq. 4.7}$$

In equation 4.7,  $|\Delta|$  is the magnitude of the time displacement of the symbols of the small signal as compared to the large signal symbol, as illustrated previously in Figure 4-3.  $SIR$  is the signal to interference ratio  $A_{l\text{arge}}^2/A_{small}^2$ .  $n(t)$  is the AWGN process with noise power  $\sigma^2$  and noise spectral density  $N_o$ .

Since the symbol position on the signal constellation is symmetric, it is sufficient to evaluate the symbol error probability of just one symbol  $a_{l\text{arge},m}$  specifically when  $a_{l\text{arge},m} = +1$ . The conditional probability for detecting one symbol in the large signal, with respect to the phase difference  $(\theta_{l\text{arge}} - \theta_{small})$  and symbol displacement  $|\Delta|$ , is shown below in equation 4.8 [Jans97]:

$$\Pr(\text{error} | (\theta_{l\text{arge}} - \theta_{small}), |\Delta|, a_{l\text{arge},m} = +1) = \frac{1}{4} \sum_{\text{All States of } A_{l\text{arge},m} \text{ \& } A_{l\text{arge},m+1}} Q \left[ \sqrt{\frac{E_{b_{l\text{arge}}}}{N_o}} \left[ 1 + \frac{(|\Delta| a_{small,n} + (1-|\Delta|) a_{small,n+1}) \cos(\theta_{l\text{arge}} - \theta_{small})}{\sqrt{SIR_{l\text{arge}}}} \right] \right] \quad \text{Eq. 4.8}$$

The average probability of error for detecting the large signal can then be found by averaging the previous equation over the phase difference  $(\theta_{l\text{arge}} - \theta_{small})$  and time displacement  $|\Delta|$  as:

$$Pe_{l\text{arge},B\text{-FSK}} = \frac{1}{4\pi} \int_0^{2\pi} \int_0^{0.5} \sum_{\text{All States of } A_{l\text{arge},m} \text{ \& } A_{l\text{arge},m+1}} Q \left[ \sqrt{\frac{E_{b_{l\text{arge}}}}{N_o}} \left[ 1 + \frac{(|\Delta| a_{small,n} + (1-|\Delta|) a_{small,n+1}) \cos(\theta_{l\text{arge}} - \theta_{small})}{\sqrt{SIR_{l\text{arge}}}} \right] \right] d|\Delta| d(\theta_{l\text{arge}} - \theta_{small}) \quad \text{Eq. 4.9}$$

where  $E_{b_{l\text{arge}}}/N_o$  is bit energy of the large signal divided by noise spectral density,  $Q(z)$  is the error function and is defined as:

$$Q(z) = \frac{1}{\sqrt{2\pi}} \int_z^{\infty} e^{-\frac{\lambda^2}{2}} d\lambda \quad \text{Eq. 4.10}$$

### B. Decoding the small signal

This section is to derive complete analytical BER performance for decoding the small signal  $s_{small}$ . The analysis for decoding the small signal is similar to decoding the large signal. However, it is a more computationally involved. Figure 4-4 shows the time domain representation of the small signal and the large signal. In general, the probability of detecting a symbol of the small signal is conditioned upon the overlap of at most two adjacent symbols from the large signal. These symbols are residues after detecting the large signal, as shown previously, and have different amplitude values.

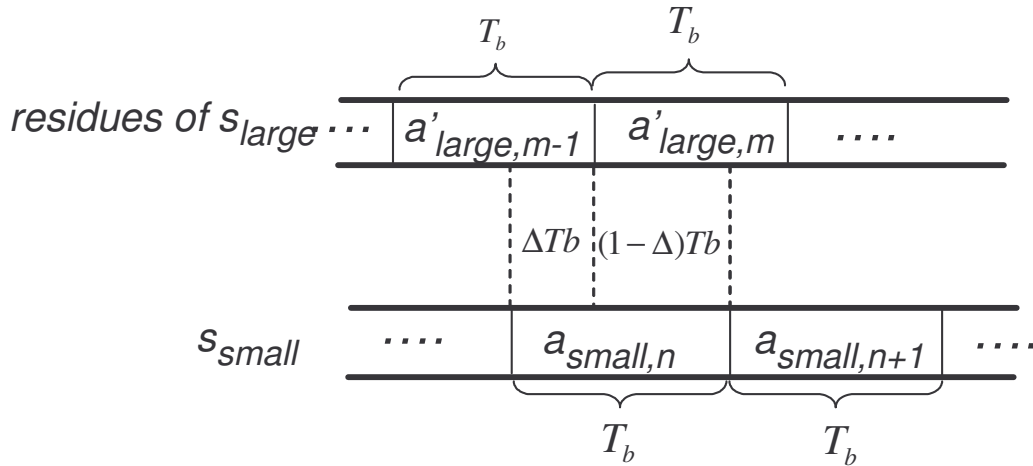


**Figure 4-4. Detecting the small signal in the presence of interference from the large signal**

The received signal, as perceived at the input of the small signal detector, is as follows:

$$r_{small} = \Delta s_{large}(t) + s_{small}(t) + n(t) \quad \text{Eq. 4.11}$$

$$= A_{large} a'_{large}(t) \cos(\theta_{large} - \theta_{small}) + A_{small} a_{small}(t) \quad \text{Eq. 4.12}$$

where  $a'_{large}(t) = \alpha_{large,m} a_{large}(t)$  and where  $\alpha_{large,m}$  is the attenuation factor of the detected amplitude of the large signal, denoted as [Jans02]:

$$\hat{A}_{large} = (1 - 2Pe_{large} |\Delta|)(1 - |\Delta|) \quad \text{Eq. 4.13}$$

This factor, which also represents the amplitude error in detecting  $a_{large,m}$  is

$$\gamma = \frac{A_{large} - \hat{A}_{large}}{A_{large}} = 1 - (1 - 2Pe_{large} |\Delta|)(1 - |\Delta|) \quad \text{Eq. 4.14}$$

The amplitude error depends on whether an error was made in detecting the large symbol previously and is equal to [More98]:

$$\alpha_{large,m} = \begin{cases} \gamma = 1 - (1 - 2Pe_{large})(1 - |\Delta|)(1 - \eta) & \text{if NO error occurs in detecting } a_{large,m} \\ 2 - \gamma = 1 + (1 - 2Pe_{large})(1 - |\Delta|)(1 - \eta) & \text{if an error occurs in detecting } a_{large,m} \end{cases} \quad \text{Eq. 4.15}$$

Where  $\eta$  represents the phase error and possible signal leakage and is assigned a value of -30 dB. Assuming perfect phase and clock reference in the receiver, the matched filter output for symbol  $a_{small,n}$  is:

$$\hat{d}_{small} = \frac{1}{T_b} \int_{1-(n-1)T_b}^{nT_b} A_{large} a'_{large}(x) \cos(\theta_{large} - \theta_{small}) + A_{small} a_{small}(x) dx \quad \text{Eq. 4.16}$$

$$= \frac{1}{T_b} \left[ A_{small} a_{small,n} T_b + A_{large} \left( |\Delta| T_b a_{large,m-1} + (1 - |\Delta|) T_b a_{large,m} \right) \cos(\theta_{large} - \theta_{small}) \right] \quad \text{Eq. 4.17}$$

$$= A_{small} \left[ a_{small,n} + \frac{A_{large}}{A_{small}} \left( |\Delta| \alpha_{large,m-1} a_{large,m-1} + (1 - |\Delta|) \alpha_{large,m} a_{large,m} \right) \cos(\theta_{large} - \theta_{small}) \right] \quad \text{Eq. 4.18}$$

$$= A_{small} \left[ a_{small,n} + \frac{\left( |\Delta| \alpha_{large,m-1} a_{large,m-1} + (1 - |\Delta|) \alpha_{large,m} a_{large,m} \right) \cos(\theta_{large} - \theta_{small})}{\sqrt{SIR_{small}}} \right] \quad \text{Eq. 4.19}$$

where  $SIR_{small} = A_{small}^2 / A_{large}^2$

The conditional probability for detecting the small signal, specifically detecting symbol  $a_{small,n}$ , is:

$$\Pr(\text{error} / a_{small,n}, a'_{large,m}, a'_{large,m-1}, |\Delta|, (\theta_{large} - \theta_{small})) = Q \left[ \sqrt{\frac{E_{b,small}}{N_o}} \times \left[ 1 + \frac{\left( |\Delta| \alpha_{large,m-1} a_{large,m-1} + (1 - |\Delta|) \alpha_{large,m} a_{large,m} \right) \cos(\theta_{large} - \theta_{small})}{\sqrt{SIR_{small}}} \right] \right] \quad \text{Eq. 4.20}$$

In detecting  $a_{small,n}$ , three possibilities could occur:

### 1. No errors detected in the two overlapping symbols

If no error occurs in detecting both of the two overlapping symbols  $a_{large,m-1}$  and  $a_{large,m}$ , we would obtain attenuation factor  $\gamma = 1 - (1 - 2Pe_{large})(1 - |\Delta|)(1 - \eta)$  for both signal amplitudes. This case would occur at a probability of  $P_o = (1 - Pe_{large})^2$ . Each  $(1 - Pe_{large})$  represents the probability for successfully decoding a single symbol of the large signal with no error. The conditional probability for detecting symbol  $a_{small,n}$ , then becomes:

$$\Pr(\text{error} / a_{small,n}, |\Delta|, (\theta_{large} - \theta_{small})) = \frac{1}{4} \sum_{\substack{\text{All states} \\ a_{large,m-1} \& a_{large,m}}} Q \left[ \sqrt{\frac{E_{b\ small}}{N_o}} \times \left[ 1 + \frac{(|\Delta| \gamma a_{large,m-1} + (1 - |\Delta|) \gamma a_{large,m}) \cos(\theta_{large} - \theta_{small})}{\sqrt{SIR_{small}}} \right] \right] \quad \text{Eq. 4.21}$$

The summation should be computed over 4 possible states of  $a_{large,m}$  and  $a_{large,m-1}$ , namely  $\{1,1\}$ ,  $\{1,-1\}$ ,  $\{-1,1\}$ , and  $\{-1,-1\}$ .

The error probability of detecting no error can be found by averaging over  $|\Delta|$  and  $(\theta_{large} - \theta_{small})$  as:

$$Pe_{small\_o} = \frac{1}{4\pi} \int_0^{2\pi^{0.5}} \int_0^1 \sum_{\substack{\text{All states} \\ a_{large,m-1} \& a_{large,m}}} Q \left[ \sqrt{\frac{E_{b\ small}}{N_o}} \times \left[ 1 + \frac{(|\Delta| \gamma a_{large,m-1} + (1 - |\Delta|) \gamma a_{large,m}) \cos(\theta_{large} - \theta_{small})}{\sqrt{SIR_{small}}} \right] \right] d|\Delta| d(\theta_{large} - \theta_{small}) \quad \text{Eq. 4.22}$$

### 2. One single error is detected in the two overlapping symbols

If only one single error is detected for the two overlapping symbols, this means that  $\alpha_{large,m} = 2 - \gamma = 1 + (1 - 2Pe_{large})(1 - |\Delta|)(1 - \eta)$  and  $\alpha_{large,m-1} = \gamma = 1 - (1 - 2Pe_{large})(1 - |\Delta|)(1 - \eta)$  or  $\alpha_{large,m} = \gamma$  and  $\alpha_{large,m-1} = 2 - \gamma$ . This case would occur at a probability of  $P_1 = 2Pe_{large}(1 - Pe_{large})$ . The conditional probability for detecting symbol  $a_{small,n}$ , then becomes:

$$\Pr(\text{error} / a_{small,n}, |\Delta|, (\theta_{l \arg e} - \theta_{small})) = \frac{1}{4} \sum \sum Q \left[ \sqrt{\frac{E_{b \ small}}{N_o}} \times \left[ 1 + \frac{(|\Delta| \alpha_{l \arg e, m-1} a_{l \arg e, m-1} + (1-|\Delta|) \alpha_{l \arg e, m} a_{l \arg e, m}) \cos(\theta_{l \arg e} - \theta_{small})}{\sqrt{SIR_{small}}} \right] \right] \quad \text{Eq. 4.23}$$

where the two summations represent all states of  $\alpha_{l \arg e, m-1}$  and  $\alpha_{l \arg e, m}$  and  $a_{large, m-1}$  &  $a_{l \arg e, m}$ .

The double summation should be computed over 16 possible states of  $a_{large, m}$  and  $a_{large, m}$ , and  $\alpha_{l \arg e, m}$  and  $\alpha_{l \arg e, m-1}$ . Let  $\kappa = 2 - \gamma$ , the 16 possible states are:

$$\begin{Bmatrix} \alpha_{l \arg e, m} \\ \alpha_{l \arg e, m-1} \\ a_{l \arg e, m} \\ a_{l \arg e, m-1} \end{Bmatrix} = \begin{Bmatrix} \gamma & \gamma & \gamma & \gamma & \kappa & \kappa & \kappa & \kappa & \gamma & \gamma & \gamma & \gamma & \kappa & \kappa & \kappa & \kappa \\ \gamma & \gamma & \gamma & \gamma & \kappa & \kappa & \kappa & \kappa & \kappa & \kappa & \kappa & \kappa & \gamma & \gamma & \gamma & \gamma \\ 1 & -1 & 1 & -1 & 1 & -1 & 1 & -1 & 1 & -1 & 1 & -1 & 1 & -1 & 1 & -1 \\ 1 & 1 & -1 & -1 & 1 & 1 & -1 & -1 & 1 & 1 & -1 & -1 & 1 & 1 & -1 & -1 \end{Bmatrix}$$

The error probability of detecting no error can be found by averaging over  $|\Delta|$  and  $(\theta_{l \arg e} - \theta_{small})$  as:

$$Pe_{small\_1} = \frac{1}{4\pi} \int_0^{2\pi} \int_0^{0.5} \sum \sum Q \left[ \sqrt{\frac{E_{b \ small}}{N_o}} \times \left[ 1 + \frac{(|\Delta| \alpha_{l \arg e, m-1} a_{l \arg e, m-1} + (1-|\Delta|) \alpha_{l \arg e, m} a_{l \arg e, m}) \cos(\theta_{l \arg e} - \theta_{small})}{\sqrt{SIR_{small}}} \right] \right] d|\Delta| d(\theta_{l \arg e} - \theta_{small}) \quad \text{Eq. 4.24}$$

In equation 4.24, the two summations represent all the states of  $\alpha_{l \arg e, m-1}$  and  $\alpha_{l \arg e, m}$  and

$a_{large, m-1}$  &  $a_{l \arg e, m}$

### 3. Both overlapping symbols are errors

If both overlapping symbols are errors, this means that both  $\alpha_{l \arg e, m}$  and  $\alpha_{l \arg e, m-1}$  can be set to be equal to  $\kappa = 2 - \gamma = 1 + (1 - 2Pe_{l \arg e})(1 - |\Delta|)(1 - \eta)$ . This case



occurs at a probability of  $P_2 = Pe^2_{large}$  since each symbol error is  $Pe_{large}$  and the error occurs independently of each other. The conditional probability for detecting symbol  $a_{small,n}$ , then becomes:

$$\Pr(\text{error} / a_{small,n}, |\Delta|, (\theta_{large} - \theta_{small})) = \frac{1}{4} \sum_{\substack{\text{All states} \\ a_{large,m-1} \& a_{large,m}}} Q \left[ \sqrt{\frac{E_{b,small}}{N_o}} \times \left[ 1 + \frac{(|\Delta| \kappa a_{large,m-1} + (1-|\Delta|) \kappa a_{large,m}) \cos(\theta_{large} - \theta_{small})}{\sqrt{SIR_{small}}} \right] \right] \quad \text{Eq. 4.25}$$

The summation should be computed over 4 possible states of  $a_{large,m}$  and  $a_{large,m-1}$ , namely  $\{1,1\}$ ,  $\{1,-1\}$ ,  $\{-1,1\}$ , and  $\{-1,-1\}$ .

The error probability of detecting no error can be found by averaging over  $|\Delta|$  and  $(\theta_{large} - \theta_{small})$  as:

$$Pe_{small\_2} = \frac{1}{4\pi} \int_0^{2\pi} \int_0^{0.5} \sum_{\substack{\text{All states} \\ a_{large,m-1} \& a_{large,m}}} Q \left[ \sqrt{\frac{E_{b,small}}{N_o}} \times \left[ 1 + \frac{(|\Delta| \kappa a_{large,m-1} + (1-|\Delta|) \kappa a_{large,m}) \cos(\theta_{large} - \theta_{small})}{\sqrt{SIR_{small}}} \right] \right] d|\Delta| d(\theta_{large} - \theta_{small}) \quad \text{Eq. 4.26}$$

Finally, the probability of error for detecting one symbol of the small signal  $a_{small,n}$  is expressed as:

$$Pe_{small} = P_0 Pe_{small\_0} + P_1 Pe_{small\_1} + P_2 Pe_{small\_2} \quad \text{Eq. 4.27}$$

The complete analytical expression for finding the probability of error of the small signal is:

$$\begin{aligned}
Pe_{small,B-FSK} &= \frac{1}{4\pi} \int_0^{2\pi 0.5} \int_0^{\pi} \left( (1 - Pe_{l \arg e})^2 \sum Q \left[ \sqrt{\frac{E_{b,small}}{N_o}} \times \left[ 1 + \frac{(|\Delta| \gamma a_{l \arg e, m-1} + (1-|\Delta|) \gamma a_{l \arg e, m}) \cos(\theta_{l \arg e} - \theta_{small})}{\sqrt{SIR_{small}}}} \right] \right] \right) + \\
2Pe_{l \arg e} (1 - Pe_{l \arg e}) &\sum \sum Q \left[ \sqrt{\frac{E_{b,small}}{N_o}} \times \left[ 1 + \frac{(|\Delta| \alpha_{l \arg e, m-1} a_{l \arg e, m-1} + (1-|\Delta|) \alpha_{l \arg e, m} a_{l \arg e, m}) \cos(\theta_{l \arg e} - \theta_{small})}{\sqrt{SIR_{small}}} \right] \right] + \\
Pe_{l \arg e}^2 &\sum Q \left[ \sqrt{\frac{E_{b, \arg e}}{N_o}} \times \left[ 1 + \frac{(|\Delta| \kappa a_{l \arg e, m-1} + (1-|\Delta|) \kappa a_{l \arg e, m}) \cos(\theta_{l \arg e} - \theta_{small})}{\sqrt{SIR_{small}}} \right] \right] \Big) d|\Delta| d(\theta_{l \arg e} - \theta_{small})
\end{aligned}$$

Eq. 4.28

Where the single summation depicts all states of  $a_{large, m-1}$  &  $a_{l \arg e, m}$  and the double summation depicts all states of  $\alpha_{l \arg e, m-1}$  and  $\alpha_{l \arg e, m}$  and  $a_{large, m-1}$  &  $a_{l \arg e, m}$ .

### 4.3.2 Case 1. Performance of SIC for decoding two overlapping co-channel FSK signals

This section provides the results for *Case 1*, which shows how an SIC receiver can decode *two* overlapping co-channel FSK channels. In *Case 1*, we assume that two co-channel signals (both are either FSK or PSK signals) overlap each other. Figure 4-5 illustrates how these two signals can overlap for different configurations. One signal is the large signal and is denoted as  $S_1$ ; the other is the small signal and is denoted as  $S_2$ . Together, they create mutual interference on one another when overlaps occur.

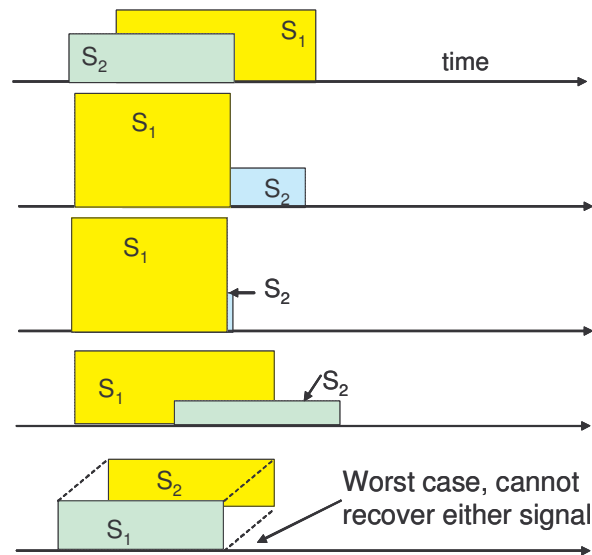
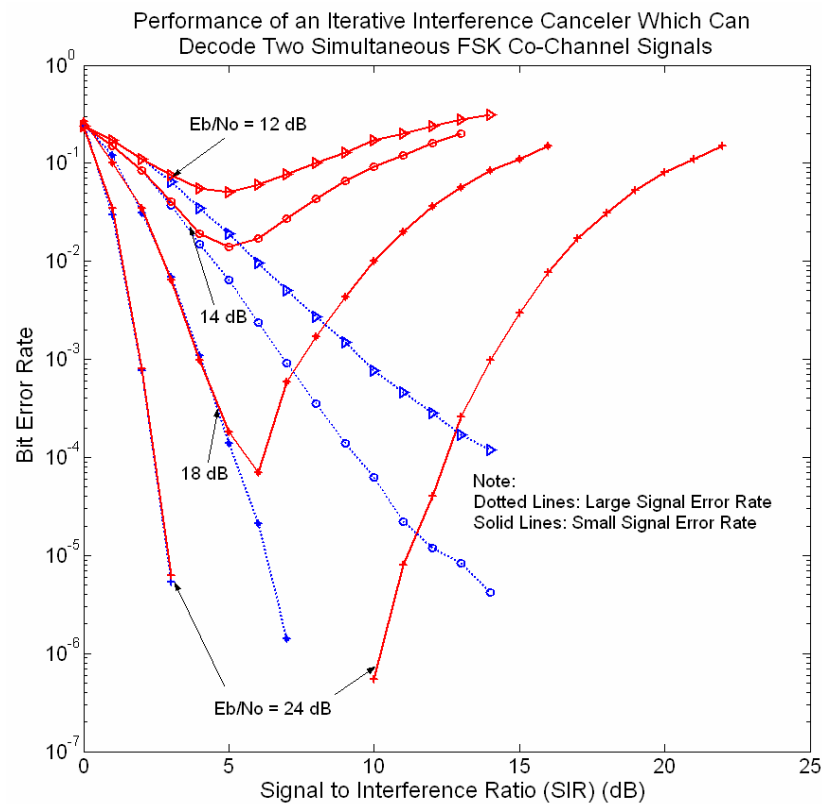


Figure 4-5. Two co-channel signal overlaps.

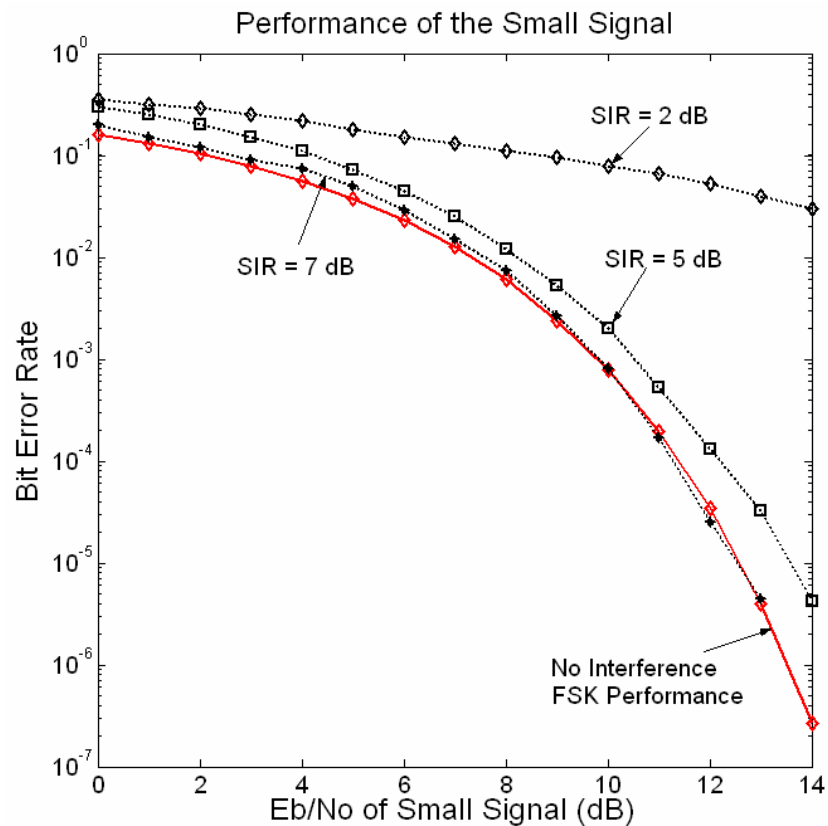
These two FSK signals arrive at the interference cancellation receiver as described in Figure 4-2, and their performance is shown in Figures 4- 6 through 4-9.

Figure 4-6 shows that the performance of the two signals are very dependent on the amount of separation between their received power levels (Signal to Interference Ratio [SIR]). Therefore, when two signals with equal power overlap each other entirely, neither one can be recovered, as shown in Figure 4-5. In general, the performance of both signals is poor for low SIRs. As SIR increases, the performance of each signal improves, until an optimum point of about 6 dB is reached, where the noise starts to dominate the SIR and degrades the performance of the small signal. However, the performance of the large signal keeps improving for higher SIRs because a larger separation (SIRs) between the signals results in a small interference coming from the small signal.



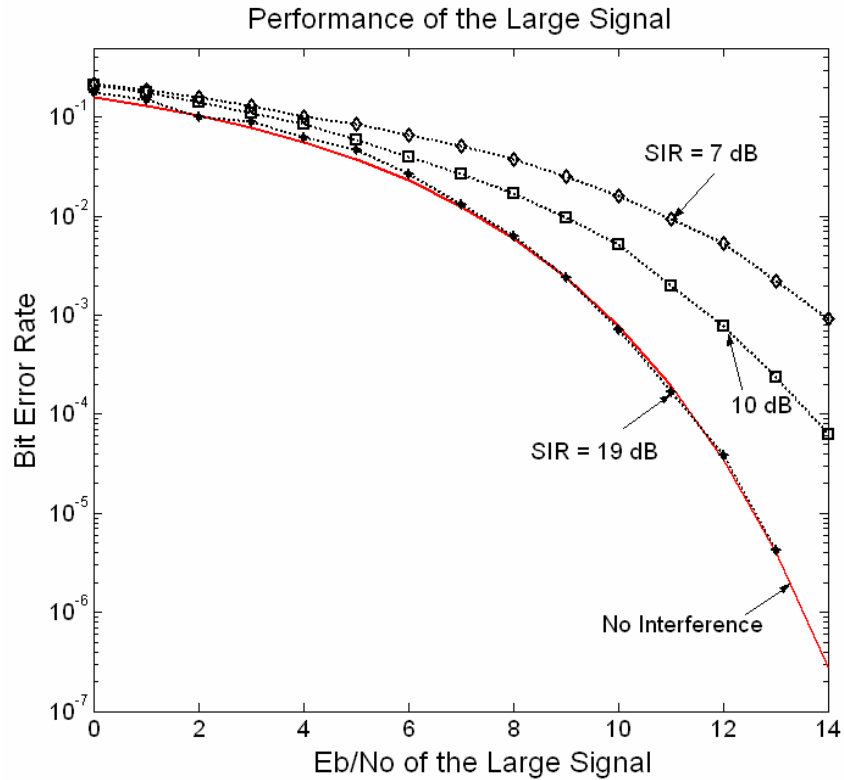
**Figure 4-6. BER vs SIR performance of the two B-FSK signals.**

Figure 4-7 focuses on the performance of the small signal. It can be seen that when the error probability of the large signal is sufficiently low, the performance of the small signal is influenced mainly by noise. The performance results show that only about 7 dB of separation in power (SIR) is needed to obtain ideal performance of the small signal; where ideal performance is defined to be the optimum system performance in the presence of AWGN (interference is not included).



**Figure 4-7. Performance of the small B-FSK signal.**

Figure 4-8 shows the performance of the large signal. It can be seen that an SIR of about 19 dB is needed to achieve ideal performance. This is because the small signal always interferes with the large signal. However, an SIR of about 10 dB can result in decent performance, where decent performance refers to performance within 2-3 dB's from ideal performance.



**Figure 4-8. Performance of the large B-FSK signal.**

Figure 4-9 shows the composite performance of both large and small signals at an SIR of 7 dB. We select 7 dB to represent the optimum SIR as illustrated in Figure 4-6. It is important to note that with a small degradation of about 4.5 dB of the large signal, the two co-channel signals can in fact be decoded simultaneously with low probability of error. Therefore, any separation (SIR) greater than 7 dB certainly improves the performance. For example, a separation of 10 dB results in performance only 2 – 2.5 dBs from ideal performance, as shown in Figure 4-8. This is a significant improvement from most of today's radios, which cannot perform this multi-signal decoding function on a single channel.

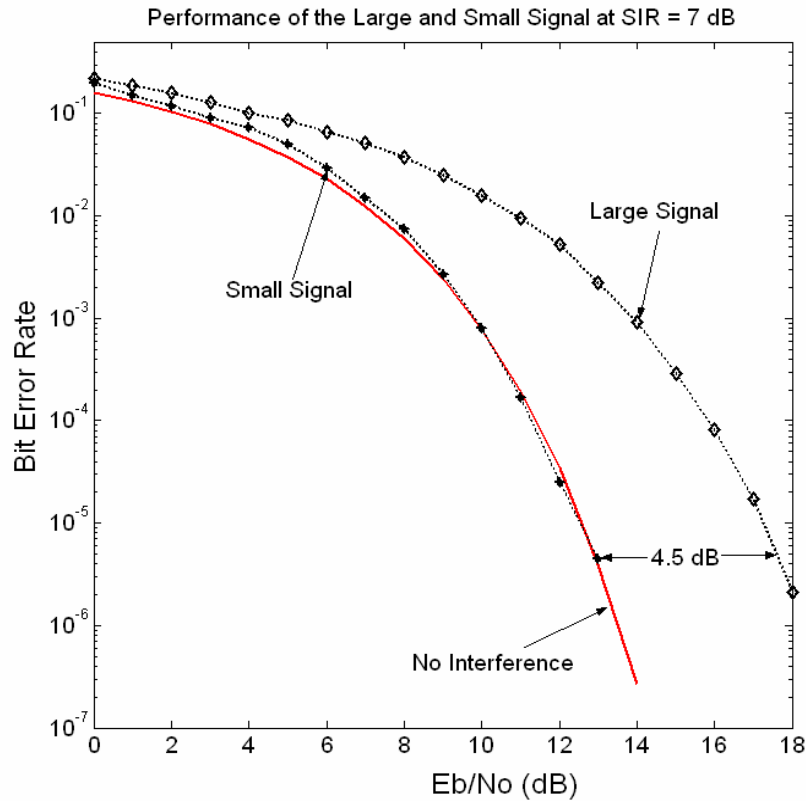
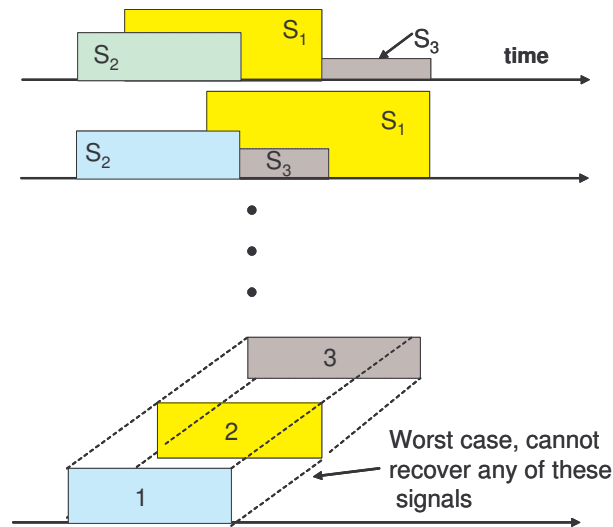


Figure 4-9. Performance of large and small FSK signals at SIR = 7 dB.

### 4.3.3 Case 2. Performance of SIC for decoding *three* overlapping co-channel FSK signals

This section provides the results for *Case 2*, which shows how an SIC receiver can decode *three* overlapping co-channel FSK signals. In *Case 2*, we assume that *three* co-channel signals overlap each other. We let  $S_1$ ,  $S_2$ , and  $S_3$  to represent the large, medium, and small signals, respectively. Figure 4-10 illustrates several possible configurations of how the *three* co-channels overlap.



**Figure 4-10. Three co-channel signal overlaps.**

The performance of each FSK signal is shown in Figures 4-11 through 4-15. Similar to *Case 1*, Figure 4-11 shows that the performance of each of the three signals is significantly dependent on SIR. Again, this is why when three co-channel signals with equal powers overlap one another entirely; neither signal can be recovered, as illustrated in Figure 4-10. In general, the performance is poor for low SIRs. As SIR increases, the performance of each signal improves, until an optimum point (around 6-7 dB) is reached, then the noise starts to dominate the SIR and degrades the performance of the small and medium signals. However, the performance of the large signal always continues to get better for higher SIRs because interference from the small and medium signals becomes smaller for larger SIRs.

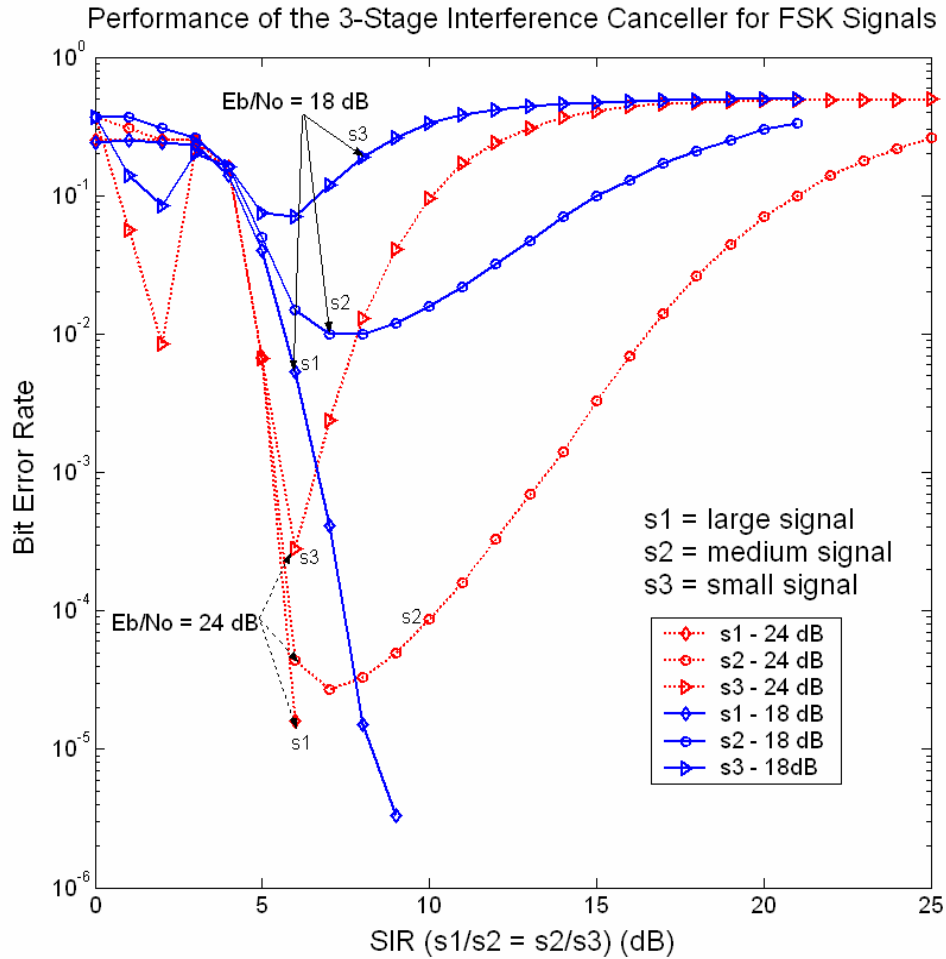


**Figure 4-11. BER vs SIR performance of the three B-FSK signals.**

The results in Figure 4-12 show that in order to achieve ideal performance, an SIR of 19 dB is needed. This is because the medium and small signals always interfere with the large signal. However, decent performance can be achieved with SIR equal to 10 dB.



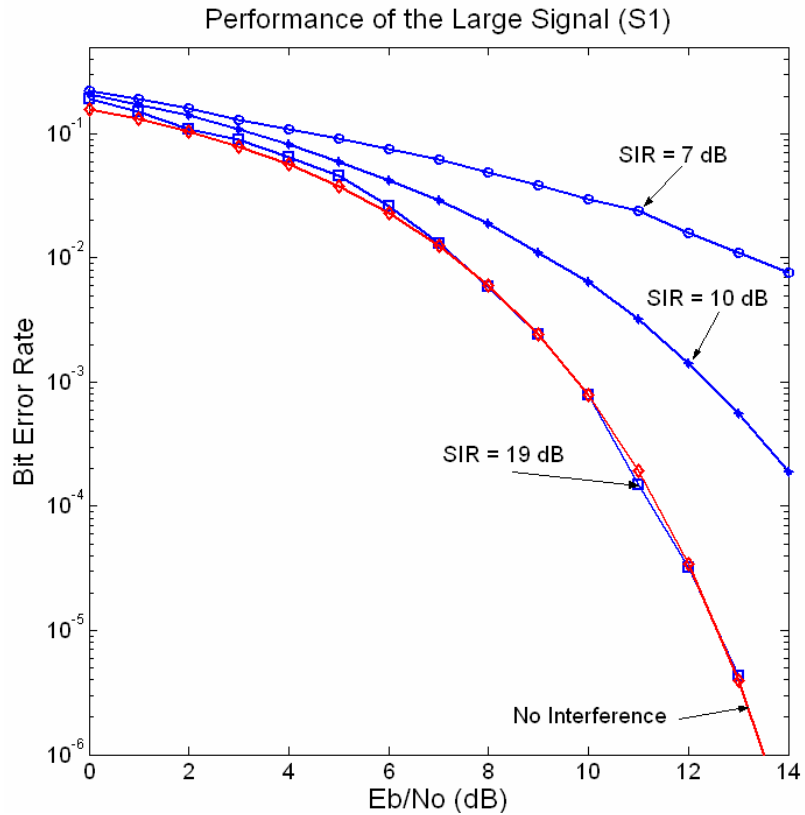


**Figure 4-12. Performance of the large B-FSK signal.**

The results in Figure 4-13 indicate that the performance of the medium signal requires about 18 dB of SIR to obtain ideal performance. However, any SIRs at or above 10-12 dBs would provide decent performance.

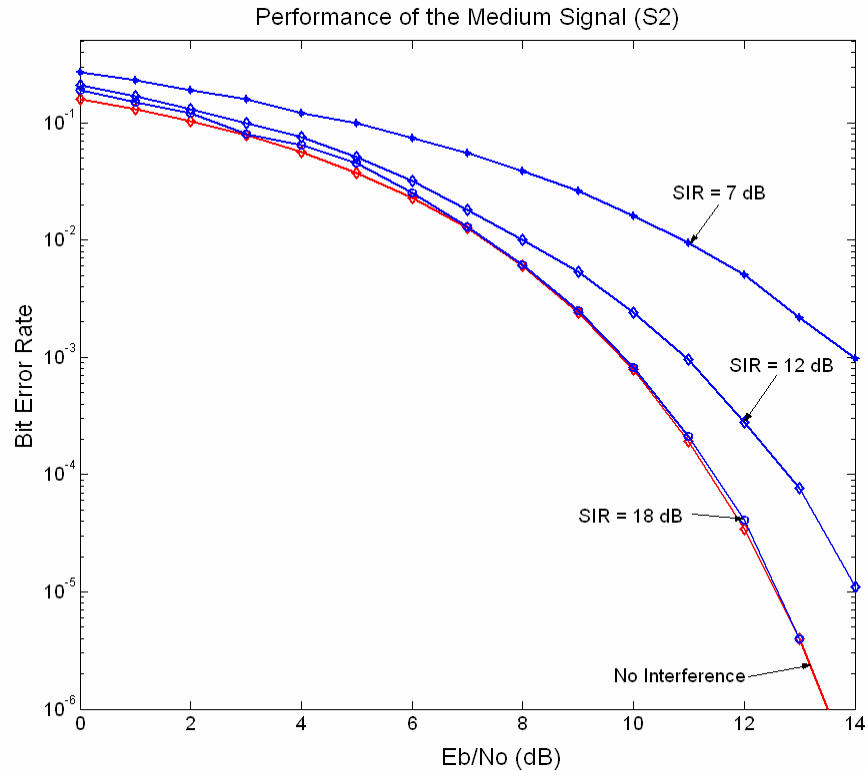


**Figure 4-13. Performance of the medium B-FSK signal.**

As for the small signal, an SIR of 6 dB is sufficient to obtain ideal performance, as shown in Figure 4-14. However, note that the small signal is more sensitive to SIR in *Case 2* as compared to *Case 1*. With a small decrease of SIR to 5 dB, the performance becomes much worse. This is because of the correlated noise and residual interference from the other two signals propagating from the preceding stages.

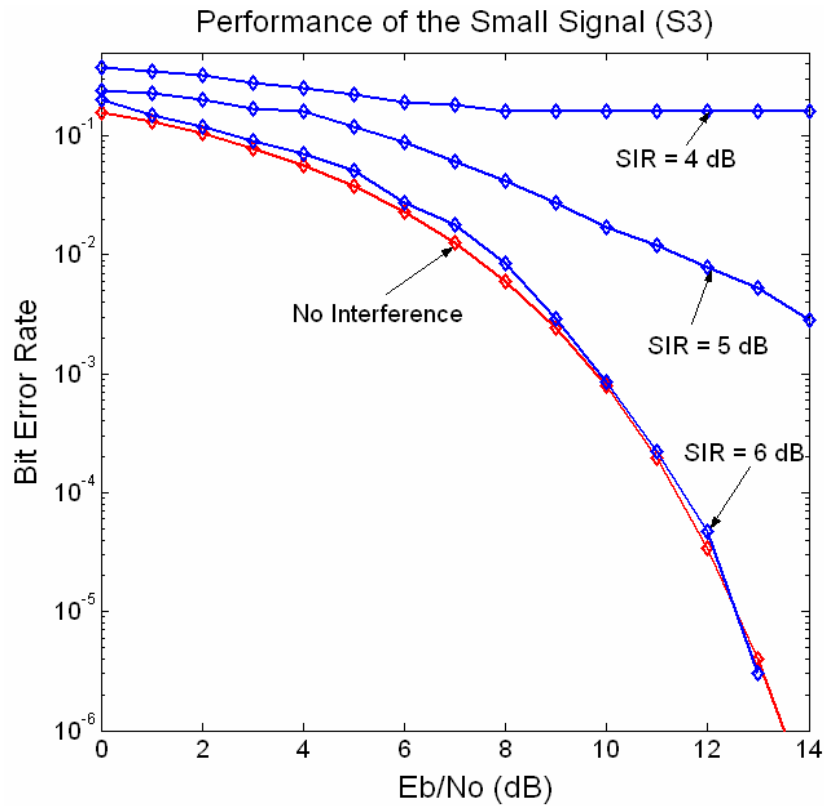


**Figure 4-14. Performance of the small B-FSK signal.**

Figure 4-15 shows the performance of all three signals at SIR equal to 7 dB. It can be seen that in order to decode all three signals successfully at a low bit error rate, a cost of 8 dBs in  $E_b/N_o$  beyond ideal performance is expected. However, if SIR is increased 10 dB for example, the performance will improve to be within 2-3 dBs from ideal, as shown in Figure 4-12.

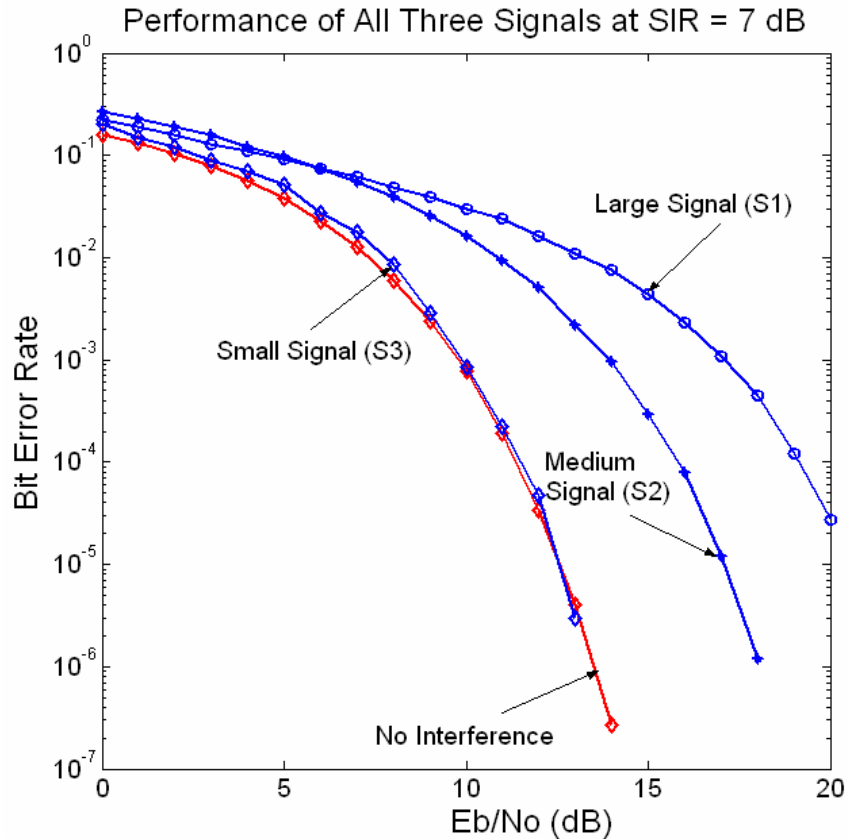


Figure 4-15. Performance of all three signals at SIR = 7 dB.

In general, we showed in *Case 2* that it is possible to decode three overlapped co-channel signals. However, signal-to-noise ratio ( $E_b/N_o$ ) must be increased by several dBs to achieve desirable performance. Although there is a small cost in performance, we emphasize that this is a significant improvement from today's radio, which cannot decode multiple signals.

#### 4.4 SIC based on B-PSK De/modulation

The previous section performs simulations and analyses based on frequency modulated signal, which is the modulation of choice for this particular avionic communication system under investigation. Other commercial, civil and military communication systems might use phase modulations. This section further investigates the use and the performance of SIC using binary phase shift keying (B-PSK) modulation and demodulation method.

### 4.4.1 Analytical performance evaluation

The derivation for probability of bit errors for B-PSK is similar to that of B-FSK, except that the Q function is now equal to

$$Pe_{BPSK} = Q\left(\sqrt{\frac{2E_b}{N_0}}\right) \quad \text{Eq. 4.29}$$

therefore the probability of error for the large signal then becomes:

$$Pe_{l_{arg e}, BPSK} = \frac{1}{4\pi} \int_0^{2\pi} \int_0^{0.5} \frac{1}{4} \sum_{\text{All States of } A_{large, m} \& A_{l_{arg e}, m+1}} Q\left[\sqrt{\frac{2E_{b_{l_{arg e}}}}{N_0}} \left[1 + \frac{(|\Delta| a_{small, n} + (1-|\Delta|) a_{small, n+1}) \cos(\theta_{l_{arg e}} - \theta_{small})}{\sqrt{SIR_{l_{arg e}}}}\right]\right] \quad \text{Eq. 4.30}$$

$$d|\Delta| d(\theta_{l_{arg e}} - \theta_{small}) d|\Delta| d(\theta_{l_{arg e}} - \theta_{small})$$

And the probability of error for the small signal then becomes:

$$Pe_{small, BPSK} = \frac{1}{4\pi} \int_0^{2\pi} \int_0^{0.5} \left( (1 - Pe_{l_{arg e}})^2 \times \sum Q\left[\sqrt{\frac{2E_{b_{small}}}{N_0}} \times \left[1 + \frac{(|\Delta| \gamma_{l_{arg e}, m-1} + (1-|\Delta|) \gamma_{l_{arg e}, m}) \cos(\theta_{l_{arg e}} - \theta_{small})}{\sqrt{SIR_{small}}}\right]\right]\right) +$$

$$2Pe_{l_{arg e}}(1 - Pe_{l_{arg e}}) \times \sum \sum Q\left[\sqrt{\frac{2E_{b_{small}}}{N_0}} \times \left[1 + \frac{(|\Delta| \alpha_{l_{arg e}, m-1} a_{l_{arg e}, m-1} + (1-|\Delta|) \alpha_{l_{arg e}, m} a_{l_{arg e}, m}) \cos(\theta_{l_{arg e}} - \theta_{small})}{\sqrt{SIR_{small}}}\right]\right] +$$

$$Pe_{l_{arg e}}^2 \times \sum Q\left[\sqrt{\frac{2E_{b_{l_{arg e}}}}{N_0}} \times \left[1 + \frac{(|\Delta| \kappa_{l_{arg e}, m-1} + (1-|\Delta|) \kappa_{l_{arg e}, m}) \cos(\theta_{l_{arg e}} - \theta_{small})}{\sqrt{SIR_{small}}}\right]\right] \quad \text{Eq. 4.31}$$

$$d|\Delta| d(\theta_{l_{arg e}} - \theta_{small})$$

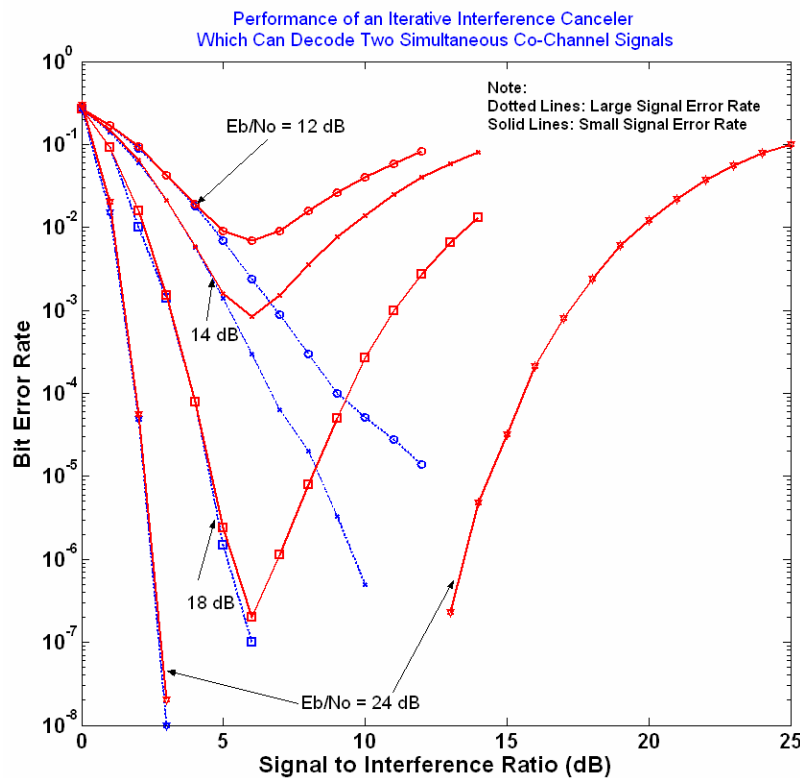
where the single summation depicts all states of  $a_{large, m-1}$  &  $a_{l_{arg e}, m}$  and the double

summation depicts all states of  $\alpha_{l_{arg e}, m-1}$  and  $\alpha_{l_{arg e}, m}$  and  $a_{large, m-1}$  &  $a_{l_{arg e}, m}$ .

### 4.4.2 Case 1. Performance of SIC for decoding two overlapping co-channel B-PSK signals

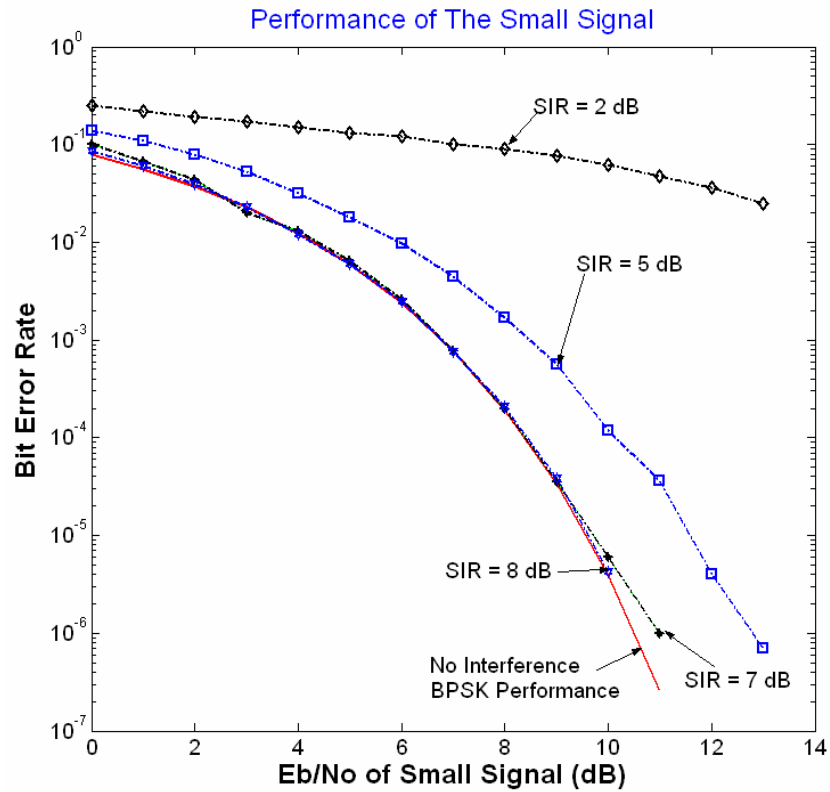
These two B-PSK signals arrive at the interference cancellation receiver as depicted in Figure 4-2, and their performance is shown in Figures 4-16 through 4-19. Figure 4-10 shows that the performance of the two signals are very dependent on how

much separation their power levels have (Signal to Interference Ratio [SIR]). In general, the performance of both signals is poor for low SIRs. As SIR increases, the performance of each signal improves, until an optimum point (around 6-7 dB) is reached, where the noise starts to dominate the SIR and degrades the performance of the small signal. However, the performance of the large signal keeps improving for higher SIRs because a larger separation (SIRs) between the signals results in a small interference coming from the small signal. This behavior is similar to FSK signaling shown in Figure 4-11.



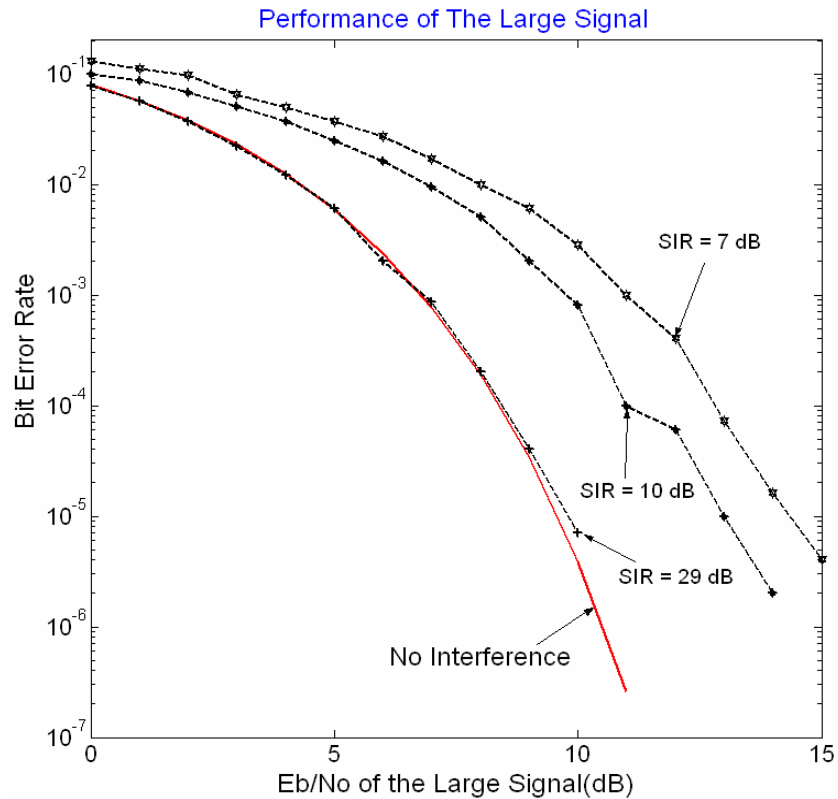
**Figure 4-16. BER vs SIR performance of the two B-PSK signals.**

Figure 4-17 focuses on the performance of the small signal. It can be seen that when the error probability of the large signal is sufficiently low, the performance of the small signal is influenced mainly by noise. The performance results in Figure 4-17 show that only about 7 dB of separation in power (SIR) is needed to obtain ideal performance of the small signal.



**Figure 4-17. Performance of the small B-PSK signal.**

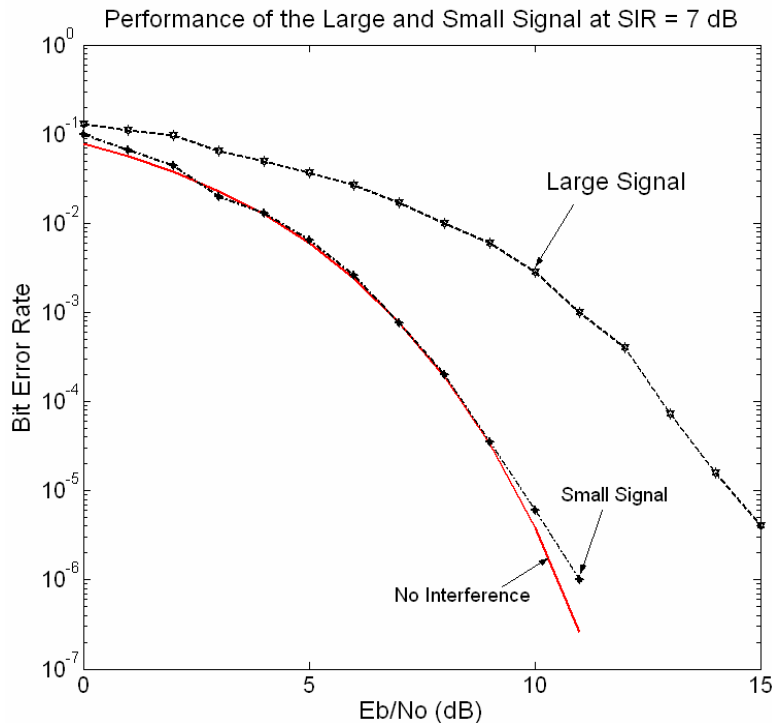
Figure 4-18 shows the performance of the large signal. An SIR of about 29 dB is needed to have ideal performance. This is because the small signal always interferes with the large signal. However, an SIR of 10 dB can lead to decent performance within 2-3 dBs of ideal performance.



**Figure 4-18. Performance of the large B-PSK signal.**

Figure 4-19 shows the composite performance of both large and small signals at an SIR of 7 dB. We select 7 dB to represent the optimum SIR as illustrated in Figure 4-16. It is important to note that with a small degradation of about 4.5 dB of the large signal, the two co-channel signals can in fact be decoded simultaneously with low probability of error. If SIR is increased to 10 dB, the performance is expected to improve to be within 2-3 dBs from ideal performance. This is a significant improvement from today's radio which cannot perform multi-signal decoding on a single channel.

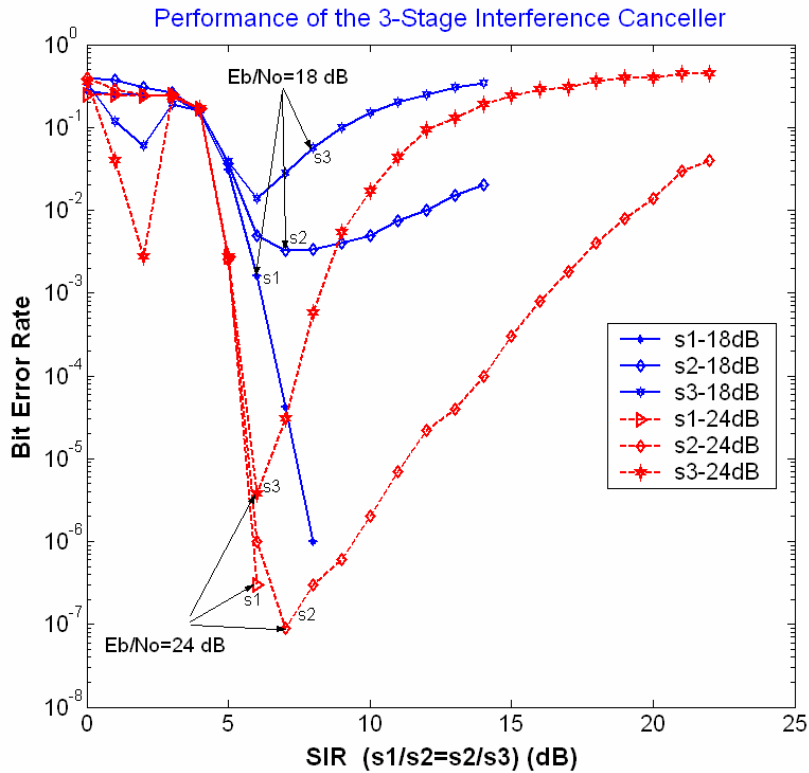




**Figure 4-19. Performance of large and small B-PSK signals at SIR = 7 dB.**

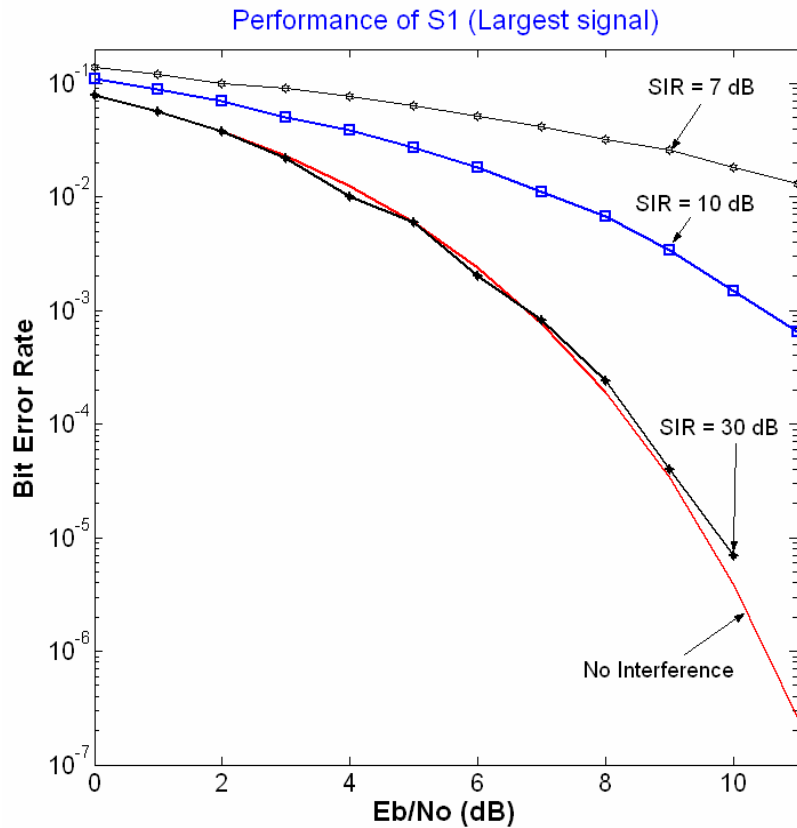
#### 4.4.3 Case 2. Performance of SIC for decoding three overlapping co-channel B-PSK signals

The performance of each of the three signals is shown in Figures 4-20 through 4-25. Figure 4-20 shows that the performance of each of the three signals is very dependent on SIR. Again, the performance is poor for low SIRs. As SIR increases, the performance of each signal improves, until an optimum point (around 6-7 dB) is reached, then the noise starts to dominate the SIR and degrades the performance of the small and medium signals. However, the performance of the large signal always continues to get better for higher SIRs because interference from the small and medium signals becomes smaller for larger SIRs.



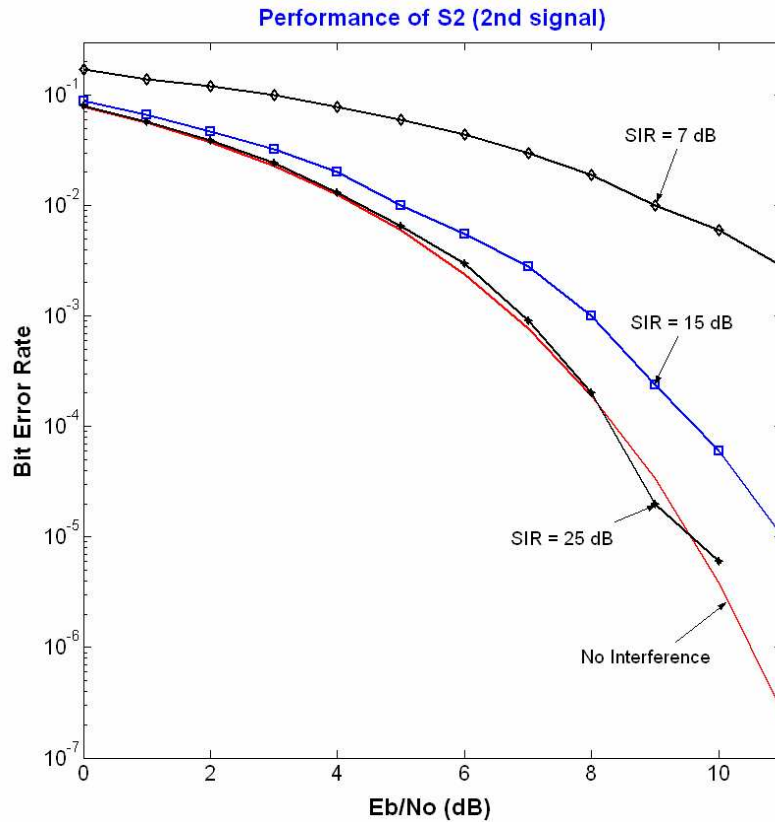
**Figure 4-20. BER vs SIR performance of the two signals.**

Figure 4-21 shows the performance of the large signal. In order to achieve ideal performance, an SIR of 30 dB is needed. This is because the medium and small signals always interfere with the large signal. However, a decent performance can be achieved for SIR at about 14-15 dB.



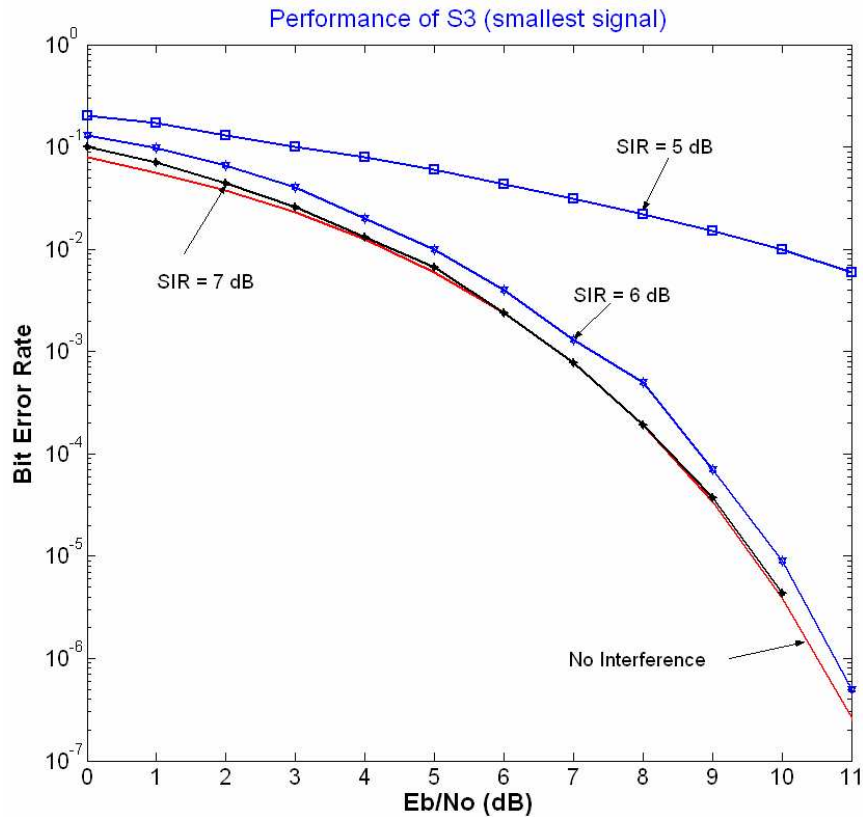
**Figure 4-21. Performance of the large B-PSK signal.**

Figure 4-22 shows that the performance of the medium signal requires about 25 dB of SIR to obtain ideal performance. However, an SIR at or above 14-15 dB provides decent performance.



**Figure 4-22. Performance of the medium B-PSK signal.**

As for the small signal, an SIR of 6-7 dB is sufficient to obtain ideal performance. However, note that the small signal is more sensitive in *Case 2* as compared to *Case 1*, as shown in Figure 4-23. With a small decrease of SIR to 5 dB, the performance becomes much worse. This is because of the correlated noise and residual interference from the other two signals propagating through the preceding stages.



**Figure 4-23. Performance of the small B-PSK signal.**

Figure 4-24 shows the performance of all three signals at SIR equal to 7 dB. So in order to decode all three signals successfully at low bit error rate, a cost of 9 dB in  $E_b/N_o$  above ideal performance as expected. However, if SIR is increased to 10 dB, as shown in Figure 4-25, the cost reduces significantly to about 4.5 dB. Higher SIRs would certainly reduce the performance cost to a lower value.

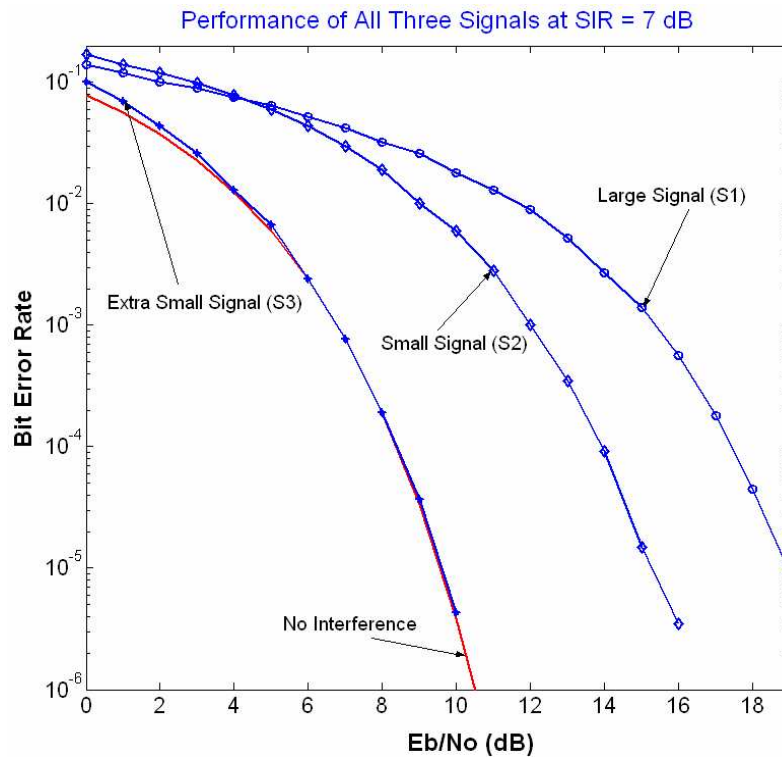


Figure 4-24. Performance of all three B-PSK signals at SIR = 7 dB.

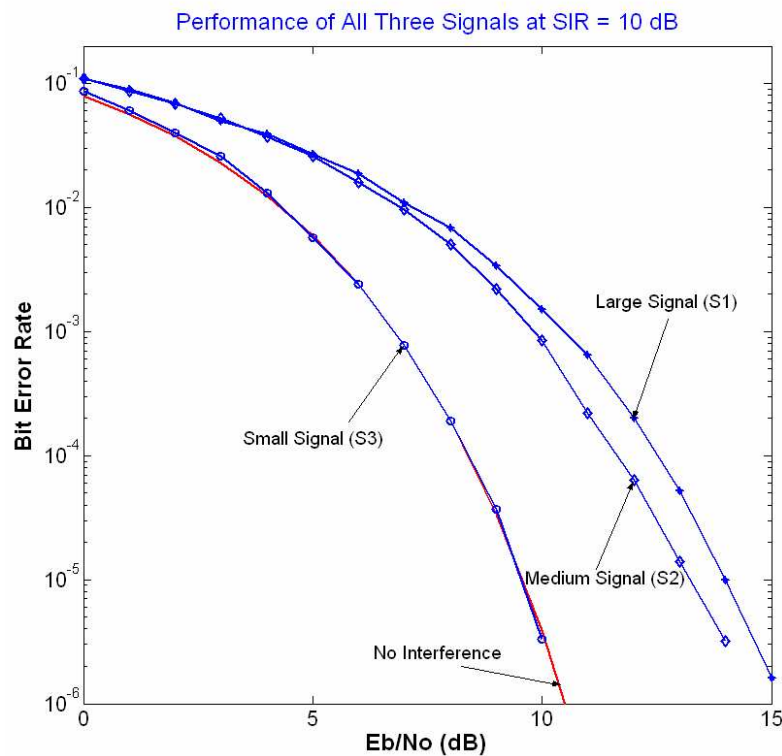


Figure 4-25. Performance of all three B-PSK signals at SIR = 10 dB.

## 4.5 Conclusion and recommendation

This chapter presents an interference cancellation technique and findings that hold the key to increasing aeronautical communication system capacity and allowing for a more efficient use of the scarce spectrum resources for aeronautical mobile communication applications. This chapter also presents a simple radio receiver architecture with powerful interference cancellation capability, and shows how this special receiver can successfully decode multiple overlapping co-channel signals on a single channel; a capability not available in today's avionic radio receivers.

The interference cancellation receiver performs well, especially in heavy-traffic environments that exhibit strong co-channel interference (e.g., the heavy-traffic aeronautical mobile environment that contains thousands of aircraft around Los Angeles airport). This special receiver can recover very weak signals that might be completely buried inside much stronger ones. We demonstrate the multi-signal decoding capability of the interference cancellation receiver based on various performance graphs for different values of signal-to-interference (SIR) ratios.

We found that the multi-signal decoding capability for *three* FSK signals can be achieved at a small cost of about 2 to 3 dBs in system performance when there is sufficient separations ( $SIR \geq 10 \text{ dB}$ ) among interfering signals. Operating at SIRs below 10 dB is also possible; however it requires a small additional performance cost. For example, that additional cost is about 2 dBs for SIR equal to 7 dB. As for BPSK signals, the cost is 2-3 dBs higher than that of the FSK case.

In evaluating the interference cancellation capability for both FSK and B-PSK de/modulations, we found that decoding *two* co-channels signals only requires SIR to be in the range from 7-10 dB to achieve decent performance, as shown in Table 4-1. However, the decoding of three signals requires an additional 2-3 dBs to achieve decent performance. We notice that the small signal, although buried inside more powerful signals, requires the least SIR. This is because interference from other signals has been

successfully extracted out from the preceding stages.

We also note that B-PSK seems to be more sensitive and less robust than FSK when using this interference cancellation technique. As shown in Table 4-1, an SIC receiver using B-PSK is penalized more in  $E_b/N_o$  as compared to SIC using B-FSK. For example, when three co-channel signals overlap, decoding the large signal (SIR=10 dB) costs 4-5 dBs while the cost is only around 2-3 dBs for FSK signal, decoding the medium B-FSK signal cost 4-5 dBs while that cost is only 2-3 dBs for B-FSK, the small signal can be decoded ideally for the B-PSK signal when SIR is conditioned at least 7 dB while it only requires 6 dBs for B-FSK signal.

**Table 4-1. SIC Receiver capability for B-FSK and B-PSK signals**

Modulation/ Demodulation Types	2-Signal Decoding Capability		3-Signal Decoding Capability		
	Large Signal	Small Signal	Large Signal	Medium Signal	Small Signal
<b>B-PSK</b>	<ul style="list-style-type: none"> <li>• SIR=7 dB, costs 4-5 dB's</li> <li>• SIR=10 dB, costs 2-3 dB's</li> </ul>	SIR=7 dB, ideal	<ul style="list-style-type: none"> <li>SIR=10 dB, costs 4-5 dB's</li> <li>SIR=15 dB, costs 2-3 dB's</li> </ul>	<ul style="list-style-type: none"> <li>• SIR=10 dB, costs 4-5 dB's</li> <li>• SIR=15 dB, costs 2-2.5 dB's</li> </ul>	SIR=7 dB, ideal
<b>B-FSK</b>	<ul style="list-style-type: none"> <li>• SIR=7 dB, costs 4-4.5 dB's</li> <li>• SIR=10 dB, costs 2-3 dB's</li> </ul>	SIR = 7 dB, ideal	<ul style="list-style-type: none"> <li>• SIR=7 dB, costs 7-9 dB's</li> <li>• SIR=10 dB, costs 2-3 dB's</li> </ul>	<ul style="list-style-type: none"> <li>• SIR=7 dB, costs 4-4.5 dB's</li> <li>• SIR=10 dB, costs 2-3 dB's</li> </ul>	SIR=6 dB, ideal

This interference cancellation technique benefits from its simple implementation and substantial performance improvement. Research needs to be done to investigate the sensitivity of this technique to incorrect estimates of phase, frequency and amplitude fluctuations, or apply this technique to other broadband multiple access schemes such as CDMA or OFDM.



## 4.6. Acknowledgement

This chapter, in part, is a reprint of the material that appears in the following conference and journal publications, in which the dissertation author was the primary author for these papers.

- M. Nguyen, A. Zaghoul, “High-Quality Communication in Heavy-Traffic ATC Environment Using Interference Cancellation Receiver”, accepted, to be published in the *Proceedings of twenty-fourth IEEE Digital Avionics System Conference*, Washington, DC, October 30<sup>th</sup> - November 3<sup>rd</sup>, 2005.
- M. Nguyen, A. Zaghoul, “Interference Cancellation Receiver,” *NASA’s Integrated Communications, Navigation and Surveillance (I-CNS) Conference*, Fairfax, Virginia, May 2-6, 2005.

## Chapter 5 : Parallel Interference Cancellation (PIC) Receiver

This chapter investigates the performance of another interference cancellation technique, namely parallel interference cancellation, which can also be used to solve the co-channel interference problem.

### 5.1 PIC receiver structure

A communication receiver structure that is capable of performing parallel interference cancellation is shown in Figure 5.1. The interference cancellation is performed in parallel between the stages, rather than sequentially as shown in Chapter 4. We assume that all co-channel signals in the collisions are desired signals and therefore will all be decoded eventually. However, while decoding one particular signal of interest (desired signal), other signals will be treated as interferers. The parallel interference cancellation works as follows. Multiple overlapping co-channel signals, or the composite

signal  $r(t) = \sum_{i=1}^k s_i$ , arrive at the receiver having  $k$  users' signals overlapping each other.

Signal  $s_1$  will be decoded first due to its highest energy level, as compared to other signals. The decoded bit stream of signal  $s_1$  is then remodulated, estimated and subtracted from the composite signal  $r(t)$ . The second signal can then be decoded without interference of the first, however, still with interference of other subsequent signals. The PIC cancellation operation of signal  $s_1$  and  $s_2$  is similar to SIC operation. However, the operation of subsequent stages is different. The third signal is demodulated by removing interference from  $s_1$  and  $s_2$  simultaneously. Similarly, the fourth signal is then demodulated by simultaneously removing interference from  $s_1$  and  $s_2$  and  $s_3$ . The operation of subsequent stages can be done in a similar manner.

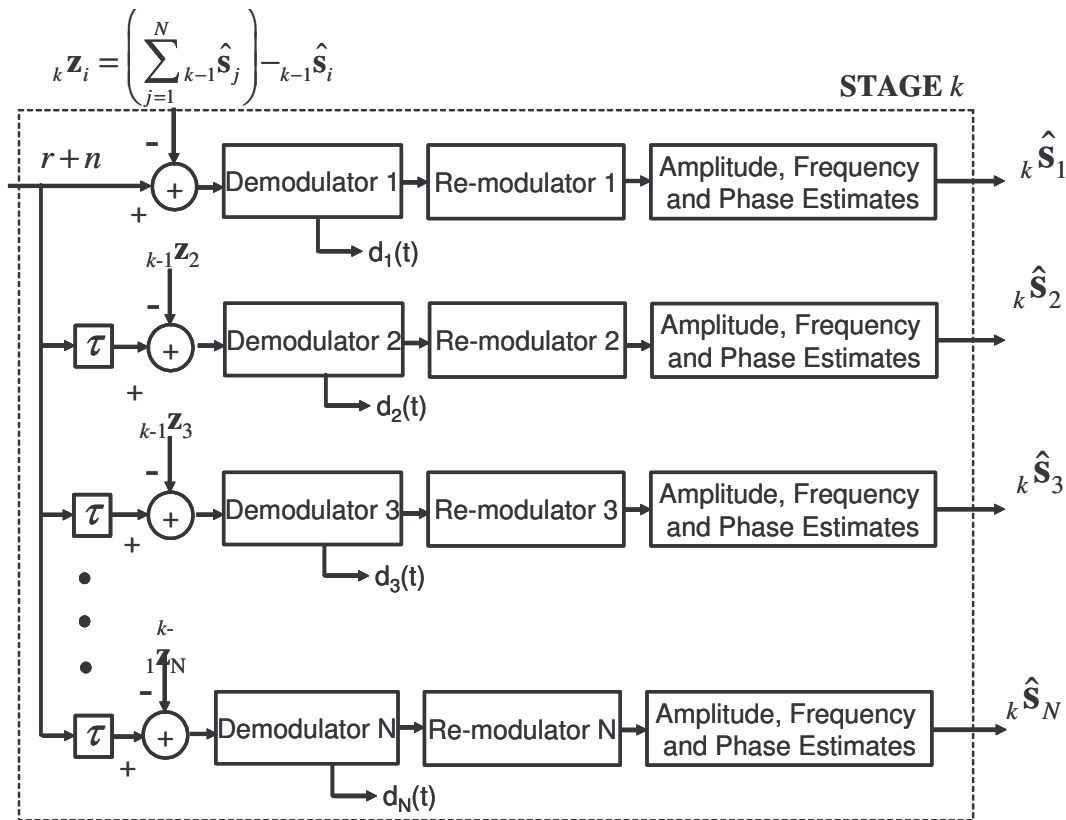


Figure 5-1. Parallel Interference Cancellation Receiver Structure

## 5.2 Simulation assumptions

Assumptions for PIC simulation are similar to those used for SIC in Chapter 4. It is repeated here for convenience. The simulation is based on the Monte Carlo computer simulation technique to show how the interference cancellation receiver can decode multiple overlapping co-channel signals simultaneously for the following two cases:

- *Case 1:* Interference cancellation receiver capable of decoding *two* co-channel Binary- FSK signals
- *Case 2:* Interference cancellation receiver capable of decoding *three* co-channel binary-FSK signals

A simulation model is developed using Matlab/Simulink based on the following

assumptions:

- Non-spread signaling scheme (CDMA signals are not yet considered)
- System is synchronous in order to analyze a worst-case lower-bound performance. (Note: An asynchronous system would be expected to perform better since signals do not overlap one another entirely);
- All co-channel signals are desired signals with similar signaling formats: modulation, carrier frequency and message formats are exactly the same (although information bits are different);
- The channels are ideal with additive white Gaussian noise (AWGN);
- Perfect cancellation of the larger signals provided by ideal recovery of system parameters: amplitude, frequency and phase have been correctly estimated before subtraction. Therefore, after subtraction, the smaller signals are only corrupted by AWGN;
- The information bits are uniformly distributed with equally probability of 0s and 1s.

### 5.3 PIC based on B-FSK De/modulation

#### 5.3.1 Case 1. Performance of PIC for decoding two overlapping co-channel B-FSK signals

*Case 1* demonstrates PIC interference cancellation capability using binary FSK modulation and demodulation method. Figure 5-2 shows the receiver structure for decoding two overlapping co-channel FSK signals. Figure 5-3 illustrates how these two signals can overlap for different configurations. One signal is the large signal and is denoted as  $S_1$ ; the other is the small signal and is denoted as  $S_2$ . Together, they create mutual interference on one another when overlaps occur.

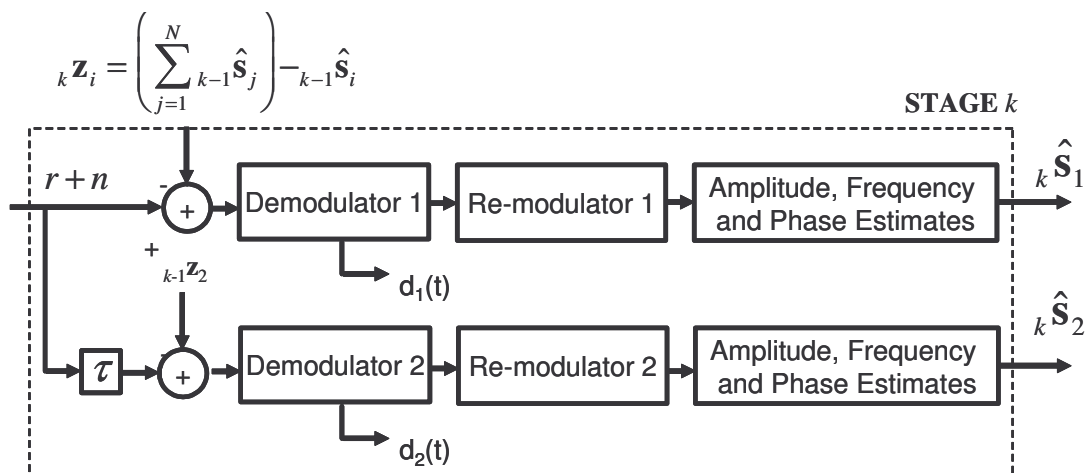


Figure 5-2. PIC Structure to Decode two Co-channel FSK Signals

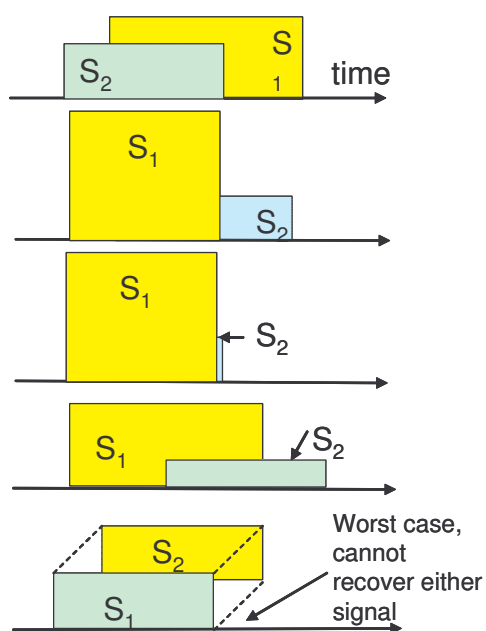
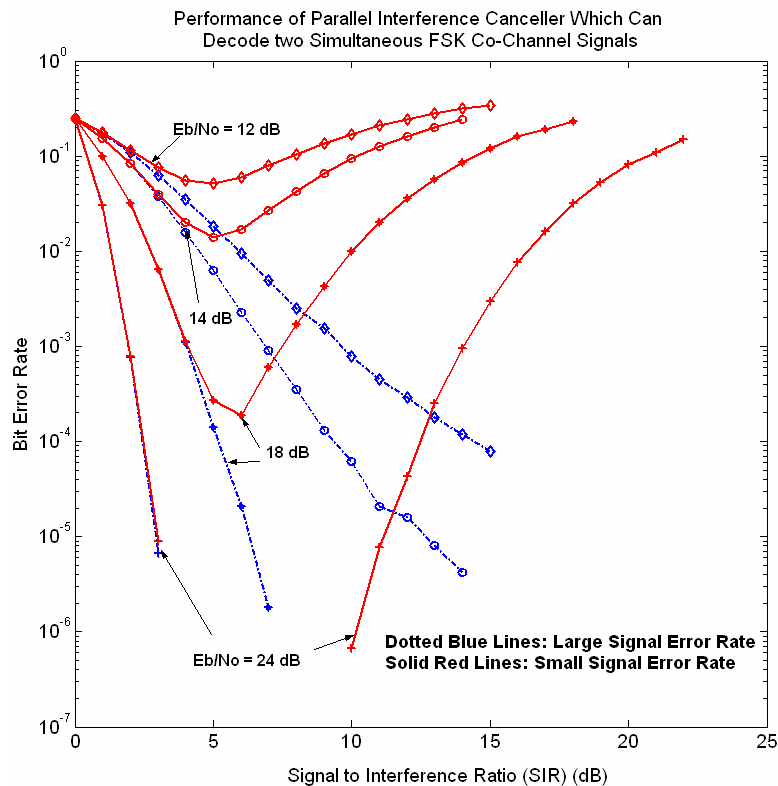


Figure 5-3. Some overlapping configurations of Two Signals

These two FSK signals arrive at the interference cancellation receiver as described in Figure 5-1, and their performance is shown in Figures 5-4 through 5-8.

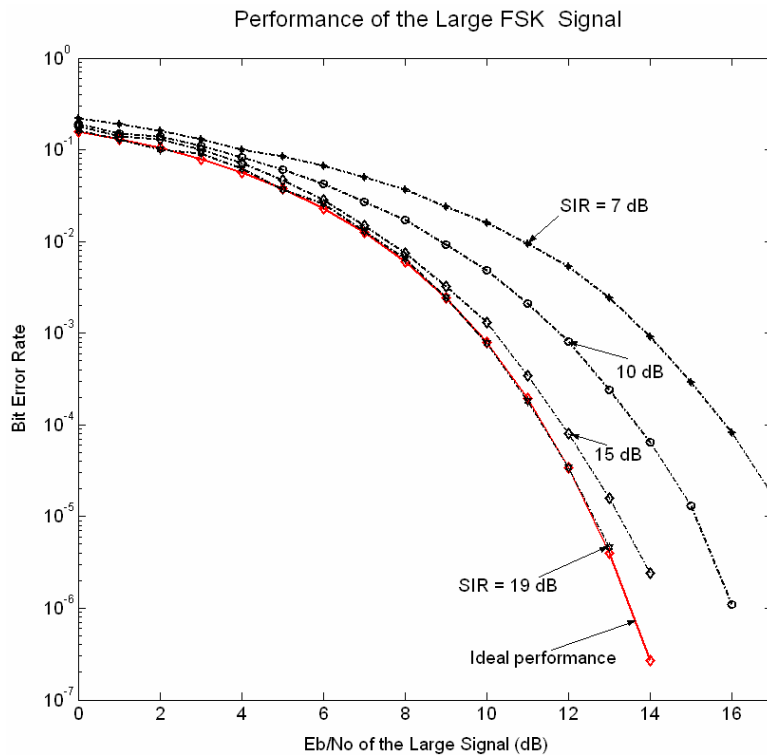
Figure 5-4 shows that the performance of the two signals is very dependent on the amount of separation between their received power levels (Signal to Interference Ratio [SIR]). Therefore, when two signals with equal power overlap each other entirely, neither

one can be recovered, as shown in Figure 5-3. In general, the performance of both signals is poor for low SIRs. As SIR increases, the performance of each signal improves, until an optimum point of about 6 dB is reached, where the noise starts to dominate the SIR and degrades the performance of the small signal. However, the performance of the large signal keeps improving for higher SIRs because a larger separation (SIRs) between the signals results in a small interference coming from the small signal.



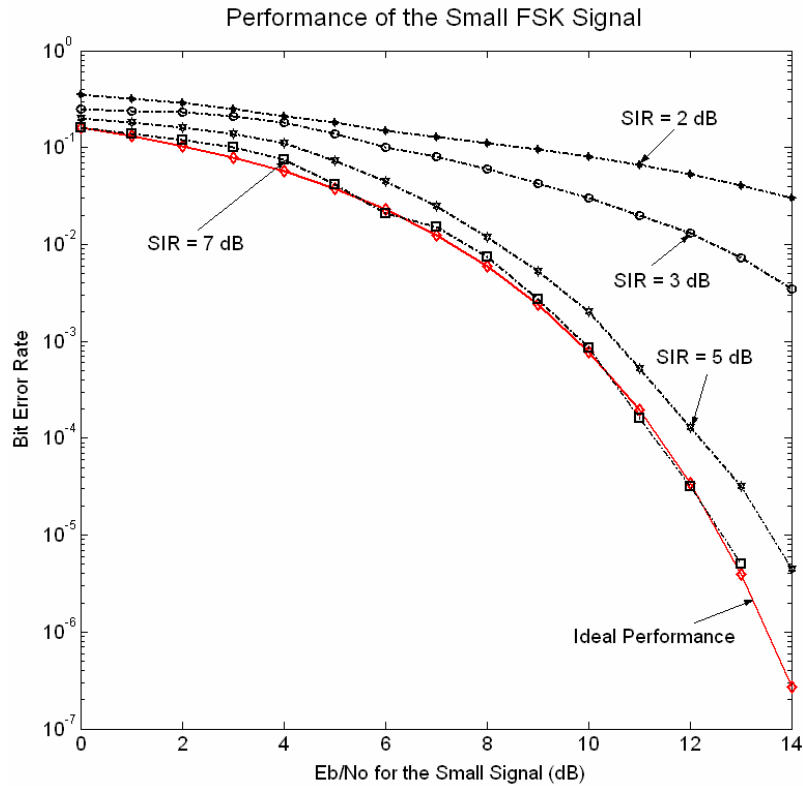
**Figure 5-4. BER vs SIR performance of two overlapping B-FSK signals (PIC)**

Figure 8 shows the performance of the large signal. It can be seen that an SIR of about 19 dB is needed to achieve ideal performance. This is because the small signal always interferes with the large signal. However, an SIR of about 10 dB can result in decent performance, where decent performance refers to performance within 2-3 dBs from ideal performance.



**Figure 5-5. Performance of the large B-FSK signal (PIC)**

Figure 5-6 focuses on the performance of the small signal. It can be seen that when the error probability of the large signal is sufficiently low, the performance of the small signal is influenced mainly by noise. The performance results show that only about 7 dB of separation in power (SIR) is needed to obtain ideal performance of the small signal; where ideal performance is defined to be the optimum system performance in the presence of AWGN (interference is not included).



**Figure 5-6. Performance of the small B-FSK signal (PIC)**

Figure 5-7 shows the composite performance of both large and small signals at an SIR of 7 dB. We select 7 dB to represent the optimum SIR as illustrated in Figure 5-4. It is important to note that with a small degradation of about 4.5 dB of the large signal, the two co-channel signals can in fact be decoded simultaneously with low probability of error. Therefore, any separation (SIR) greater than 7 dB certainly improves the performance. For example, a separation of 10 dB results in performance only 2 – 2.5 dBs from ideal performance, as shown in Figure 5-8. This is a significant improvement from most of today's radios, which cannot perform this multi-signal decoding function on a single channel.



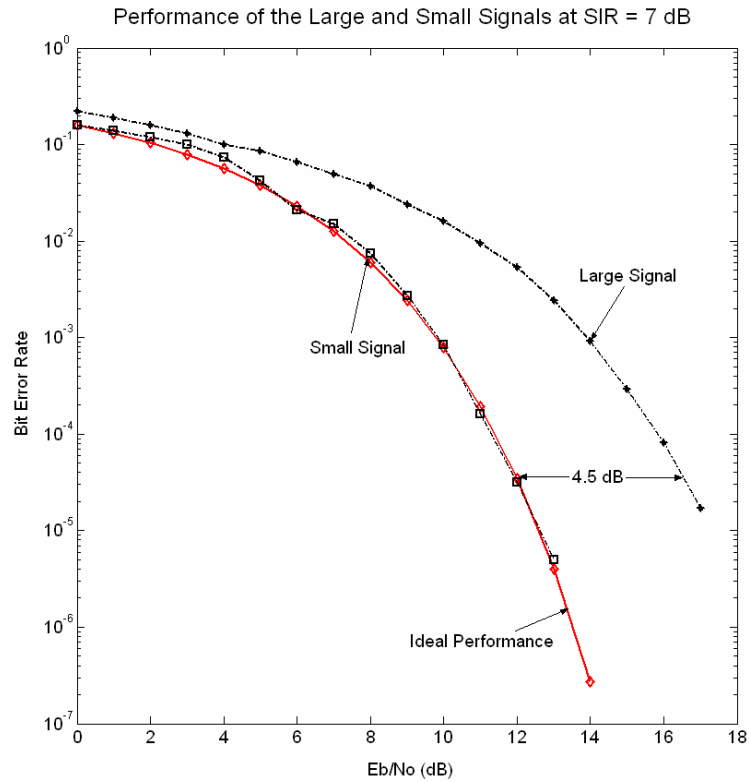


Figure 5-7. Performance of large and small signals at SIR = 7 dB

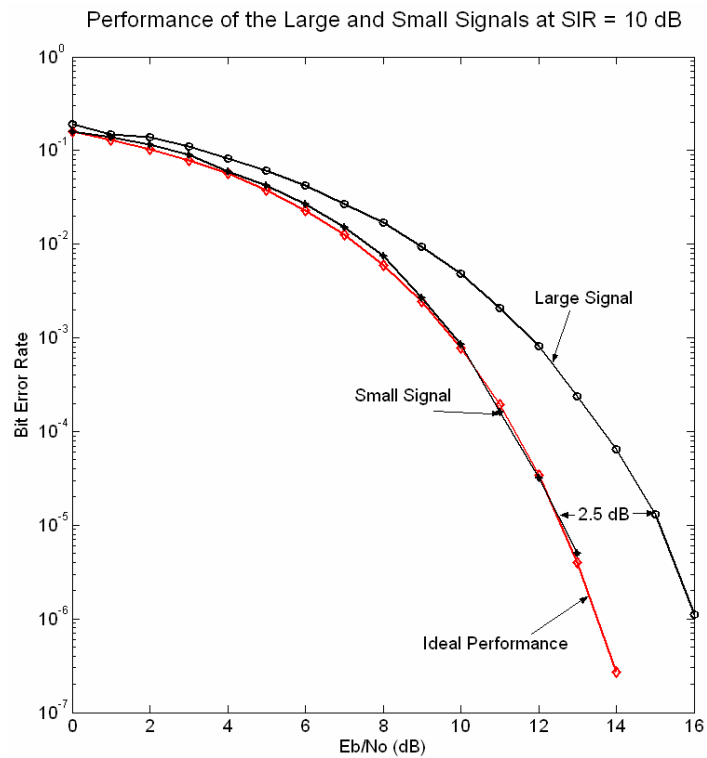


Figure 5-8. Performance of large and small signal at SIR = 10 Db

### 5.3.2 Case 2. Performance of PIC for decoding *three* overlapping co-channel B-FSK signals

Case 2 demonstrates the PIC interference cancellation capability based on FSK modulation and demodulation for *three* overlapping co-channel signals. We denote  $S_1$ ,  $S_2$ , and  $S_3$  to represent the large, medium, and small signals, respectively. Figure 5-9 shows the PIC receiver structure for decoding three overlapping co-channel FSK signals and Figure 5-10 illustrates several possible configurations of how the *three* co-channels overlap.

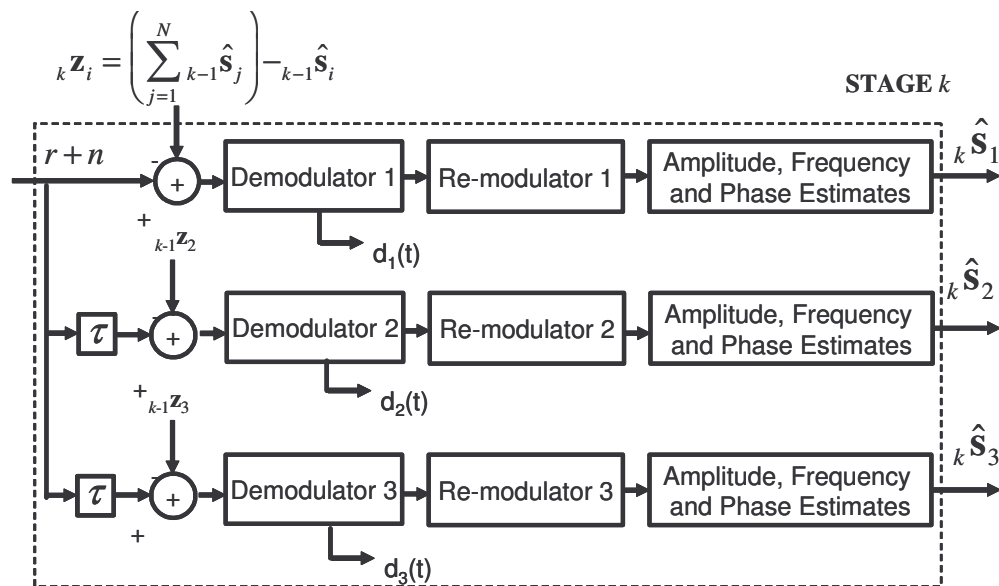
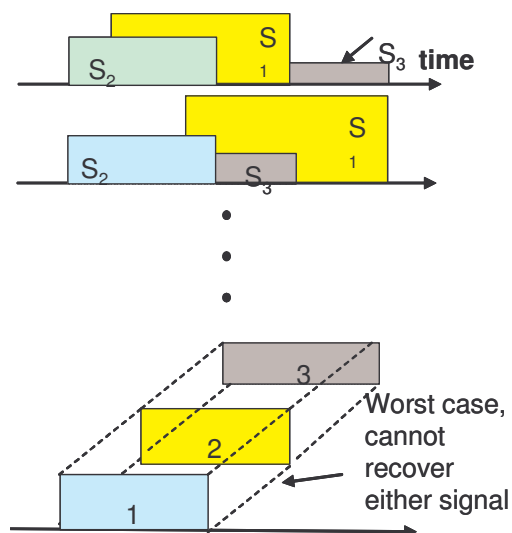
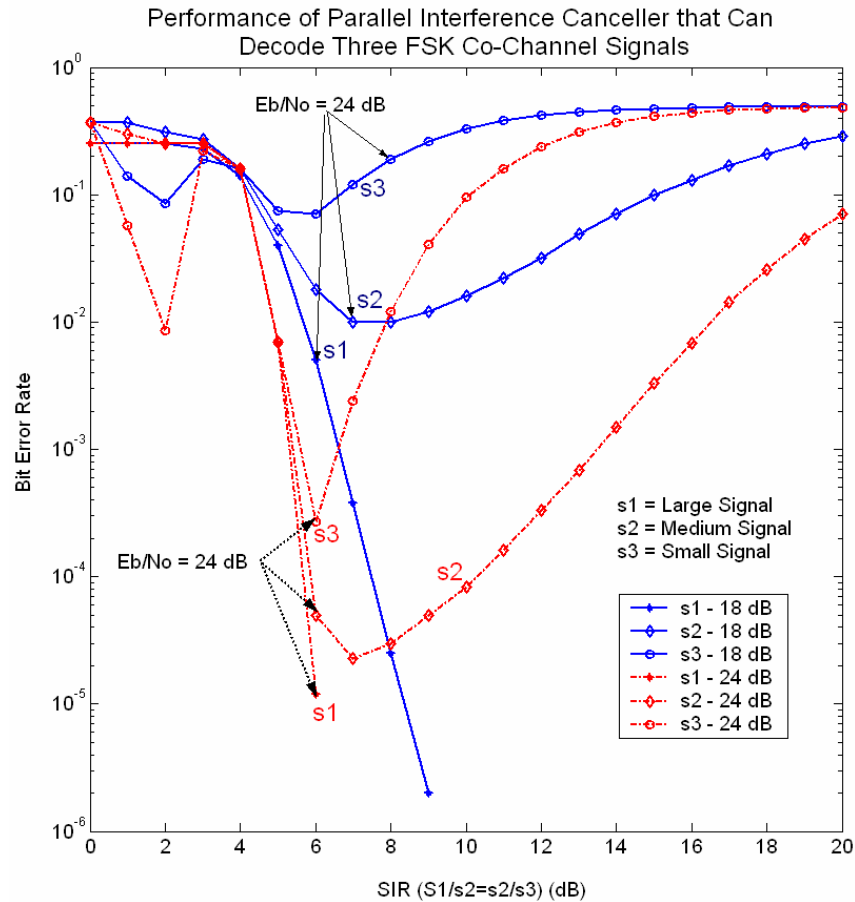


Figure 5-9. PIC structure to decode three overlapping FSK signals



**Figure 5-10. Several overlapping configurations for three signals**

The performance of each FSK signal is shown in Figures 5-11 through 5-14. Similar to *Case 1*, Figure 5-11 shows that the performance of each of the three signals is significantly dependent on SIR. Again, this is why when three co-channel signals with equal powers overlap one another entirely; neither signal can be recovered, as illustrated in Figure 5-10. In general, the performance is poor for low SIRs. As SIR increases, the performance of each signal improves, until an optimum point (around 6-7 dB) is reached, then the noise starts to dominate the SIR and degrades the performance of the small and medium signals. However, the performance of the large signal always continues to get better for higher SIRs because interference from the small and medium signals becomes smaller for larger SIRs.



**Figure 5-11. BER vs SIR performance of the three B-FSK signals.**

The results in Figure 5-12 show that in order to achieve ideal performance, an SIR of 19 dB is needed. This is because the medium and small signals always interfere with the large signal. However, decent performance can be achieved with SIR equal to 10 dB.

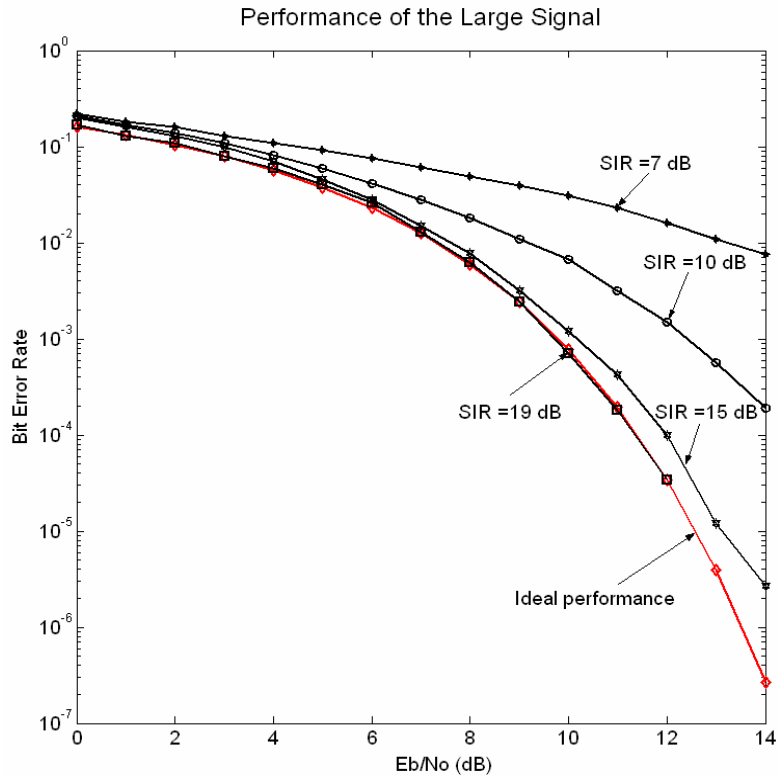


**Figure 5-12. Performance of large B-FSK signal (PIC)**

The results in Figure 5-13 indicate that the performance of the medium signal requires about 18 dB of SIR to obtain ideal performance. However, any SIRs at or above 10-12 dB would provide decent performance.

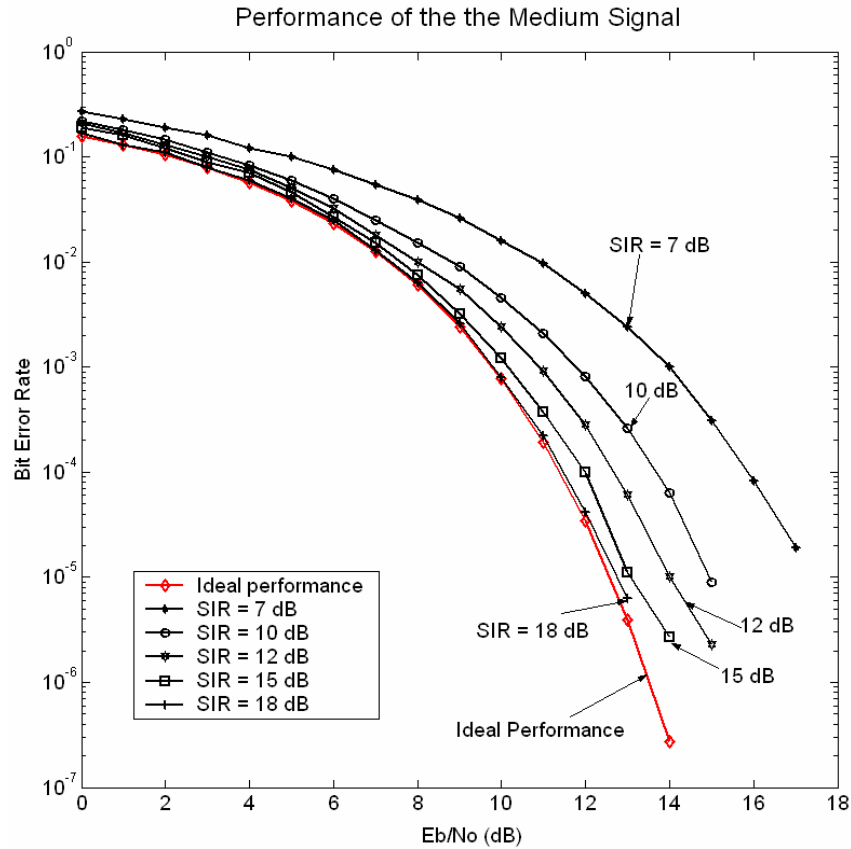


**Figure 5-13. Performance of the medium B-FSK signal.**

As for the small signal, an SIR of 6 dB is sufficient to obtain ideal performance, as shown in Figure 5-14. However, note that the small signal is more sensitive to SIR in *Case 2* as compared to *Case 1*. With a small decrease of SIR to 5 dB, the performance becomes much worse. This is because of the correlated noise and residual interference from the other two signals propagating from the preceding stages.

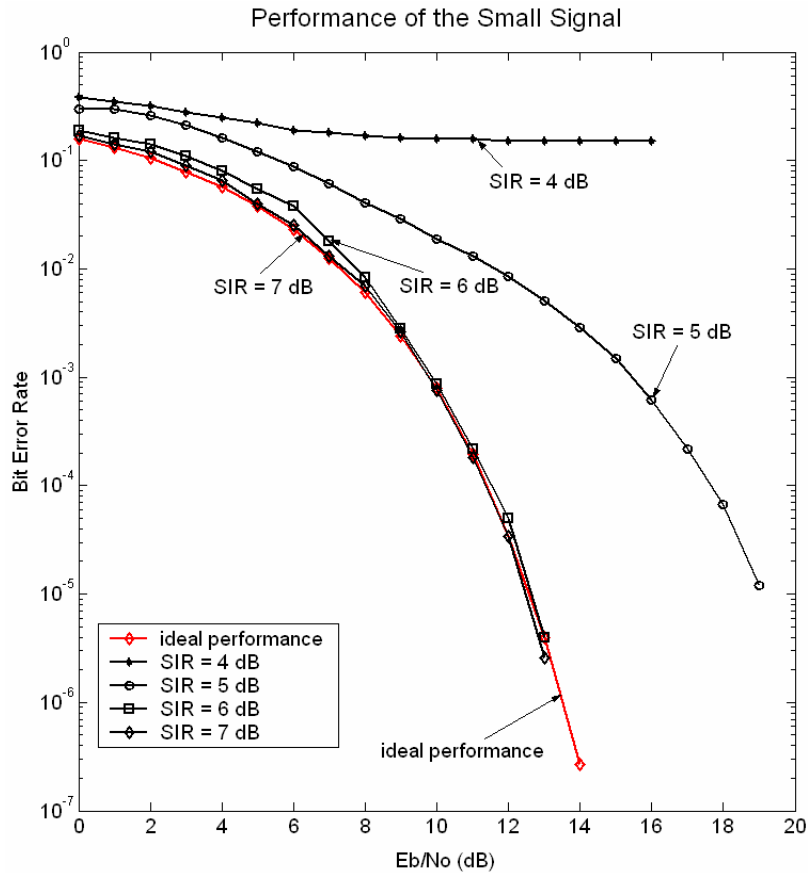


**Figure 5-14. Performance of the Small B-FSK Signal**

The following figures illustrate the improvement in performance when the power separation between signals increases. We show for SIR=7 dB, 10 dB, and 12 dB and 15 dB. Figure 5-15 shows the performance of all three signals at SIR equal to 7 dB. It can be seen that in order to decode all three signals successfully at a low bit error rate, a cost of 8 dBs in  $E_b/N_o$  beyond ideal performance is expected. However, if SIR is increased to 10 dB or 12 dB for example, the performance will improve to be within 2-3 dBs from ideal, as shown in Figures 5-16 and 5-17. When SIR is 15 dB, the performance is only within 0.5 dB from ideal, as shown Figure 5-18.

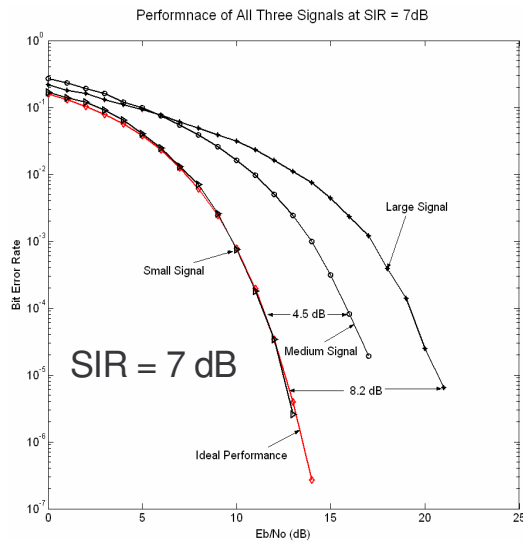


**Figure 5-15. Performance of all three signals at SIR = 7dB**

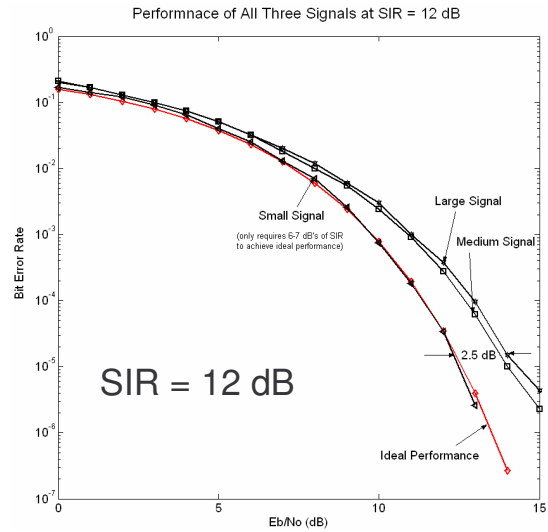


**Figure 5-17. Performance of all three signals at SIR = 12 dB**

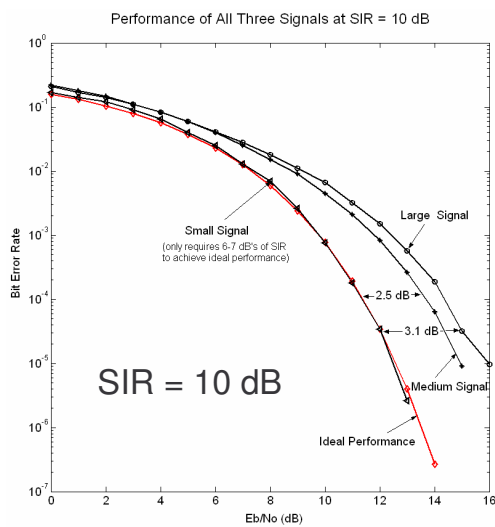


**Figure 5-16. Performance of all three signals at SIR = 10 dB**

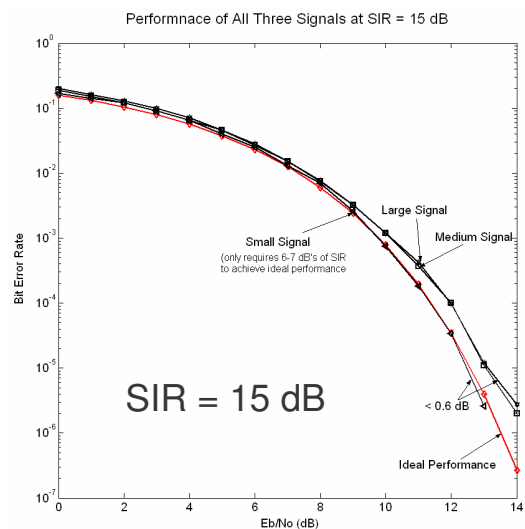


**Figure 5-18. Performance of all three signals at SIR = 15 dB**

## 5.4 Conclusion and recommendation

The receiver structure based on parallel interference cancellation is studied and its performance for each signal for various SIR values is plotted. The performance is exceptional as compared to a conventional receiver, given that amplitude, phase and frequency estimates are perfect. The general rule of thumb found is that the larger the



separation between the signals, the better the performance becomes. An SIR equal to 7 dB yields performance about 8.2 dBs worse than ideal while and SIR equal to 15 dB yields performance about 0.5 dB from ideal. It is found that an SIR of 10 dB actually yields very decent performance when decoding either the two signal-overlap scenario or three-signal overlap scenario.

Future research should take into account the incorrect estimate of phase, frequency and amplitude or extend this technique to other signaling formats such as CDMA, OFDM or ultra-wideband.

## **5.5. Acknowledgement**

This chapter, in part, is a reprint of the material that appears in “M. Nguyen, A. Zaghoul, “Parallel Interference Cancellation Receiver for Future CNS Systems, submitted to the *IEEE Transactions on Aerospace and Electronic Systems*”. The dissertation author was the primary author for the papers.

## Chapter 6 : SIC, PIC and their Implementation Considerations

This chapter discusses a receiver architecture that is feasible for the implementation and insertion of both types of interference cancellation techniques, namely the SIC and PIC. This chapter also discusses the necessary components to implement prior to implementing the SIC or PIC techniques. The performance comparison between SIC and PIC is also studied.

### 6.1 A possible receiver architecture for the implementation of SIC and PIC

A typical two-stage down-conversion heterodyne receiver is shown in Figure 6-1. In principle, this receiver structure can be used for any type of demodulation schemes since the demodulation process is done in the DSP inside the multi-signal processor block. A received signal, usually in low power (as low as -110 dBm is quite possible), is filtered using an RF bandpass filter (BPF) to reject possible interferers or noise impairments. The signal is then boosted up using a low-noise amplifier (LNA), then down converted using the 1<sup>st</sup> mixer and 1<sup>st</sup> local oscillator (LO) to step down one level of IF. The same IF step-down process is done one more time to bring the signal to IF closer to baseband, or possibly directly to baseband for signal processing. Today's software and DSP power could synthesize RF signals for low operating frequencies such as in the VHF or UHF band, one step-down RF to IF conversion can be sufficient for L band signals.

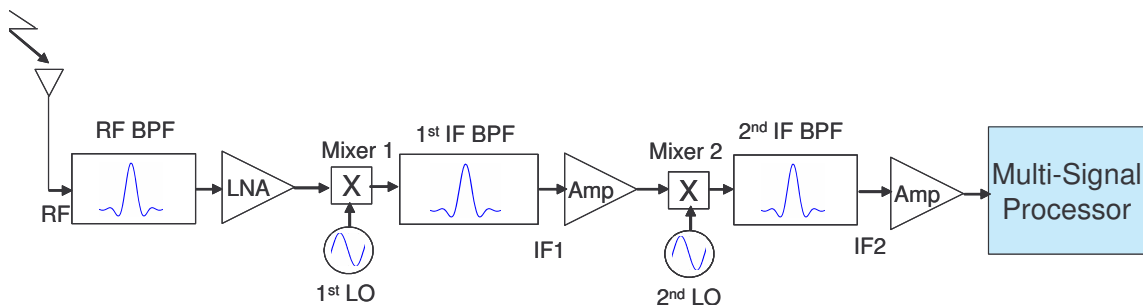


**Figure 6-1. Typical Heterodyne receiver with Multi-signal Processor**

The multi-signal processor is a DSP body that handles the demodulation of data as well as any algorithms to improve signal quality. In this case, the multi-signal processor includes a baseband conversion process, and over-sampling block, and energy detector coupled with correlator, a memory buffer and finally the SIC or PIC detector, as shown in Figure 6-2.

A baseband conversion block is used if the previous two-stage down-conversion heterodyne receiver described above does not already do this conversion. The idea is that at this time the signal should be in baseband form. An over-sampling block is used to sample the signals three times faster than the Nyquist rate ( $3 \cdot 2 \cdot R_b$ ) to allow better detection of the presence of the desired and co-channel interferers. The energy detector detects and monitors the signal(s) energy state (up or down) through continuously integrating over every symbol period to learn the presence of one or more signals. Once the energy detector knows the presence of signal(s), it would trigger the correlation process to kick in and synchronize the signal(s). Synchronization is an important step in acquiring the signals. If synchronization fails, then there is no signal to decode. Then a memory buffer is used to capture all the overlapping signals. In synchronous reception, the memory buffer can be set to contain just enough samples of one signal frame. However, in asynchronous reception, the memory buffer should be set to capture all the samples of the overlapping signal frames. Once done, signal interference cancellation is processed based on sequential interference cancellation.

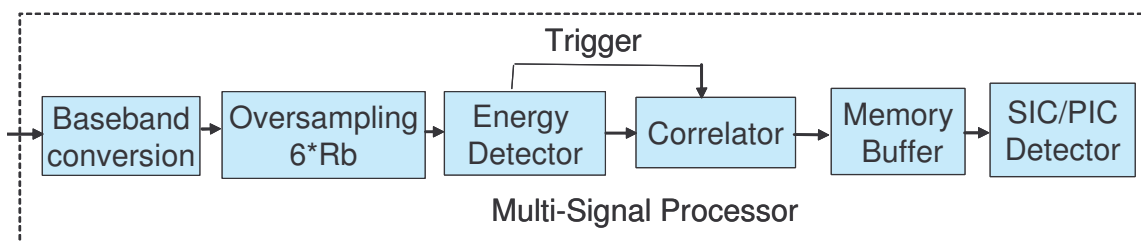


**Figure 6-2. Multi-Signal Possessor consisting SIC Detector**

The synchronization is done by the use of the correlator in the receiver. This section will study one type of correlator initially proposed to the RTCA MOPS standards

committee [Wils02b]. In this correlator structure, 3 samples of the 6 samples will not be counted towards correlation scores. Because of this reason, the highest possible synchronization score is 108. Without interference, an  $E_b/N_o$  greater than 4 dB should produce all perfect scores of 108, as shown in Figure 6-3. However, an  $E_b/N_o$  around 1 dB will not produce perfect scores.

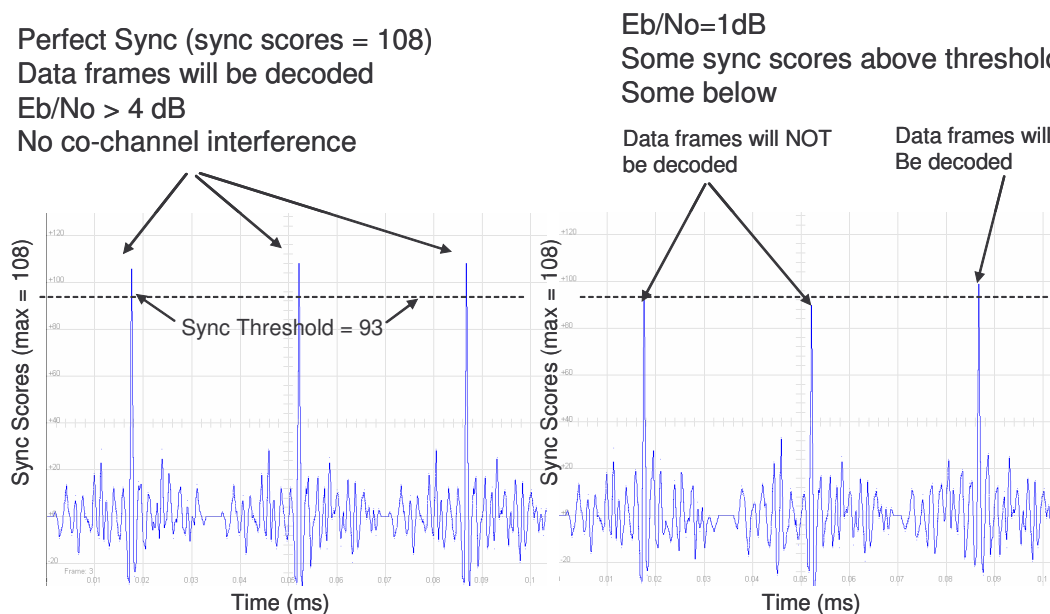


**Figure 6-3. Synchronization process for the avionic system**

Synchronization performance in AWGN is shown in Figure 6-4. It is shown that about 3.96 dB is needed to obtain 90% successful syncs in a pure AWGN environment. This is assuming FSK demodulation, no coding, raised cosine filter with roll off rate equal to 0.5, 6 samples/symbol and 3-bit blanker correlator. In the presence of one interferer (assume that S/I is high so AWGN is dominated by interference only), it was found through simulation that only about 1.3 dB is needed to obtain 90% success sync rates, as shown in Figure 6-5. The metric 90% success rate is a commonly agreed number by the standards committee to design the avionic system.

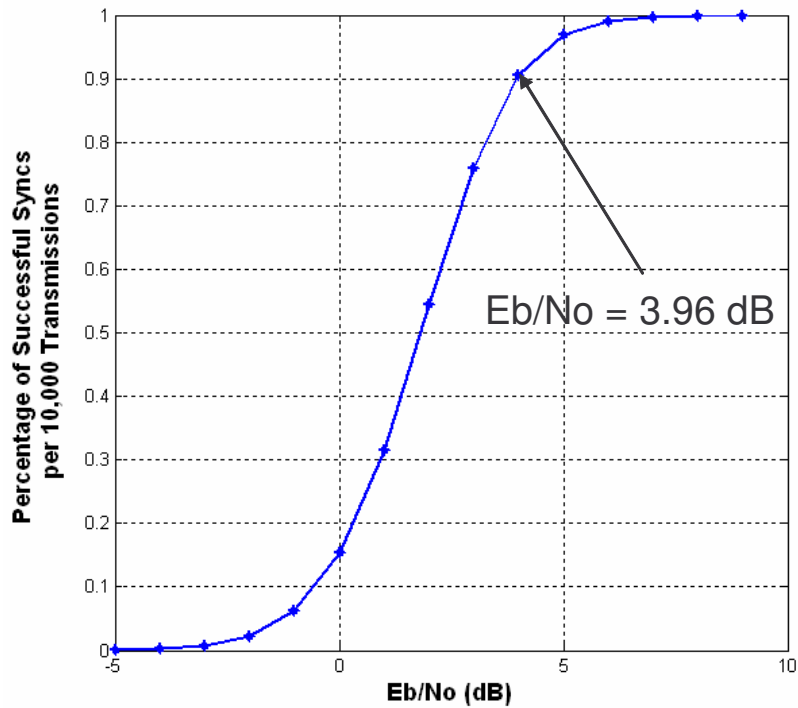


Figure 6-4. Synchronization performance in AWGN

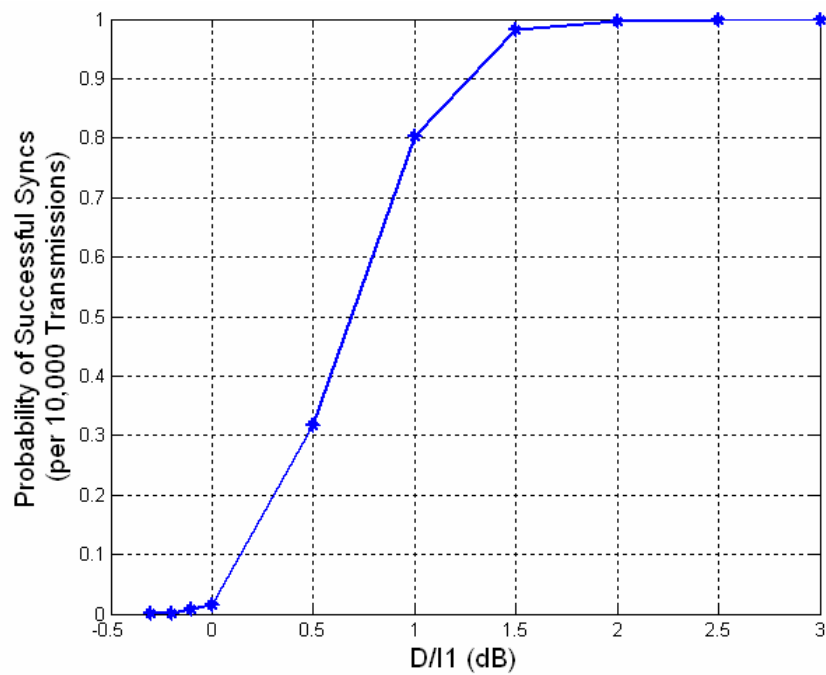


Figure 6-5. Synchronization performance in the presence of one interferer.

When there are two interferers, interference one ( $I_1$ ) and interference two ( $I_2$ ) would hold different receive power values. Some of them are shown in Table 6-1. Those header values of  $I_1$  and  $I_2$  represent the number of dBs below the desired signal power level. For example, when  $I_1=2.5$  and  $I_2=3$ , only about 53.9% of syncs are successfully detected out of 10,000 sync transmissions. Therefore, when there are two co-channel interferers, the following condition must be met in order to achieve 90% successful sync rate:

- Individual interference needs to be at least 2.5 dBs below the desired power level ( $P_d$ ), so

$$\sum_{i_j}^{\infty} I_i \geq -2.5dB \quad \text{and}$$

- Aggregate interference needs to be at least 7 dBs below  $P_d$ , so

$$\sum_{i_j}^{\infty} \sum_{i_i}^{\infty} I_{ij} \geq -7dB$$

**Table 6-1. Synchronization performance in the presence of two interferers**

$I_1$	$I_2$											
		0	0.5	1	1.5	2	2.5	3	3.5	4	4.5	5
0	0	0.0018	0.0030	0.0051	0.0061	0.0073	0.0097	0.0123	0.0138	0.0153	0.0160	0.0161
0.5	0	0.0029	0.0063	0.0095	0.0147	0.0210	0.0315	0.0429	0.0549	0.0703	0.0848	0.1012
1	0	0.0045	0.0096	0.0149	0.0279	0.0466	0.0742	0.1067	0.1468	0.1996	0.2582	0.3242
1.5	0	0.0061	0.0128	0.0277	0.0517	0.0946	0.1543	0.2323	0.3199	0.4251	0.5292	0.6215
2	0	0.0069	0.0192	0.0448	0.0944	0.1741	0.2821	0.4079	0.5395	0.6592	0.7624	0.8402
2.5	0	0.0096	0.0289	0.0712	0.1528	0.2803	0.4328	0.5914	0.7308	0.8386	0.9183	0.9676
3	0	0.0113	0.0405	0.1079	0.2318	0.4084	0.5929	0.7420	0.8716	0.9566	0.9855	0.9937
3.5	0	0.0118	0.0542	0.1487	0.3222	0.5399	0.7304	0.8699	0.9640	0.9893	0.9959	0.9979
4	0	0.0141	0.0681	0.2043	0.4244	0.6639	0.8400	0.9553	0.9885	0.9960	0.9980	0.9987
4.5	0	0.0159	0.0861	0.2619	0.5318	0.7644	0.9180	0.9840	0.9954	0.9981	0.9989	0.9990
5	0	0.0170	0.1005	0.3257	0.6302	0.8444	0.9660	0.9930	0.9977	0.9988	0.9990	0.9990

In the case of two interferers, it was found that sync performance requires 7 dB of protection among all three signals and an  $E_b/N_o$  equal to 4 dBs to meet 90% success rate while the data payload portion of the message requires 9.5 dB of protection among all

three signals and an  $E_b/N_o$  equal to 10.8 dB to meet the 90% message success rate, as shown in Figure 6-6.

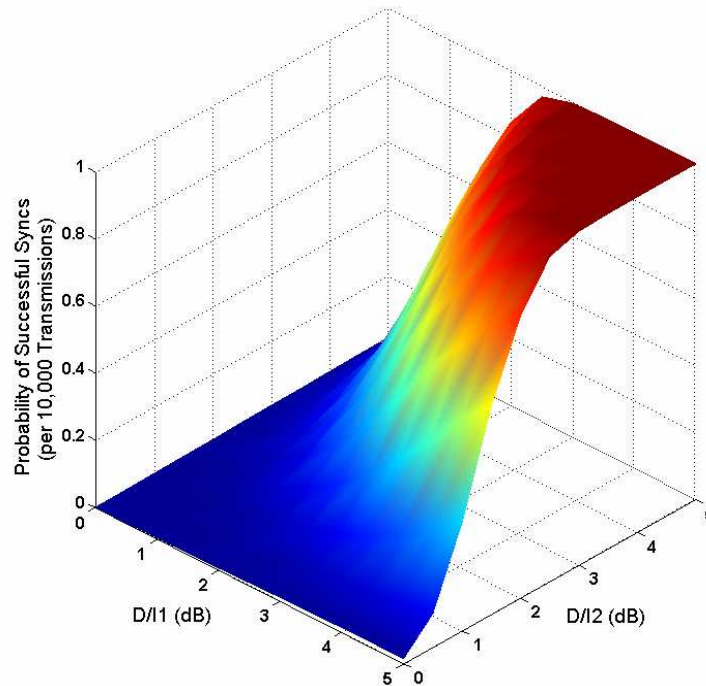


**Figure 6-6. Synchronization performance in the presence of two interferers**

The synch results are generalized as follows for two- signal overlap case

**Table 6-2. Synchronization performance summary**

<b>SYNCHRONIZATION PERFORMANCE SUMMARY</b>	
<b>Interference Type</b>	<b>Condition for 90% Successful Sync</b>
AWGN only	$E_b / N_o \geq 3.96dB$
1 co-channel interferer	$D / I \geq 1.27dB$
2 co-channel interferers	$D / I_1$ or $D / I_2 \geq 2.5dB$ and $\frac{D}{\sum_{i_j} \sum_{i_i=0}^{\infty} I_{ij}} \geq 7dB$

## 6.2 Performance comparison between SIC and PIC

This section provides a comparison in performance between SIC and PIC techniques. This section reuses most of these performance curves that are presented in Chapters 4 and 5, however, we superimpose them on the same graphs for clarity and to facilitate comparison. Figure 6-7 shows the BER performance of receivers implemented SIC or PIC techniques for various SIR values. It can be seen that the two performance results trace each other very closely. In fact, both SIC and PIC has the same performance.

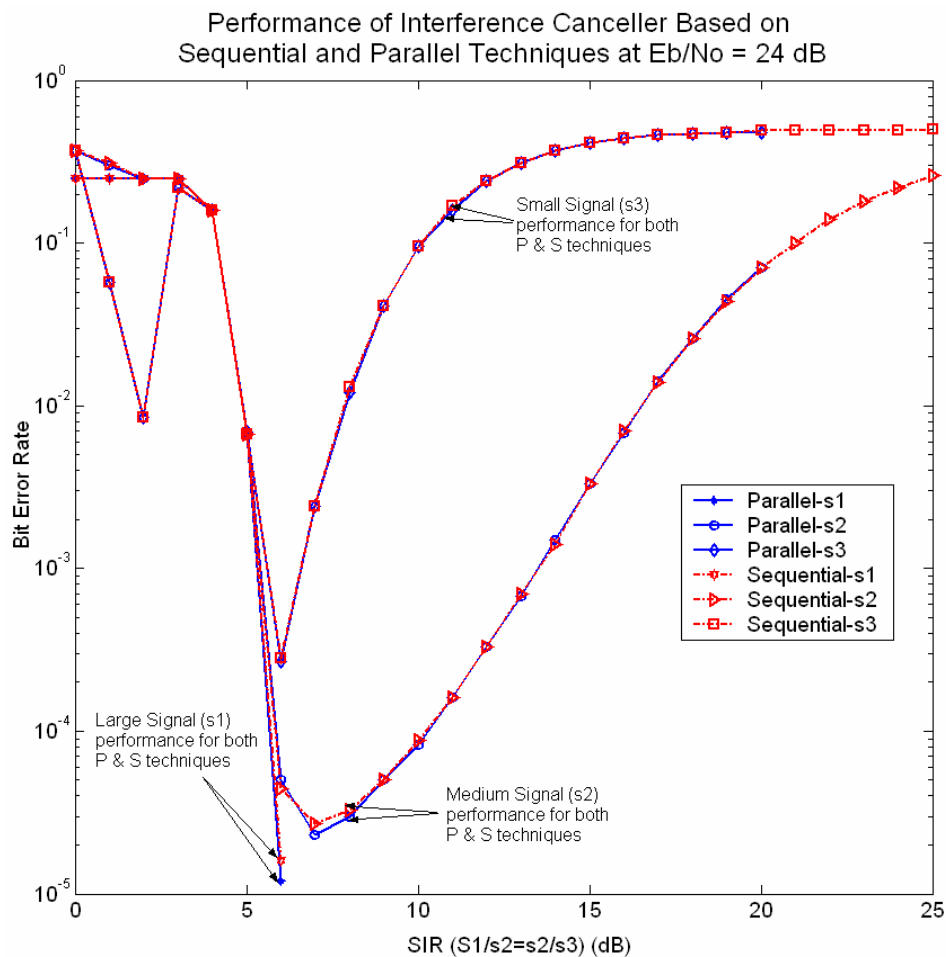
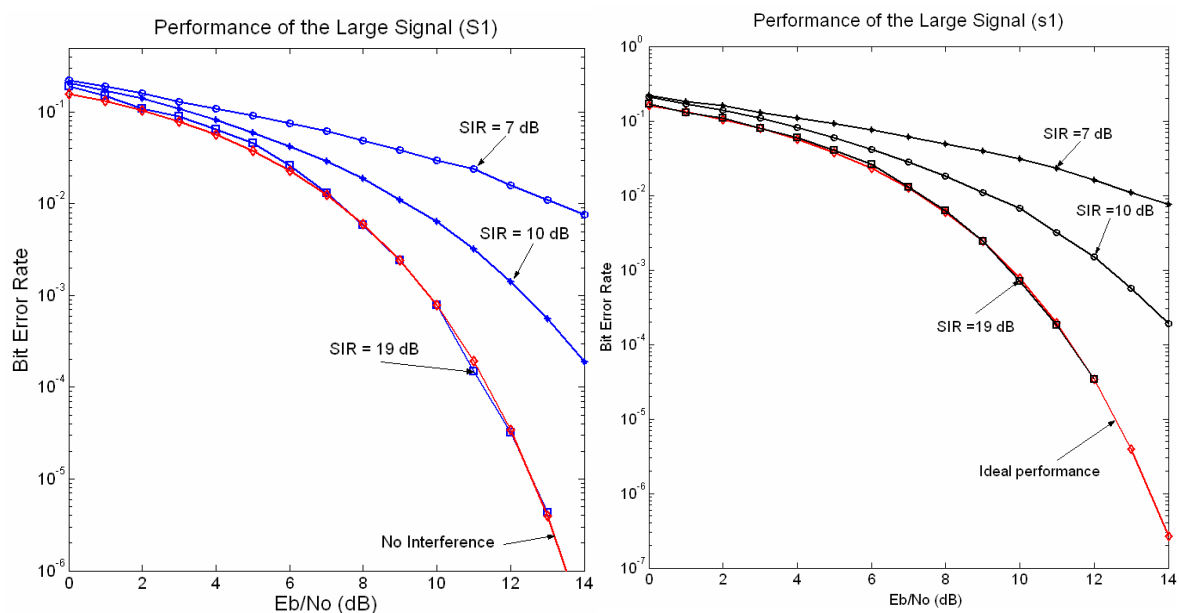


Figure 6-7. PIC and SIC performance for 3 overlapping co-channel Signals



The performance results of the individual signals, the large signals, the medium signals and the small signals for both SIC and PIC techniques are plotted below in Figures 6-8, 6-9 and 6-10. Based on the simulated results, the performance of SIC and PIC for individual signals are similar. Recall that SIC performs cancellation by sequentially removing one interferer at a time using a subtraction method. Once the stronger signals are removed, the weaker signals then can be decoded, in a sequential order. The parallel interference cancellation performs cancellation all in parallel. All interferers are removed all at once before attempting to decode the weaker signals. So, effectively, both SIC and PIC only decode weaker signals when strong interferers are successfully removed. This similarity allows for the same performance being observed by the two techniques, although the interference cancellation operation might be different. This claim can be justified by observing Figures 6-8, 6-9 and 6-10.



**Figure 6-8. Comparison between SIC (left) and PIC (right) for Large Signal**

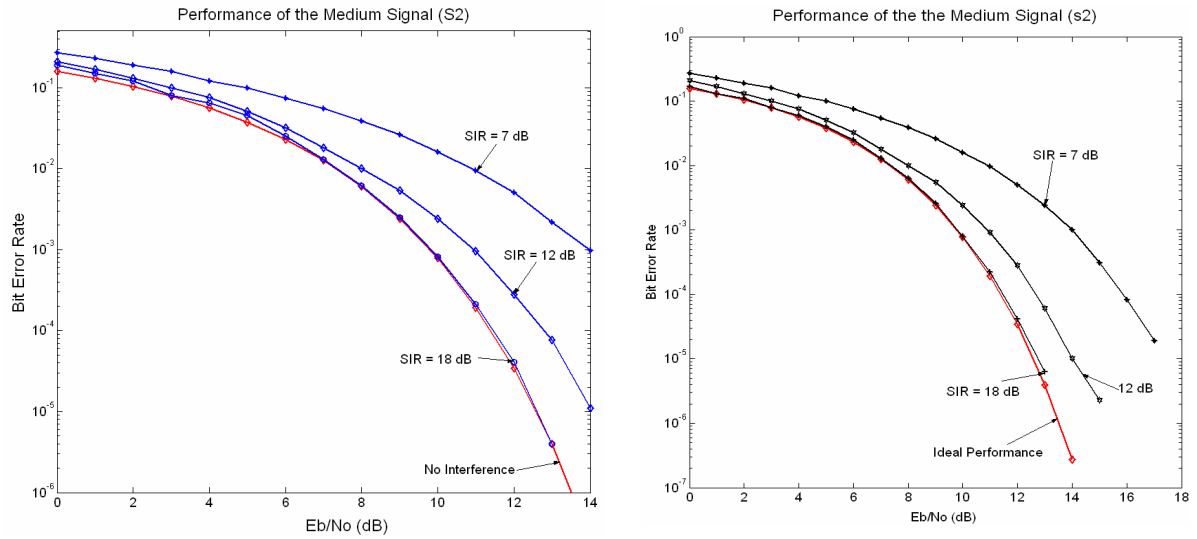


Figure 6-9. Comparison between SIC (left) and PIC (right) for Medium Signal

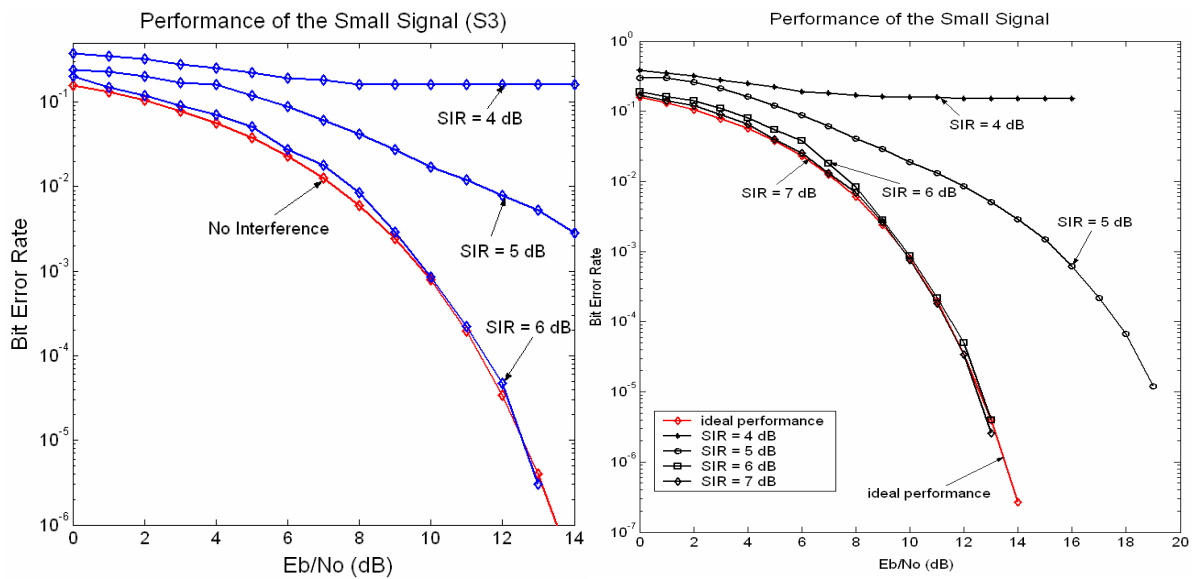


Figure 6-10. Comparison between SIC (left) and PIC (right) for Medium Signal

## Chapter 7 : Conclusion and Future Directions

The research presented in this dissertation focuses on quantifying multi-user co-channel interference and proposes interference cancellation techniques to mitigate the interference for an aeronautical (avionic) mobile communication system. The study is divided into two main parts. The first part is to propose a method to quantify the co-channel interference problem for the avionic communication system operating in a heavy-traffic aeronautical mobile environment using a visualization technique. The second part is to propose interference cancellation techniques to solve the interference problem, whose severity is defined in the first part.

The key findings for multi-user co-channel interference analysis are presented in Chapter 3. It was shown, using a Monte Carlo simulation model implemented based on the visualization method, that the co-channel interference for this aviation system using a random contention access communication protocol, can be best estimated using the statistical Poisson distribution. Various graphs are used to provide the bounds for simulation results, in terms of best-case, worst-case and most-likely-case. Several important conclusions are drawn regarding the characterization of interference for various mean and variance values and are shown in Chapter 3. The most important finding of all is that although co-channel interference, which is specified in terms of message-overlaps, could result from up to *eight* overlaps, high-quality communications, up to 98.5% success rate of signal detection, could be achieved by eliminating the interference of just *three* overlaps. In other words, achieving 98.5% success rate requires a special receiver capable of decoding successfully *three* overlapping co-channel signals. This key finding sets up the stage for multi-user interference cancellation research for the next chapters.

Next, in Chapters 4 and 5, two interference cancellation techniques are presented, namely sequential interference cancellation and parallel interference cancellation. Also, those chapters present findings that hold the key to increasing aeronautical communication system capacity and allowing for a more efficient use of the scarce

spectrum resources for aeronautical mobile communication applications. We propose a simple radio receiver architecture with powerful interference cancellation capability and show how this special receiver can successfully decode multiple overlapping co-channel signals on a single channel; a capability not available in today's avionic radio receivers.

The interference cancellation receiver performs well, especially in heavy-traffic environments that exhibit strong co-channel interference (e.g., the heavy-traffic aeronautical mobile environment that contains thousands of aircraft around Los Angeles airport). This special receiver can recover very weak signals that might be completely buried inside much stronger ones. We demonstrate the multi-signal decoding capability of the interference cancellation receiver based on various performance graphs for different values of signal-to-interference (SIR) ratios.

We found that multi-signal decoding capability for *three* FSK signals can be achieved at a small cost of about 2 to 3 dBs in system performance when there is sufficient separations ( $SIR \geq 10 \text{ dB}$ ) among interfering signals. Operating at SIRs below 10 dB is also possible; however it requires a small additional performance cost. For example, that additional cost is about 2 dBs for SIR equals to 7 dB. As for BPSK signals, the cost is 2-3 dBs higher than in FSK case. We discovered that using SIC and PIC would increase system performance by 15%. This is a substantial improvement. An 18% improvement means that critical information from 450 ( $0.15 \times 3,000$ ) aircraft in the heavy-traffic environment can be preserved.

In evaluating the interference cancellation capability for both FSK and B-PSK de/modulations, based on both SIC and PIC techniques, we found that decoding *two* co-channels signals only requires SIR to be in the range from 7-10 dB to achieve decent performance. However, the decoding of three signals requires an additional 2-3 dBs to achieve decent performance. We notice that the small signal, although buried inside more powerful signals, requires the least SIR. This is because interference from other signals has been successfully extracted out from the preceding stages. We also note that B-PSK seems to be more sensitive and less robust than FSK when using this interference

cancellation technique and SIC and PIC yield the same performance.

There are various avenues for future research associated with the work performed in this dissertation:

- The multi-user co-channel interference analysis conducted in Chapter 3 assumes equal statistical weights for all aircraft in the heavy-traffic environment. This means that information which arrives from all aircraft to the “victim” aircraft is equally important. This is a decent assumption, especially when future operational concepts would likely to transfer aircraft separation and monitoring responsibility to pilots instead of currently being managed by the controllers. Pilots then need sufficient information from all aircraft in the surrounding area in order to handle increased responsibility [Hawk04]. However, for near future operations, pilots might be only interested in knowing aircraft within their proximity, 30 nautical miles for example. One possible research topic is to divide the analysis into different segments or tiers so that the message-overlap statistics have different weights, depending on various level of importance of the arriving messages. The tiered-analysis is shown in Figure 7.1.

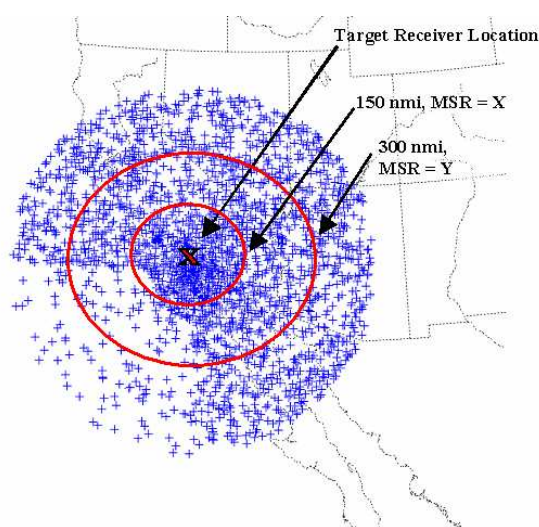


**Figure 7-1. Tiered Statistical Analysis**

- Risk analysis can also be another research topic to identify the rare events which might cause catastrophic system malfunction. For example, a possible case would be when several large signals, which come from several aircraft that are very close to the

victim aircraft, happen to collide and cannot be decoded. Although the victim aircraft could receive this information several seconds later, this can be dangerous because other aircraft already come close to the victim aircraft. Although the FAA has the Traffic Collision and Avoidance System (TCAS) to handle urgent tactical situations such as this one, this risk analysis can make an interesting research topic to compliment TCAS operation.

- Future analysis might consider including Reed-Solomon coding or Turbo coding for future use in the system. However, it should be noted that Turbo codes might cause additional delay that might not be applicable to delay-sensitive systems.
- Future analytical analysis could further enhance the multi-user co-channel interference evaluation by mathematically proving that the avionic system does exhibit Poisson properties for large number of samples, therefore converging from the binomial distribution. The traffic data could then be used for verification purposes against computer simulation, as well as estimates of mean and variances for various scenarios.
- The co-channel interference analysis above assumes omni-directional antennas, which is a decent assumption. However, enhancement on the analysis can be done to take into account the average received power gain using some antenna switching mechanism for this avionic system with the antenna not truly omni. Some initial work has been done and shown in Appendix B.
- One major assumption made in this work is the perfect cancellation of the larger signals due to perfect estimation of signal amplitudes, phase and frequencies. In a practical implementation and design, perfect estimates are tremendously difficult to achieve, especially when dealing with multipath fading causing signal fluctuations, Doppler causing frequency offsets, and other noise and impairments causing phase change. More research is needed to quantify the performance of the SIC and PIC receiver schemes under imperfect estimates of amplitudes, phase and frequency deviations.

- Further investigation can be done for multi-stage PIC. Subsequent stages of PIC could help improve the performance due to iterative estimates of the larger signals.
- In addition, one might look into a possibility of combining SIC and PIC for a hybrid solution. This is envisioned to improve the delay as experienced in SIC and reduce the complexity in multi-stage PIC.
- So far, it has been shown that the SIC and PIC receivers could be applied to communication applications. For future research, one could extend this simple concept of SIC and PIC to navigation or surveillance applications, as well as future cellular systems employing CDMA, OFDM or hybrid multi-carrier OFDM/CDMA. Furthermore, one can study how to apply this technique for ultra-wideband waveforms.
- More study is needed to quantify the signal processing delay and complexity for both synchronous and asynchronous reception for SIC, PIC and hybrid SIC-PIC techniques.
- Performance of SIC and/or PIC in the presence of multipath fading in the channel (e.g., Ricean, Rayleigh) can also be a subject for future research.
- Future work can extend this technique to show the decoding of *four*, or even *five* overlapping signals, thus achieving 99.7% or 99.9% success rate in signal detection, respectively.

## Appendix A. Simulation Integrity

### MOE Validation: Unbiased and Consistent Estimator

A parametric study is developed to ensure that the message overlap estimator (MOE) is modeled correctly thus verifying that the results it provides can be obtained with confidence (given the assumptions). Ten thousand simulations were conducted to evaluate the randomness of the results. The results, as shown in Figure A-1, yield a normal distribution. This figure implies that, for example, if the expected number of message-overlap occurrences (before normalizing the mean to zero) is 900, one would be likely to achieve that since the standard deviation of 29.2 about the mean represents a low error spread value.

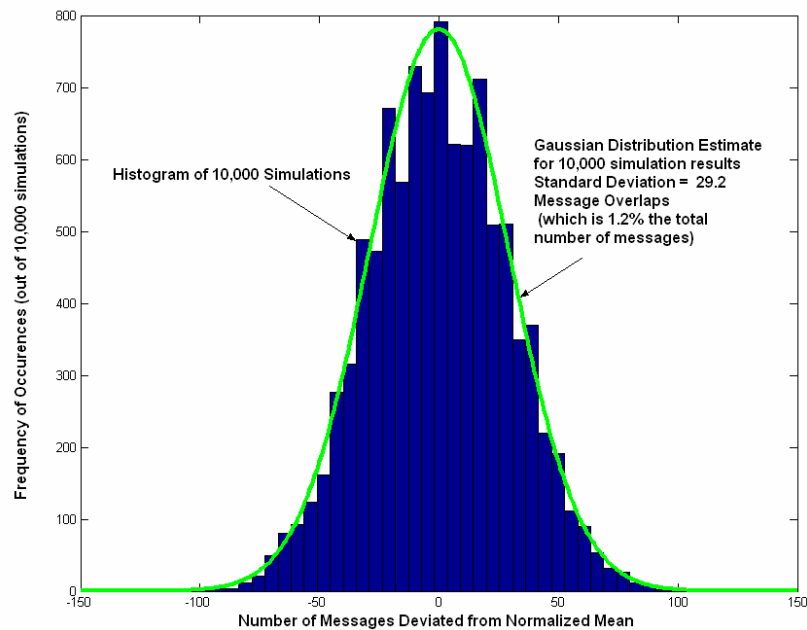


**Figure A-1. Distribution of Results from MOE**

To prove that the simulation results are unbiased and consistent, four additional sets of super simulations were created. Each set consists of ten thousand simulation runs. The results in Figure A-2 illustrate the average percent errors as the number of simulations



increase. The simulation results are unbiased because the expected values of the results converge to the actual value, which is normalized to zero in this case [Tranter] [Shamugan].

$$E\{Estimator\}=0$$

The simulation results are also consistent because the error variance ( $\sigma_e^2$ ) converges to zero as the number of simulations (N) increases to infinity [Tran] [Jeru92].

$$\sigma_e^2 \approx 0 \quad \text{as } N \rightarrow \infty$$

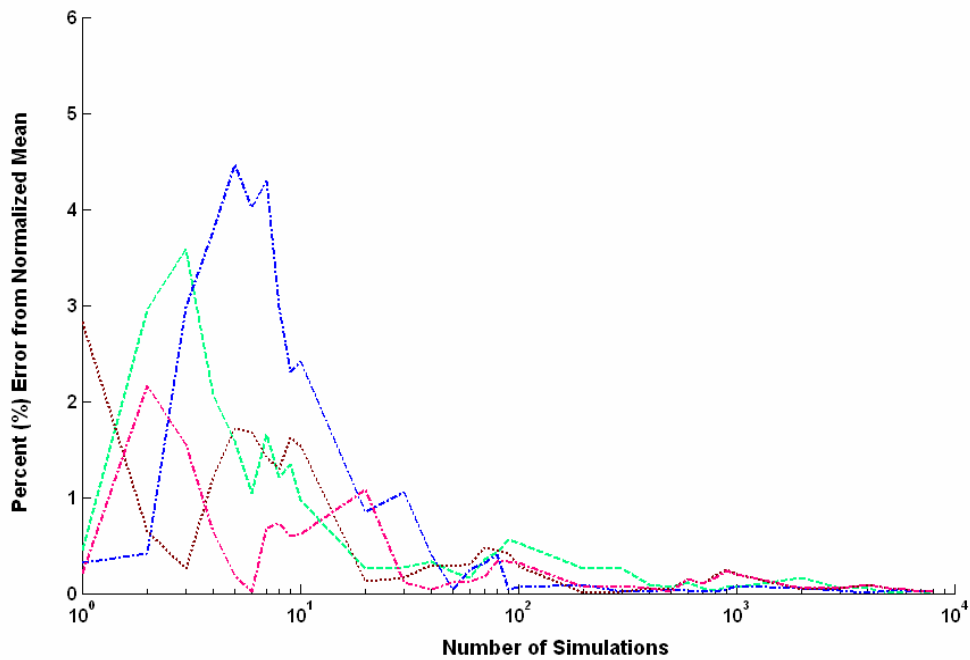


**Figure A-2. Illustration of the Unbiased and Consistent MOE**

Figure A-2 also suggests the number of simulations needed to obtain results within a particular percent error. This number is chosen to be one thousand simulations so that the results can be obtained within 0.5% accuracy (errors are bounded within less than 0.5%).

## Appendix B. Antenna and Switching Mechanism to Improve System Performance

An antenna model can be modeled to account for the RF interaction between the avionic transmitters and receivers. The heavy-traffic environment was used to create the histograms in B-1 and B-2 that depict the two cases of the received signal distribution with and without antenna, respectively. The number of aircraft from the environment is plotted against received signal power, where each bin represents a 2 dB power increment. The root-mean-square (RMS) power was calculated for both cases, which yields -128.8 dBW without antenna and -125.7 dBW with antenna. These results imply that approximately 3 dB accuracy is gained in the power-link computation by including the antenna in the model. Note that when the antenna is not accounted for, the resulting distribution appears to be a negative exponential function. However, when the antenna is taken into consideration, the resulting distribution yields a more realistically scattered function.

There are two main features of the antenna that can be implemented: the antenna pattern and the antenna switching mechanism. The following will describe in detail the characteristics and implementation aspects of the two.

The airborne antenna was modeled according to the RTCA MOPS standards [MOPS]. This antenna includes the measured  $\frac{1}{4}$  wave monopole antenna provided by UPS Aviation Technologies (UPS-AT), as shown in Figure B-3. When measurements were performed, the antenna was mounted on top of an aircraft. The bottom-mounted antenna pattern can be viewed by rotating the plot 180 degrees. The azimuth antenna pattern was assumed uniformly distributed. The antenna was classified as passive with linear polarization, mounted on a 9-inch ground plane. The operating frequency was 2.44 gigahertz (GHz).

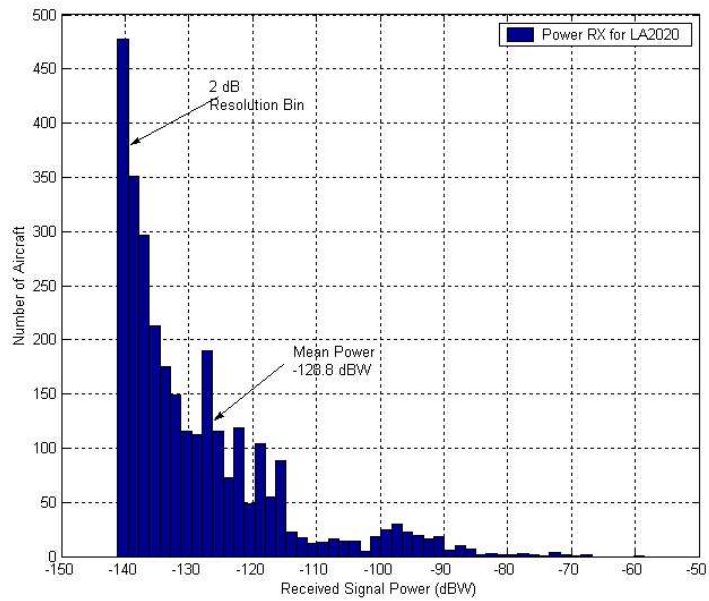


**Figure B-1. Histogram of Received Signal Power (Without Antenna)**

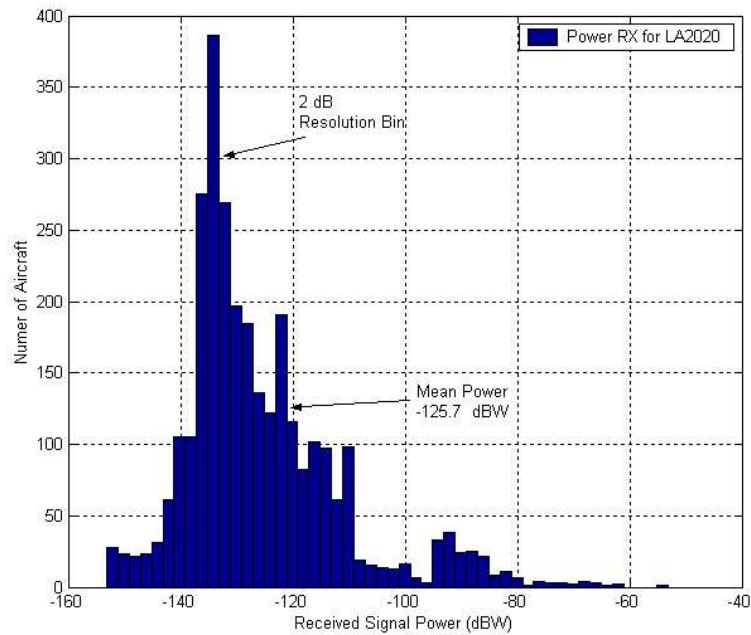


**Figure B-2. Histogram of Received Signal Power (With Antenna)**

However, the frequency was scaled down to 981 MHz to comply with the operations of an avionic system operating on 981 MHz. The scaling effect makes the 9-

inch ground plane appear as a 2-foot ground plane. The zero degree point (up) corresponds to the top of the aircraft while 180-degree point faces ground (down).

The antenna pattern model consists of a look-up table ranging from zero to 180 degrees. Due to its approximately symmetrical property, this table can also be applied to angles ranging from 180 degrees to 360 degrees. The angles falling into the range from 0 degree to 30 degrees and 130 degrees to 180 degrees are estimated using a 5 degree increment resolution to capture the effect of antenna nulls. However, a lower resolution of 10 degrees increment is used for angles starting from 30 degrees to 130 degrees.

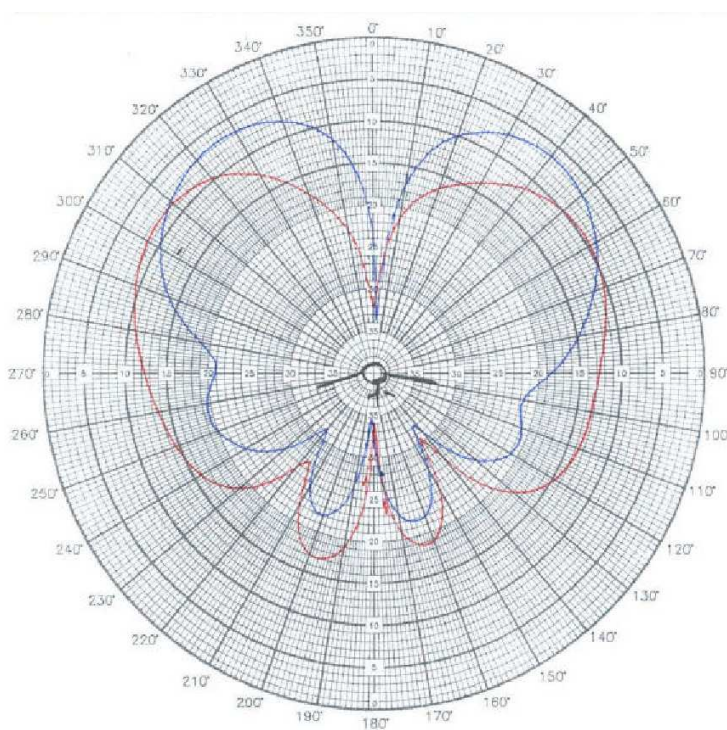


**Figure B-3. Antenna Pattern**

The Antenna Switching Mechanism represents an approach to overcome the limited area of coverage when only one antenna is mounted on an aircraft. Although the avionics antenna is approximately omni-directional, the communications range can be severely affected in the antenna nulls or aircraft banking. The signal loss could be as high as 30 dB, which is not accounted for in most link-budget calculations. Therefore, this could result in total signal loss although the aircraft is in the expected range of coverage.

To resolve this problem, the MOPS standards committee proposed two antennas, one on top of the aircraft and one on the bottom, to perform switching to whichever antenna receives the highest energy. Figure B-4 illustrates this mechanism. The victim aircraft (assumed a location at 10,000 feet above Los Angeles International Airport [LAX]) receives RF signals from its bottom or top antenna, sent by other surrounding aircraft.

The angle  $\theta$  in Figure 10 can be calculated using the following derived equation:

$$\theta = \text{Cos}^{-1} \left( \frac{\sqrt{(x_1 - x_n)^2 + (y_1 - y_n)^2}}{\sqrt{(x_1 - x_n)^2 + (y_1 - y_n)^2 + (z_1 - z_n)^2}} \right) \text{ where } x_1, y_1, z_1 \text{ represents the victim}$$

aircraft position, and  $x_n, y_n, z_n$  represents the position of any aircraft in the heavy-traffic environment.

As a result of using antenna switching, the simulated victim (i. e., receiving) aircraft, assigned at LAX or any other location for that matter, always receives more accurate signals from the surrounding aircraft. This results in a more accurate computation of the power-link budget thus enabling the model to provide more realistic performance results.

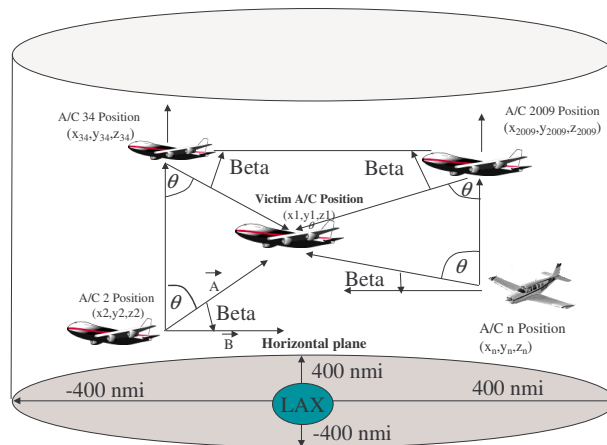


**Figure B-4. Antenna Switching Mechanism for Aircraft in Heavy-Traffic Environment**

Note: The work presented in Appendix B is extracted from a previously published paper by Nguyen et al at IASTED conference in 2003, in which the dissertation author was the primary author of the paper.

- Nguyen, Minh A., Liedman, David., Monticone, Leone C., *The Communications Adaptive Design and RFI Environment (CADRE) Tool for Radio System Design*. Proceedings of the International Association of Science and Technology for Development Conference (IASTED) on Modeling and Simulation, p 7-17, ACTA Press, February 24, 2003.

## Appendix C. SIC Receiver for Decoding Four BFSK and BPSK Signals

The dissertation focuses on SIC and PIC that have the capability to decode *three* overlapping co-channel signals. The SIC and PIC receivers can actually decode more than three signals. The performance of a SIC receiver for decoding *four* overlapping co-channel FSK signals is shown in Figure C-1.

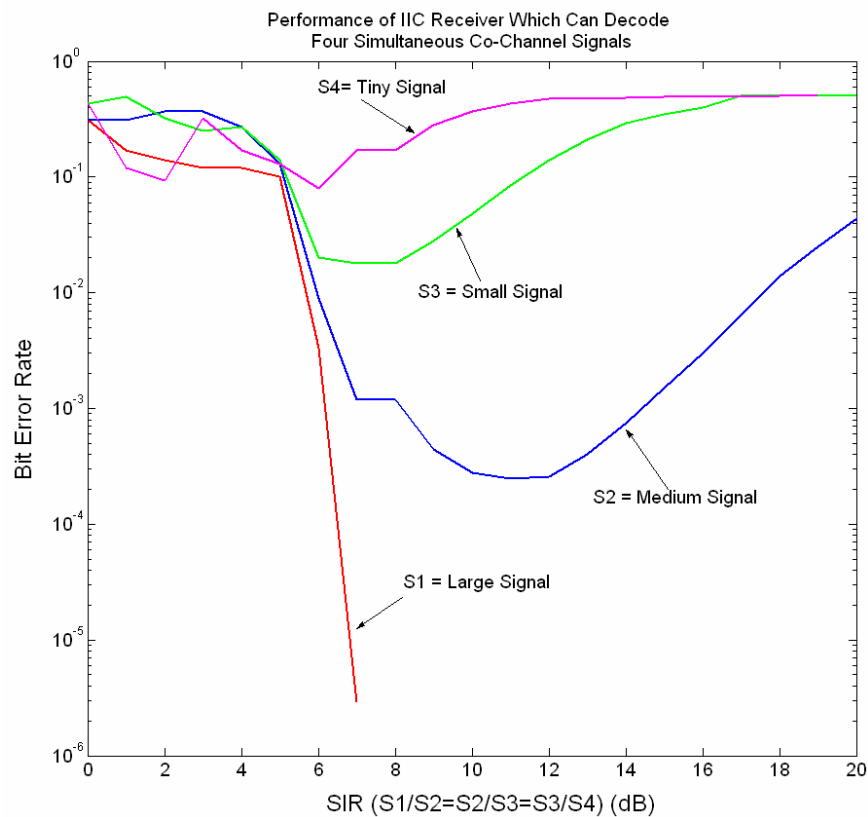


**Figure C-1. SIC to Decode 4 Co-channel B-FSK signals**

Similarly, the BER vs SIR performance for an SIC receiver trying to decode 4 overlapping BPSK co-channel signals can be simulated and shown in Figure C-2. Performance of the small signal S4 is shown with better resolution in Figure C-3.

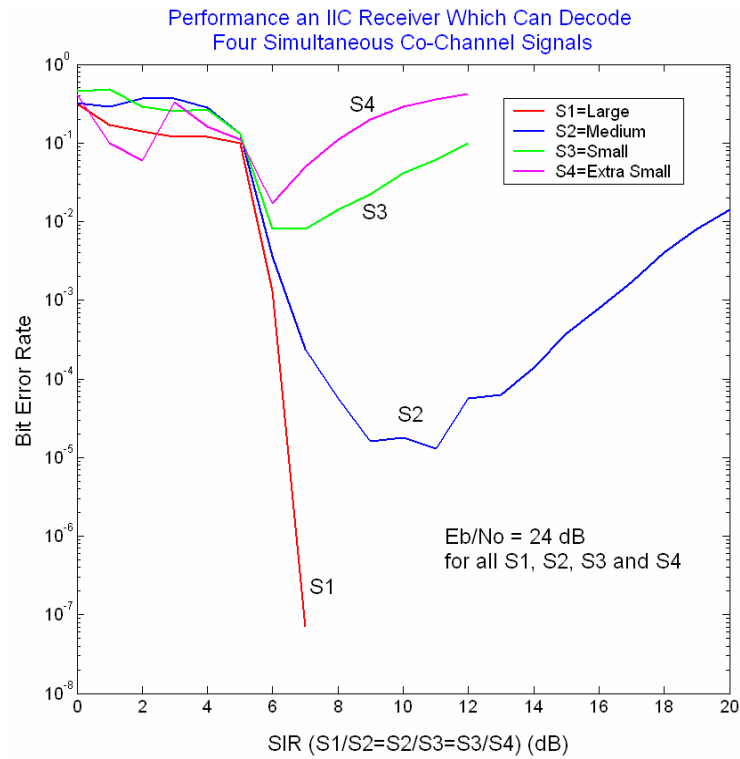


Figure C-2. SIC to Decode 4 Cochannel B-PSK signals

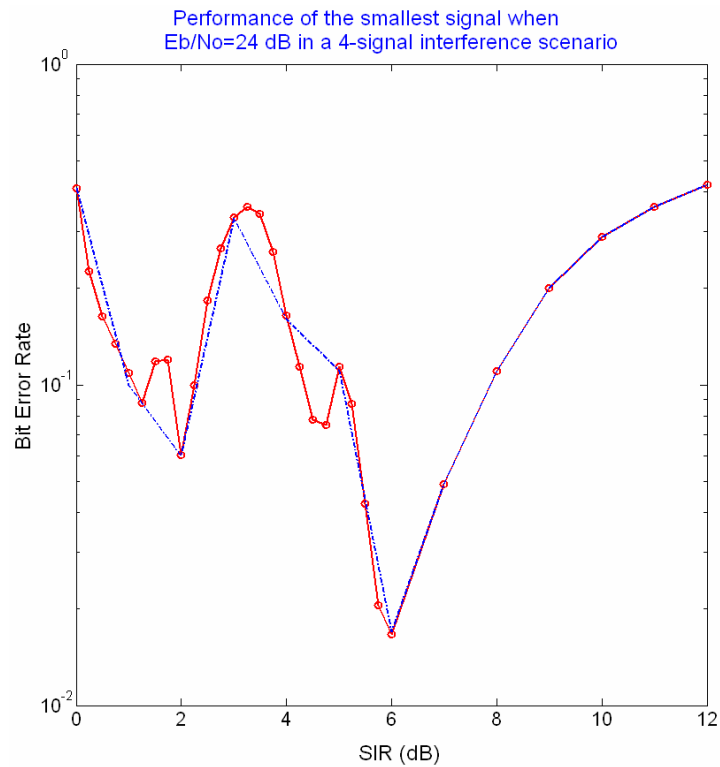


Figure C-3. SIC to Decode 4 Cochannel B-PSK signals (for Tiny signal) at 0.25 dB SIR resolution



## References

- [Abra] T. Abrao, P. Jeszensky. Successive Parallel interference canceller for asynchronous multirate DS-CDMA systems, not dated.
- [Abra70] N Abramson, "The Aloha System-Another alternative for computer communications," in Proc. Fall Joint Computer Conf., 1970
- [Abra85] N. Abramson, "Development of the ALOHANET," IEEE Transactions on Information Theory, Vol. IT-31, No. 2, March 1985.
- [Abra94] N. Abramson, "Multiple Access in Wireless Digital Networks," Proceedings of IEEE, Vol. 82, NO. 9, September 1994.
- [Alem80] C. Weber, W. Alem, "Performance Analysis of Demod-Remod Coherent Receiver for QPSK and SQPSK Input," IEEE Transactions on Communications, Vol. Com-28, No. 12, December 1980.
- [Arsl01] H. Arslan, K. Molnar, "Cochannel interference suppression with successive cancellation in narrow-band systems", IEEE Communications letters, vol. 5, No. 2, February 2001.
- [Bach01] Bachman, "LA 2020 Results," Presentation at the RTCA Special Committee 186, Working Group 5, Meeting 8, June 2001.
- [Bene73] S Benedetto, E. Biglieri, and V. Castellani, "Combined Effects of Intersymbol, Interchannel, and Co-Channel Interference in M-ary CPSK Systems," IEEE Transactions on Communications, Vol. COM-21, pp.997-1008, September 1973.
- [Bueh00] R.M. Buehrer, N. Mendoza, B. Woerner, "A simulation Comparison of Multiuser Receivers for Cellular CDMA", IEEE Transactions on Vehicular Technology, Vol. 49, No. 4, July 2000.
- [CAPS00] Capstone Proposed Initial Draft Standard for UAT, May 22, 2000.
- [Cho98] Y. Cho, J. Lee, "Analysis of an Adaptive SIC for Near-Far Resistant DS-CDMA", IEEE Transactions on Communications, Vol. 46. No. 11, November 1998.

- [Corr97] N. Correal, R. Buehrer, B. Woerner. "Improved CDMA performance through bias reduction for parallel interference cancellation", IEEE 1997.
- [Corr99] N. Correal, R. Buehrer, B. Woerner, "A DSP-Based DS-CDMA multiuser receiver employing partial parallel interference cancellation". IEEE Journal on selected areas in communications, Vol. 17, No. 4, April 1999.
- [Dieu01] J. Dieudonne, "Universal Access Transceiver (UAT) and MOPS Status" presentation, NASA Integrated Communications, Navigation and Surveillance Conference, May 2001.
- [Dard00] D. Dardari, V. Tralli, and R. Verdone, "On the Capacity of Slotted Aloha with Rayleigh Fading: The Role Played by the Number of Interferers," IEEE Comm. Letters, Vol. 4, NO. 5, May 2000.
- [Ette76] W. Van Etten. "Maximum likelihood receiver for multiple channel transmission systems". IEEE Transactions on Communications, COM-24(2):276-283, February 1976.
- [FAA98] FAA Order 6050.32A. Spectrum Management Regulations and Procedures Manual, Department of Transportation, Federal Aviation Administration, ASR-200, May 1, 1998.
- [Forn72] G. D. Forney, "Maximum-likelihood sequence estimation of digital sequences in the presence of intersymbol interference". IEEE Transactions on Information Theory, IT-18:363-378, May 1972.
- [Gitm75] I. Gitman, "On the Capacity of Slotted Aloha Networks and Some Design Problems," IEEE Trans. Comm., Vol. Com-23, March 1975.
- [Gold71] J. Goldman, "Multiple Error Performance of PSK Systems with Cochannel Interference and Noise," *IEEE Trans. Comm. Techno.*, Vol. COM-19, pp.420-430, August 1971.
- [Hawk04] Hawkins, P., Simons, E., and Zeitlin, A, *Controller-Assigned Airborne Separation(CAAS) Concept Exploration*, AIAA-2004-6390, The MITRE Corporation/Center for Advanced Aviation System Development, McLean, VA, September 2004.
- [Hayk96] S. Haykin. *Adaptive Filter Theory*. Prentice Hall, 1996.

- [Holt94] J. M. Holtzman, "Successive Interference Cancellation for Direct Sequence Code Division Multiple Access", IEEE, 1994.
- [Honi95] M.L. Honig, U. Madhow, S. Verdu. "Blind adaptive multiuser detection". IEEE Transactions on Information Theory, 41(4):944-960, July 1995.
- [Huan03] Y.F. Huang, "An Adaptive Multistage Parallel Interference Canceller for CDMA System over Frequency Selective Fading Channels", IEEE 2003.
- [Jans95] G. Janssen, "A Dual Receiver for Narrowband DPSK Modulation with Co-Channel Interference Cancellation," IEEE Proceedings of on Communications and Vehicular Technology in the Benelux, pp. 115-121, Eindhoven, 1995.
- [Jans02] G. Janssen, S. Slimane, "Symbol Error Probability Analysis of a Multiuser Detector for M-PSK Signals Based on Successive Cancellation," IEEE Journal on Selected Areas in Communications, Vol. 20, No. 2, February 2002.
- [Jans97] G. Janssen, "Enhancement of a Dual-Signal Receiver Using Predetection Microdiversity for Narrowband and Wideband Signals, IEEE 1997.
- [Jeru84] M. Jeruchim, "Techniques for Estimating the Bit Error Rate in the Simulation of Digital Communication Systems," IEEE Journal on Selected Areas in Comm., Vol. SAC-2 No. 1, January 1984.
- [Jeru92] M. Jeruchim, P. Balaban, and S. Shanmugan, *Simulation of Communication Systems*, Plenum Press, 1992.
- [Kama88] A. Kamal, "Semi-Synchronous ALOHA," IEEE 1988.
- [Koba77] H. Kobayashi, Y. Onozato, D Huynh, "An Approximate Method for Design and Analysis of an Aloha System," IEEE Trans. Comm., Vol. Com-25, No.1, January 1977.
- [Kohn90] R. Kohno, H. Imai, M. Hatori, and S. Pasupathy. "An adaptive canceller of cochannel interference for spread-spectrum multiple-access communication networks in a power line". IEEE Journal on Selected Areas in communications, 8(4):691-699, May 1990.

- [Lai] K.C. Lai, J. Shynk, M. Motamed, R. Gooch, Adaptive “Successive Interference Cancellation for the IS-95 Uplink”, not dated
- [Lupa89] R. Lupa, S. Verdu. “Linear multiuser detectors for synchronous Code-Division Multiple-Access Channels”. IEEE Transactions on Information Theory, 359(1):123-136, January 1989.
- [Meda04] M. Medard, J. Huang, A. Goldsmith, S. Meyn, T. Coleman, “Capacity of Time-Slotted Aloha Packetized Multiple-Access System Over the AWGN channel,” IEEE Trans. Wireless Comm., Vol. 3, No. 2, March 2004.
- [Merris01] R. Merris, *Graph Theory*, Wiley-Interscience, 2001.
- [Mood00] J. Moody, “Universal Access Transceiver System Description” presentation, RTCA Special Committee, Working Group 5, December 2000.
- [Mood03] J. Moody, “Universal Access Transceiver System Description” presentation,, December 2003.
- [MOPS02] Minimum Operational Performance Specifications (MOPS) meetings and working papers for ADS-B systems using Universal Access Transceiver (UAT), Appendix K. FAA System Development 2002.  
<http://adsb.tc.faa.gov/ADS-B/186-subf.htm>
- [More99] M. Moretti, U. Pezzano, G. Janssen, D. Sparreboom, Performance evaluation of a mobile communication system implementing the dual-signal receiver, IEEE 1999.
- [Mont03] Monticone, M. Nguyen., D. Liedman, F. Box, T. Kim, P. Purcell, and J. Barrows, *The Communications Adaptive Design and RFI Environment (CADRE) Tool Suite for L-Band Spectrum Management*, The MITRE Corporation, McLean, VA, July 2003.
- [Nguy04a] M. Nguyen, A. Zaghoul, “A Method for Characterizing Packet Interference in a High-Density Traffic Environment,” IEEE Proceedings of Vehicular Technology, September 2004.

- [Nguy04b] M. Nguyen, A. Zaghoul, "Extension on Characterizing Packet Interference in a High-Density Traffic Environment," Proceedings of Digital Avionics System Conference, October 2004.
- [Nguy05] M. Nguyen, A. Zaghoul, "On the Characterization of Co-Channel Interference in an Aeronautical Mobile Environment," accepted to be published in the IEEE Transactions on Vehicular Technology, May 2005.
- [McLa75] P. McLane, "Error Rate Lower Bounds for Digital Communication with Multiple Interferers," IEEE Trans. Comm., Vol. COM-23, pp. 539-543, May 1975.
- [Meda99] M. Medard, A. Goldsmith, "Capacity of Time-Slotted Aloha System," IEEE 1999.
- [Meda04] M. Medard, J. Huang, A. Goldsmith, S. Meyn, T. Coleman, "Capacity of Time-Slotted Aloha Packetized Multiple-Access System Over the AWGN channel," IEEE Trans. Wireless Comm., Vol. 3, No. 2, March 2004.
- [Mill96] S.L. Miller. "Training analysis of adaptive interference suppression for direct sequence code-division-multiple access." IEEE Transactions on Communications, 44(4):488-195, April 1996.
- [More98] M. Moretti, G. Janssen, and R. Prasad, "Performance Evaluation of the Dual Signal Receiver for a Quadrature Modulation Scheme," IEEE, 1998.
- [Lai00] K. Lai, J. Shynk, M. Motamed, and R. Gooch, "Adaptive Successive Interference Cancellation for the IS-95 Uplink," IEEE, 2000.
- [Oon00] T. Oon, R. Steele, Y. Li, "Performance of an adaptive Successive serial-parallel CDMA cancellation schme in flat Rayleigh fading channels", IEEE Transactions on Vehicular Technology, Vol. 49, No. 1, January 2000.
- [Pate94] P. Patel, J. Holtzman, "Analysis of a Simple Successive Interference Cancelaltion Scheme in a DS/CDMA System. IEEE Journal on Selected Areas in Communications". Vol. 12, No. 5, June 1994.

- [Pede] K.I. Pedersen, T.E. Kolding, I. Seskar, J.M. Holtzman, "Practical Implementation of Successive Interference Cancellation in DS/CDMA System". IEEE, not dated.
- [Reed97] D. Reed, L. Sundell, "Performance of A d=0 Demod/Remod Detector with Partial Erasure Matching," IEEE Transactions on Magnetics, Vol. 33, No. 5, September 1997.
- [Rom90] R. Rom, M. Sidi., *Multiple Access Protocols: Performance and Analysis*, p 47 – p 77, Springer-Verlag, New York Inc., 1990.
- [RTCA02] RTCA, SC-186, *Minimum Operational Performance Standards for UAT*, RTCA Document Number DO-282, Appendix K, RTCA, Washington, D.C., August 2002.
- [Schn76] K.S. Schneider, "Optimum detection of code division multiplexed signals", IEEE Transactions on Aerospace and Electronic Systems, AES-15(1), January 1976.
- [Star94] H. Stark, J. W. Woods, Probability, Random Process, and Estimation Theory for Engineers, 2<sup>nd</sup> edition, Prentice Hall 1994.
- [Tran] W. Tranter, *Computer-Aided Design and Analysis of Communication Systems*, to be published, not dated.
- [Tran94] W. Tranter, K. Kosbar, "Simulation of Communication Systems," IEEE Comm. Magazine, July 1994.
- [Tral99] V. Tralli, "Performance Characterization of Digital Transmission Systems with Cochannel Interference," IEEE Trans. on Vehicular Technology., Vol. 48, NO. 3, May 1999.
- [Unge74] G. Ungerboeck. "Adaptive maximum-likelihood receiver for carrier-modulated data-transmission systems". IEEE Transactions on Communications, COM-22:624-636, 1974.
- [UPS03] Presentation from UPS Aviation Technologies, Inc. *Universal Access Transceiver*, 2003

- [Vara90] M.K. Varanasi, Aazhang, "Multistage detection in asynchronous Code-Division Multiple Access Communications", *IEEE Transactions on Communications*, 38(4):509-519, April 1990.
- [Verd98] S. Verdu. *Multiuser Detection*. Cambridge Press, 1998.
- [Verd86] S. Verdu. "Minimum probability of error for asynchronous gaussian multiple access channels", *IEEE Transactions on Information Theory*, IT-32(1):85-96, January 1986.
- [Wils02] W. Wilson, "Message Overlap Statistics," presentation at the RTCA Special Committee 186, Working Group 5, Meeting #10, January 2002.
- [Wils02b] W. Wilson, "UAT Synchronization Issues", RTCA Special Committee 186, Working group 5, ADS-B UAT MOPS, Meeting #11, Third Draft of Appendix H, UAT-WP-11-02R1, March 4, 2002.
- [Woer94] B. Woerner, J. Reed, T. Rappaport, "Simulation Issues for Future Wireless Modems," *IEEE Communications Magazine*, July 1994.
- [Xie90] Z. Xie, C.K. Rushforth, and R.T. Short, "Multiuser signal detection using sequential decoding", *IEEE Transactions on Communications*, 38(5):578-583, May 1990.
- [Zeit02] A. Zeitlin and R. Strain, "Augmenting ADS-B with Traffic Information Services-Broadcast," *IEEE Digital Avionics Systems Conference Proceedings*, Volume: 1 pp 3D2-1 – 3D2-7, 2002.

## Vita

Minh A. Nguyen was born in Vietnam on April 21, 1975. He received his Bachelor of Science and Master of Science degrees in Electrical and Computer Engineering from Virginia Polytechnic Institute and State University (Virginia Tech) in 1999 and 2000, respectively. He worked at the Naval Research Laboratory (NRL) in Washington, DC, as an electronics engineer in 1999. While at NRL, he evaluated CDMA receivers for Very Small Aperture Terminal (VSAT) SATCOM applications. He then worked at the MITRE Corporation in McLean, Virginia, as a Senior Communication System Engineer in 2000. Some of his work include FAA next-generation air/ground communication system-VDL-3, adapting commercial and military (JTRS/SCA) software radio architectures for civil aviation, adapting commercial WLAN/MAN (802.11 a/b/g, 802.16e, 802.20) for high-speed airport communications, evaluating commercial cellular technologies (cdma2000, WCDMA, Inmarsat), military (JTIDS/MIDS), and public safety (P-25, P-34) for aviation use.

In 2002, he was selected to join MITRE's fast-paced advanced graduate degree program, which funds for his Ph.D. work in Electrical and Computer Engineering at Virginia Tech as a part time student while continued working at MITRE full-time. He obtained his PhD degree in 2005.

His research interests include multiple access interference, mutual system-to-system interference, broadband spectral overlay, spread-spectrum CDMA communications, OFDM, multi-user detection, and implementation of advanced digital receivers. He has published 30 publications consisting of IEEE journals, conference papers and MITRE technical reports. He is a member of Eta Kappa Nu.